Material and Flexural Properties of Fiber-reinforced Rubber Concrete

A Thesis

Presented to the

Graduate Faculty of the

University of Louisiana at Lafayette

In Partial Fulfillment of the

Requirements for the Degree

Master of Science

Nicholas P. Helminger

Fall 2014

Material and Flexural Properties of Fiber-reinforced Rubber Concrete

Nicholas P. Helminger

APPROVED:

Chris Carroll, Chair Assistant Professor of Civil Engineering	Matthew Fadden Assistant Professor of Civil Engineering
Mohammad Jamal Khattak Professor of Civil Engineering	Mary Farmer-Kaiser Interim Dean of the Graduate School

ACKNOWLEDGMENTS

I would like to extend my thanks to Dr. Khattak and Dr. Fadden in helping me to achieve success in my graduate school research. I would especially like to thank my advisor, Dr. Chris Carroll, for his guidance and encouragement throughout the process. This project could not have been accomplished without the dedicated help of my fellow graduate and undergraduate classmates including Jacob Benton, Michelle Campbell, Dylan Hardy, and Algy Semien. A special thanks to Mr. Mark Leblanc for his laboratory assistance for this project.

TABLE OF CONTENTS

LIST OF TABLES

LIST OF FIGURES

LIST OF FIGURES AND TABLES IN APPENDICES

Appendix A Figures:

Appendix A Tables:

Appendix B Figures:

Appendix B Tables:

Appendix C Figures:

Appendix C Tables:

LIST OF ABBREVIATIONS

a	Depth of the equivalent rectangular stress block (in)
A_1	Area under the load-deflection plot up to $P_{100\%}$
A_2	Area under the load-deflection plot from $P_{100\%}$ to $P_{95\%}$
A_s	Area of tensile steel (in^2)
b_w	Width of beam (in)
C	Compressive force of concrete (kips)
c	Depth to the neutral axis (in)
d	Depth from extreme compressive fiber to center of tensile reinforcement (in)
E	Modulus of elasticity (ksi)
f'_c	Ultimate concrete compressive strength (psi)
f_c	Concrete compressive strength (psi)
f_r	Concrete split tensile strength (psi)
f_s	Stress in reinforcing steel (ksi)
h	Height of beam (in)
M	Moment (k-in)
P	Load (kips)
$P_{100\%}$	Ultimate load (kips)
$P_{90\%}$	90% of ultimate load on descending branch of load-deflection plot (kips)
$P_{95\%}$	95% of ultimate load on descending branch of load-deflection plot (kips)
P_{cr}	ACI Cracking Load (kips)
P_n	Nominal Load per ACI (kips)
P_u	Ultimate Load (kips)

$T_{90\%}$	Toughness index corresponding to $P_{90\%}$
$T_{95\%}$	Toughness index corresponding to $P_{95\%}$
T_{F1}	Tensile force of fiber concrete in the pre-crack region (kips)
T_{F2}	Tensile force of fiber concrete in the post-crack region (kips)
T_{steel}	Tensile force of reinforcing steel (kips)
V_c	Shear capacity of beam (kips)
x	Distance from neutral axis to limit of un-cracked tensile region (in)
y_c	Distance from neutral axis to centroid of concrete compressive force (in)
z	Distance from un-cracked tensile region to extreme tensile fiber (in)
β_1	Concrete strength adjustment factor
Δ	Deflection (in)
Δ_u	Deflection at ultimate load (in)
Δ_y	Deflection at yielding load (in)
ε_c	Concrete strain (in/in)
ε_{cr}	Tensile cracking strain of concrete (in/in)
ε_{cu}	Ultimate concrete compressive strain (in/in)
ε_o	Strain corresponding to f'_c (in/in)
ε_s	Strain in steel reinforcement (in/in)
ε_t	Concrete tensile strain (in/in)
ε_{tu}	Ultimate concrete tensile strain (in/in)
μ	Percentage of σ_{cr} experienced after first crack
σ_{cr}	Ultimate tensile stress of concrete (ksi)
σ_p	Stress in fiber-reinforced concrete cracked tensile region (ksi)

σ_t	Tensile stress of concrete (ksi)
ϕ	Curvature (in^{-1})
ϕ_u	Curvature at ultimate moment (in^{-1})
ϕ_y	Curvature at yielding moment (in^{-1})

CHAPTER 1: Introduction and Objectives

1.1 Introduction

Over the past two decades, more and more attention has been given to the use of recycled materials and sustainable design. Waste products have traditionally been disposed of in landfills, but in recent years, those landfills are beginning to fill with materials that are not biodegradable. This buildup of waste products is resulting in a significant and urgent need for other alternatives. Rather than discarding waste products, an entire industry in recycled materials has begun to thrive in an effort to minimize the amount of waste sent to landfills each year. In addition to the visible, everyday recycling of aluminum cans, plastic bottles, and paper, there is also recycling of industrial by-products, glass, and even tires. Beyond the recycling process, there must also be a market for the recycled product to fully enclose the sustainability loop, which in some cases is the true challenge. With respect to construction materials, the use of a wide variety of materials in concrete mixes has been attempted. Industrial by-products such as fly ash and silica fume have for many years been used in concrete with much success. Glass has been successfully developed into tensile reinforcement and in some cases used as aggregates in both asphalt and concrete. While recycled tires have a more general use in playgrounds and athletic fields, there have been a number of studies completed, looking at the use of recycled tire particles as aggregates in both asphalt and concrete in an effort to dispose of the millions of scrap tires generated each year in the United States (Environmental Protection Agency 2013; Rubber Manufacturers Association 2013).

Although sustainable design and the use of recycled materials have become the popular trend, structural performance still remains as the foundation to sustainable design.

Thus, the appropriate use of recycled materials must be considered based on the type of structure being designed. Additionally, performance-based design is also being implemented more and more as engineers find new innovations to combat extreme events such as earthquakes, tsunamis, hurricanes, and unfortunately, terrorist attacks. In such events, the key is to design and detail with ductile components, a structure with the ability to absorb high amounts of energy and sustain loadings under excessive deflections.

While it is unlikely that the use of recycled tire particles in concrete mixes will ever significantly reduce the volume of scrap tires generated each year in the United States, their use in concrete mixes could be beneficial in the design of structural elements for extreme events. A number of studies have shown concrete containing recycled tire particles to have less compressive strength than conventional concrete and to have less workability, both of which are directly proportional to the percentage of aggregate (fine/coarse) replaced with recycled tire particles (Eldin and Senouci 1993; Khatib and Bayomy 1999; Toutanji 1996). On the contrary, in almost all studies undertaken, the concrete containing recycled tire particles was shown to have a ductile failure mechanism and increased toughness in comparison to a conventional concrete with the same compressive strength **(**Eldin and Senouci 1993; Topçu 1995; Toutanji 1996**)**. A ductile failure mechanism and increased toughness are both desirable characteristics of a material used in the design of structural elements for extreme events. Numerous recommendations have been made regarding the use of concrete in this form **(**Eldin and Senouci 1993; Aiello and Leuzzi 2010; Taha et al. 2008**)**. However, no studies to date have investigated its behavior in any structural applications.

Historically, conventional reinforced concrete has not exhibited ductile behavior without the addition of large amounts of steel. Spiral reinforcing, closer tie spacing, and

tighter grid spacings make its use possible, but also increase both material and labor costs. Over the past few decades, research has shown that the addition of fibers to conventional concrete mixes can significantly increase ductility and toughness. The degree to which the properties of the concrete are affected by the fibers depends on the geometry of the fiber, and the type of material of which the fiber is made. A great deal of research has been done which investigates the performance of fiber-reinforced concrete, but little, if any, has been done on the addition of fibers to rubberized concrete. The purpose of the proposed research is to determine the applicability of using concrete containing both recycled tire particles and fibers as an energy-absorbent material for potential structural applications.

1.2 Objectives

The purpose of the research is to determine the applicability of using concrete containing fiber reinforcement and recycled tire particles as an energy absorbent material. The primary purpose of this study was to determine the basic structural properties for fiber-reinforced rubber (FRR) concrete for potential structural applications. Comparisons were made between rubber concrete with and without fibers in order to determine the effect of fibers on rubberized concrete. The rubber concrete was comprised of two different sizes of rubber: larger rubber particles, around 3/8 in, classified as coarse and smaller rubber particles, passing #8 sieve, classified as fine or crumb rubber. Along with the two types, three concentrations of rubber were used to generate eighteen mixes: nine with fibers and nine without fibers. In addition to the eighteen mixes, four control mixtures that do not contain rubber (two with fibers and two without) were also included for comparison.

For each of the 22 mixes, the following test specimens were cast: 4 in x 8 in cylinders and 8 in x 4 in beam specimens, 54 inches long. Fresh concrete properties were obtained including slump, air content, and the unit weight. Compression tests, split tensile tests, and modulus tests of elasticity were performed on hardened concrete cylinder specimens. Finally, the beam specimens were subjected to flexural loading, from which ductility and toughness were determined.

The main objectives of this research are:

1) Determine fresh concrete properties to:
    - Assess the practicality of the performing these mixes in a real world scenario with respect to workability.

- Determine the differences in unit weight and air content of rubber concrete and fiber rubber concrete versus a conventional concrete mix.

2) Determine hardened concrete properties to:
   - Assure a practical compressive strength range.
   - Compare the effects of rubber addition and rubber/fiber addition to conventional concrete with respect to compressive strength and split tensile strength.
   - Determine the change in the modulus of elasticity of the composite material when compared to conventional concrete as well as ACI predictions.
3) Determine flexural behavior of beam specimens to:
   - Determine the change in toughness and ductility due to addition of rubber and addition of fiber and rubber to conventional concrete.
   - Determine the change in ductility due to addition of rubber and addition of fiber and rubber to conventional concrete.
   - Create a model to predict behavior of flexural beam specimens.

This research achieves the goal of determining the basic structural properties of fiber-reinforced rubber concrete by analyzing data from all properties collected, comparing the data to what is expected from past research, and drawing conclusions about the structural properties that are improved or degraded with the addition of fiber to rubber concrete.

1.3 Research Plan

Literature Review

- Fiber-reinforced concrete and rubber concrete

Preliminary Mix Design

- Determine mix proportions
- Determine fiber type and percentage
- Determine high-range water reducer

Develop Mix Matrix

- Define rubber percentage range and particle size
- Define control mixes

Final Mixes

- Develop mixing procedure and carry out mixes

Fresh Concrete Tests

- Unit weight, workability, air content

Hardened Concrete Tests

- Compressive strength, split tensile strength, modulus of elasticity

Flexural Specimen Tests

- Collect load deflection data
- Determine toughness index and ductility displacement factor

Flexural Beam Model

- Obtain stress-strain relationship of rebar specimens in tension
- Quantify contribution of fiber-reinforced concrete in tension
- Compare experimental versus theoretical data

CHAPTER 2: Literature Reviewed

2.1 Fiber-reinforced Concrete

2.1.1 Types of Fibers

Discontinuous short fibers used in fiber-reinforced concrete can be characterized by the fiber's material properties, physical/chemical properties, and mechanical properties. The material properties of the fiber can be related to whether the fiber is a natural organic material, natural mineral material, or man-made. Natural organic fibers include those obtained from cellulose, sisal, jute, or bamboo. Natural mineral fibers are those made of asbestos or rock-wool. Examples of man-made fibers are those made from steel, titanium, glass, carbon, polymers, or synthetics. The physical/chemical properties of fibers include the fiber's density, roughness, and chemical stability. The mechanical properties that characterize fibers are the fiber's tensile strength, elastic modulus, stiffness, ductility, elongation to failure, and surface adhesion property (Naaman 2003).

Most of the fibers used today are man-made due to optimized properties that are far more effective as reinforcement than natural organic or natural mineral fibers. Common types of man-made fibers used in fiber-reinforced composites (FRCs) today are made of steel, glass, carbon, polymers, and synthetics (Naaman 2003). These include ultra-high molecular weight polyethylene (Spectra) fibers, low-density polyethylene fiber, polypropylene fiber, polyvinyl alcohol (PVA) fibers, Nylon fibers, hooked steel fibers, twisted steel fibers, straight steel fibers, and crimped steel fibers.

Polyvinyl alcohol (PVA) fibers are made by forming PVA powder and extruding it into a fiber-like shape (Noushini et al. 2013). The PVA powder contains hydroxyl groups, which can form hydrogen bonds, increasing the bond between the fibers surface and the

concrete matrix (Toutanji et al. 2010). The PVA fibers are a cheaper alternative to the ultra-high molecular weight polyethylene (Spectra) fibers. They are also desirable due to a higher tensile strength and modulus of elasticity in comparison to Nylon, low-density polyethylene fibers, and polypropylene fibers (Li et al. 2002).

The different types of steel fibers all have advantages and disadvantages that are sensitive to the concrete matrix being used. For example, some types of steel fibers may create a stronger bond with the concrete due to the deformations on the fiber itself but create workability problems when placed in that concrete matrix. The steel fiber type used should be selected with regard to the properties desired within the concrete matrix, as each will produce a different outcome.

2.1.2 Fiber Volume Fraction: Practical and Economic Viewpoint

It has been shown that increasing the volume fraction of fibers in a concrete matrix enhances the toughness and post cracking behavior of the concrete. Increasing the fiber volume fraction can hinder the growth of microcracks and suppress localization (Shao and Shah 1997). Increasing the fiber volume fraction beyond a certain point, however, is not practical due to workability issues. When fibers are added to a cement matrix, the viscosity of the matrix tends to increase. This results in poor workability (Shao and Shah 1997). If the concrete matrix is difficult to mix and place, the hardened concrete properties could be affected by the lack of bond between the cement matrix and the fibers or the other aggregates.

The desire to increase the fiber volume fraction beyond those that are capable of being mixed by conventional mixing procedures has created the need for special processing technology. Two of these processing techniques are slurry-infiltrated fiber concrete

(SIFCON) and slurry infiltrated mat concrete (SIMCON). These techniques allow steel fiber volume fractions ranging from 5 to 20 percent to be used. Although they produce a composite that exhibits the desired strain-hardening response with no workability issues, the practical use of these techniques is limited. This is due not only to the need for special processing, but also the high cost of putting 5 to 20 percent volume fractions of steel fibers into a concrete matrix (Li et al. 2002). It has been noted that when using conventional mixing techniques the volume fraction of fibers should not exceed 1 percent to avoid workability problems (Shao and Shah 1997).

Past research discussed that strain-hardening behavior can be achieved with relatively low fiber volume fractions in comparison to the 5 to 20 percent mentioned previously. Fiber volume fractions between 1 and 2 percent along with the proper matrix constituents and fiber type can produce a composite that produces strain-hardening behavior (Chao et al. 2006).

Overall, from a practical, advantageous, and economic point of view, the fiber volume fraction should remain between 1 and 2 percent. Increasing the volume fraction more than this creates the need for special processing, and higher volume fractions of fibers are expensive.

2.1.3 Types of Fiber-reinforced Cementitious Composites

In 1996, a system for classifying fiber-reinforced cementitious composites (FRCCs) was proposed by Naaman and Reinhardt (1996). The system was based on the behavior of the composites under bending and direct tension tests. From a bending test, the composite can be classified as either a deflection-softening material or a deflection-hardening material. If the composite under bending exhibited a decrease in load carrying capacity after first cracking, the composite is classified as deflection-softening material. If the composite

experienced an increase in load carrying capacity after first cracking, the composite is classified as deflection-hardening material. From a direct tension test, the composite can be classified as either a strain-softening material or a strain-hardening material. If the composite under direct tension exhibited a decrease in load carrying capacity after first cracking, the composite is classified as strain-softening material. If the composite experienced an increase in load carrying capacity after first cracking, the composite is classified as strain-hardening material. Strain-hardening and deflection-hardening materials show increased amounts of shear strength and ductility in comparison to strain and deflection-softening materials. The performance of FRCCs depends on many factors, including the type, amount, and geometry of fibers used and the composition of the cementitious matrix itself (Parra-Montesinos and Chompreda 2007). It is difficult to classify the composite based on the composition alone since many factors can affect it, thus, classification is based on behavior under loading.

2.1.4 Hardened Concrete Properties

2.1.4.1 Compressive Strength

The compressive strength of fiber-reinforced concrete (FRC) depends on many factors, such as water cement ratio, age, particle grading, the composite fabrication process, and chemical admixtures. In addition to these, the fiber type and fiber volume fraction also have some affect on the compressive strength of the FRC. Past research shows both an increase and decrease in compressive strength of FRC with different fiber types and fiber volume fractions in comparison to conventional concrete. For a similar matrix, the compressive strength can increase at first, then decrease with increasing fiber volume fraction (Li 1992). Again, the compressive strength of a given matrix is not solely dependent

upon the fiber type or the fiber volume fraction; however, past research provides observed relationships between these two factors and the compressive strength of FRC.

Li (1992) provides an explanation on the strengthening and weakening effect of increasing the fiber volume fraction within a given concrete matrix. Concrete in compression fails due to crack-to-crack interaction, which, in turn, depends on voids and crack density. A likely place where cracks initiate are void defects in the concrete matrix, which create weak zones. The greater the number of weak zones, the lower the ultimate compressive strength of the concrete. Li (1992) states that the strengthening effect of the fiber addition may be due to the ability of the fibers to aid in resisting sliding of microcracks, which eliminates wing-cracks from initiating. Once the cracks are formed, the fibers also decrease the crack growth rate, thus hindering crack-to-crack interaction and allowing the FRC to reach higher loads before failure occurs. The weakening effect created by the addition of fibers is caused by the introduction of more pores and microcracks into the matrix. An increase in pores may be due to the poor workability of a larger fiber volume fraction, which creates compaction issues. The increased number of microcracks with high fiber volume fractions is due to fibers touching one-another, resulting in fibers that are poorly bonded or even unbonded in the matrix. This creates weak zones (Li 1992). Others suggest that introducing more fibers into the matrix, in turn, leads to more pores, leading to a decreased composite ultimate strength (Noushini et al. 2013; Ward et al. 1989).

Research over the years supports the aforementioned theories. Wu and Li (1994) incorporated steel fibers into conventional concrete ranging from 3 to 8 percent fiber volume fraction. Using 3, 6, and 8 percent steel fibers increased the compressive strength by 10, 95, and 44 percent respectively. The results show that increasing the fiber volume fraction past 6

percent is useless in terms of gaining compressive strength. It was stated that the decrease in compressive strength gain may be due to the poor workability of the concrete when adding 8 percent fiber addition (Wu and Li 1994). Noushini et al. (2013) introduced PVA fibers ranging from 0 to 0.5 percent into a concrete mixture. Results show that matrices with lower fiber additions have higher compressive strength when compared to the control matrix. It was also noticed that matrices with short fibers have a higher compressive strength than those with long fibers. It was suggested that introducing higher volume fractions or longer length fibers into a matrix creates workability problems, which in turn produces a porous composite. Porous composites have lower ultimate strengths (Noushini et al. 2013). The use of synthetic fibers such as polypropylene fibers exhibited similar results (Soulioti et al. 2011; Mydin and Soleimanzadeh 2012).

In general, selecting a fiber type and fiber volume fraction, which either does not affect or increases the compressive strength, is dependent upon many factors that are sensitive to a given concrete matrix. Increases in compressive strength of less than 10 percent using 1.5 percent steel fibers have been observed (Shao and Shah 1997). Others state that using 1-2 percent fibers did not significantly increase or decrease the compressive strength of the composite (Chao et al. 2006). Li (1992) stated that the ultimate strength of FRC is typically reached between fiber volume fractions of 0.5 to 1 percent. Again these results were all based on different concrete matrices, which have different properties. The effects of fiber type and fiber volume fraction on compressive strength are dependent upon these individual matrix properties.

2.1.4.2 Tensile Strength

One of the main reasons for the addition of fibers into concrete is to increase the tensile strength. Research proves this objective is achieved. Thomas and Ramaswamy (2007) incorporated 1.5 percent steel fibers into conventional concrete and discovered an increase in split tensile strength of nearly 40 percent. The increased tensile strength is created from the fibers' interaction with cracks in the matrix similar to that of fiber interaction in concrete in compression. Significant enhancement to post-cracking behavior was also observed (Thomas and Ramaswamy 2007). Incorporation of PVA fibers into conventional concrete has also shown increased split tensile strength. An increase in tensile strength of 11 percent was observed for 12mm length fibers incorporated at a 0.5 percent fiber volume fraction. An increase in tensile strength of 32.5 percent was observed for 6mm length fibers incorporated at 0.25 percent fiber volume fraction. It was also noticed that using a longer length fiber with the same fiber volume fraction did not enhance the tensile strength further. This is due to the creation of a more porous structure, again, relating to workability issues (Noushini et al. 2013). Others compared the tensile strength of concrete, incorporating different types of fibers to see which performed the best. For the concrete matrix tested, when comparing the performance of twisted steel fibers, spectra fibers, and PVA fibers, the twisted steel fibers provided the greatest increase in tensile strength (Chandrangsu and Naaman 2003).

Just as the matrix properties affect the behavior of a FRC in compression, the properties also have an effect on the FRC tensile behavior. In other words, changing the matrix constituents or mixing process may cause different fibers to perform better than others. Overall, adding fibers to conventional concrete increases the tensile strength significantly.

2.1.4.3 Flexural Behavior

Since the addition of fibers to concrete increases its tensile strength, the bending strength of concrete containing fibers also increases. The fibers act as tensile reinforcement when a specimen containing fibers is subjected to flexural loads. The contribution of fibers is similar to that of rebar in reinforced concrete. An increase in ultimate load and higher deflections before ultimate failure are observed.

The question of which fiber performs the best under flexure is also dependent on the properties of the concrete matrix, similar to performance in compression and tension. Chandrangsu and Naaman (2003) investigated the bending strength of three different fiber-reinforced composites. When comparing twisted steel fibers, spectra fibers, and PVA fibers, the twisted steel fibers performed the best under flexure. Other comparative research performed between the fiber types mentioned previously, along with hooked steel fibers, show that the twisted steel fibers perform optimally under flexure. Although the specimens containing twisted steel fibers exhibited the highest load carrying capacity, the spectra fiber specimens were found to have a higher deflection capacity at modulus of rupture. Overall, the equivalent bending strength of the specimens cast of different fiber-reinforced composites in order from highest to lowest was twisted steel fibers, hooked steel fibers, spectra fibers, then PVA fibers (Kim 2008). For this particular concrete matrix, it is evident that the twisted steel fibers perform the best. However, in a different concrete matrix, a different fiber type may perform better.

2.1.4.4 Toughness

Toughness is defined as the ability of a material to absorb energy (Wang and Backer 1989). Since the area under the stress strain curve for a material is energy absorbed by that material, one way of representing an increase of toughness of a material is by decreasing the slope of the descending branch of the curve. Decreasing the slope of the descending branch will increase the area under the stress strain curve, which, in turn, represents an increase in energy absorbed. The toughness of concrete in compression is ordinarily increased by the placement of transverse reinforcement. Transverse reinforcement creates hoop tension in the concrete by confining the lateral expansion of the concrete in compression. As lateral expansion continues in the concrete, the transverse reinforcement experiences inelastic behavior. The deformation caused by the inelastic behavior of the transverse reinforcement is how the toughness of the concrete is increased. In place of, or in addition to, transverse reinforcement, fibers can be used to increase the toughness of concrete. Fibers bridge the cracks in concrete, deterring the lateral expansion of the concrete in compression. As lateral expansion of the concrete continues, the cracks bridged by the fibers widen and the fibers pull out of the concrete. The pull-out of the fibers from the concrete increases the toughness of the concrete (Ou et al. 2012).

The fiber type, fiber volume fraction, and fiber geometry are of concern when determining the most effective way to increase toughness. Comparative research between hooked end fibers, corrugated fibers, and end deformed fibers led to the conclusion that the toughness of the concrete was enhanced the most with the incorporation of hooked end steel fibers (Balaguru et al. 1992). Other research shows the toughness of concrete to increase with a fiber volume fraction of 2 percent when using steel fibers. It was also noted that longer

fibers increased the toughness of the concrete more than short fibers (Ou et al. 2012). Increasing the product of fiber volume fraction and fiber aspect ratio has been proven to increase the toughness of steel fiber-reinforced concrete (Otter and Naaman 1988; Soroushian and Bayasi 1991; Ezeldin and Balaguru 1992; Hsu and Hsu 1994; Mansur et al. 1999; Nataraja et al. 1999; Bhargava et al. 2006; Bencardino et al. 2008; Dhonde et al. 2007).

2.1.4.5 Modulus of Elasticity

There is limited information on the affect that fibers have on the modulus of elasticity of concrete, but available information suggests that little variations are noticed. Research shows that incorporating steel fibers into concrete changed the modulus of elasticity very little (Ou et al. 2012). Other research using PVA fibers at fiber volume fractions of 0.25 and 0.5 percent showed similar results (Noushini et al. 2013). More evidence provides that the modulus of elasticity is only slightly altered when using various fiber types at low fiber volume fractions (Corinaldesi and Moriconi 2011). Though little variation is found at low fiber volume fractions, increasing the fiber volume fraction or the fiber length may decrease the modulus of elasticity of the concrete (Noushini et al. 2013).

2.1.5 Post Cracking Behavior

Regardless of the loading condition, conventional concrete with no reinforcement is known to have a brittle failure mode. Introducing discontinuous fibers into a conventional concrete matrix can change the fracture mode from brittle to a somewhat ductile failure mode. The post-cracking behavior of the concrete is what is ultimately enhanced. The way the fiber interacts with its surrounding matrix is what determines the degree to which the post-cracking behavior is improved.

Once cracks form in a FRC matrix there are forces created by either the fiber or the matrix or a combination of the two, which resist further widening of the cracks. It has been suggested that these forces may form due to the following: debonding of the wire from the concrete matrix (Outwater and Murphy 1969), overcoming interfacial forces that oppose the pull-out of the wires (Cottrell 1964), or deforming of the wire by some means (Helfet and Harris 1972; Morton and Groves 1974). Preventing the propagation and widening of cracks can provide residual strength (Morton and Groves 1974).

The bond between the fiber and the matrix can exist in two forms: physiochemical (chemical) bond and mechanical bond. A chemical bond can be created when substances such as latex or an epoxy resin are added to the concrete matrix. The chemicals increase the adhesive properties between the fibers and the matrix (Naaman 2003). One example of altering the bond properties between the fiber and the matrix is through the use of PVA. Research has shown that due to the presence of hydroxyl groups in PVA fibers, a strong chemical bond exists (Kanda and Li 1998). The bond between steel fibers and the concrete matrix is almost always improved through the use of mechanical deformations on the fiber. Mechanical bond can be created by deforming the fiber such as in the case of twisted or hooked-end steel fibers (Naaman 2003). Improving the bond increases the load required to pull the fiber from the matrix.

In order for the fiber to be completely removed from the matrix, the fiber must overcome frictional forces and either deform or rupture. The fiber must overcome the frictional forces, which are always present as long as the fiber and matrix are in contact (Naaman 2003). In the case of steel fibers with deformations, the deformations must be overcome in order for the fiber to pull out. For example, the hook on hooked-end steel fibers

must straighten out in order for pull-out to occur. In the case of twisted steel fibers, the fiber must un-twist for the fiber to be removed from the matrix. These additional required deformations result in increased pull-out resistance (Willie and Naaman 2012). In the case of PVA fibers where the bond strength is extremely high, the fiber will rupture before pull-out can occur (Kanda and Li 1998).

2.2 Rubber Concrete

2.2.1 Mix Composition

The first challenge in creating rubberized concrete is to determine in what way the rubber should be incorporated into conventional concrete in order to produce the most effective results. A conventional concrete mix design that includes aggregates, cement, and water is modified to rubberized concrete by replacing the mineral aggregates with rubber particles. The process and amount in which they are incorporated has varied over the years through research pertaining to rubberized concrete.

One of the most common ways of replacing the mineral aggregates with rubber particles is by comparing the particle size of the rubber particles to the mineral aggregates. Mineral aggregates include sand and either gravel or limestone. If the size of rubber aggregate to be used is similar to the size of the fine mineral aggregate such as sand, the sand should be replaced by the rubber aggregate. Likewise, if the rubber particles to be tested more closely match the size of the coarse aggregate like gravel or limestone, the coarse aggregate would be replaced by the rubber particles. Over the past decade or so, most of the research done on rubberized concrete followed this methodology (Eldin and Senouci 1993; Khatib and Bayomy 1999; Ghaly and Cahill (IV) 2005; Khaloo et al. 2008; Taha et al. 2008; Aiello and Leuzzi 2010).

The amount of rubber substitution, whether fine or coarse, has been widely investigated, the most common of which is by volume. This means that a certain volume of rubber being incorporated into a conventional mix is substituting for the same volume of aggregate being removed from the mix. Replacement levels from 0 to 100 percent by volume of the total aggregate volume have been investigated (Toutanji 1996; Taha et al. 2008).

However, the high replacement levels produce workability problems and severe strength reduction. It was recommended that the replacement level be no greater than 50 percent by volume to prevent severly altering the properties of rubberized concrete in comparison to conventional concrete (Khatib and Bayomy 1999). Even lower amounts should be used to maintain concrete properties that are practical for use in engineering applications.

2.2.2 Fresh Rubber Concrete Properties

2.2.2.1 Workability

Workability has been defined as "the ease with which concrete can be mixed, transported, and placed" (Khaloo et al. 2008). Khaloo et al. (2008) state that workability is influenced by the interaction between mineral aggregates and tire particles. Results from experiments performed by this group on rubberized concrete show that up to 15 percent replacement levels, fine rubber tends to increase the workability while coarse rubber tends to decrease the workability. Beyond 15 percent replacement, mixes containing either fine or coarse rubber exhibit decreased workability. Biel and Lee (1996) and Toutanji (1996) also reported decreased workability with the addition of coarse rubber particles. Though adding rubber particles may influence the mechanical properties of concrete, if the workability is not practical, then the mixture is not practical.

Khatib and Bayomy (1999) also made observations on the workability of rubberized concrete. According to the research, the workabilty is dependent on the percentage of rubber in the mixture. It was stated that replacement for both coarse and fine rubber particles beyond 40 percent by volume exhibited severe workablitiy issues. Results showed a slump value of near zero with vibratory compaction required to consolidate the concrete sufficiently. The fact that the workability is dependent upon the rubber content in the mixture was further

acknowledged by Taha et al. (2008). Results showed that while both coarse and fine rubber particles exhibit negative effects on the workablity of concrete, coarse rubber particles tend to cause a greater effect.

2.2.2.2 Unit Weight

Over the past decade, existing research conducted on rubberized concrete shows a consistent reduction in unit weight with increased amounts of rubber particles (Topçu 1995; Biel and Lee 1996; Khatib and Bayomy 1999; Khaloo et al. 2008; Taha et al. 2008; Zheng et al. 2008). Topçu (1995) stated that the relationship between the reduction in unit weight with increasing amounts of rubber particles is "systematic". Khatib and Bayomy (1999) stated that the unit weight of rubberized concrete can be as little as 75 percent of normal weight concrete.

There are two suggested reasons for this reduction in unit weight. First, the rubber particles have lower specific gravity values when compared to conventional aggregates and are therefore lighter than the mineral aggregates they are replacing in the concrete mixture (Khaloo et al. 2008; Taha et al. 2008; Zheng et al. 2008). Lighter particles in place of heavier particles in the same volume will result in a decrease in unit weight. The second suggested reason for the reduction in unit weight involves the ability of the rubber particles to entrap air in their jagged surfaces (Khatib and Bayomy 1999; Taha et al. 2008). If air gets entrapped on the surface of the rubber particles while it is being incorporated into the mix, the air will remain in the mixture and cause a higher air content in the concrete. A higher air content means that instead of mineral aggregates or even rubber particles taking up space in a specific volume, there are actually voids in which air is present. The lighter air, instead of

heavier mineral aggregates or rubber, will certaintly cause a decrease in unit weight of the concrete.

2.2.2.3 Air Content

Past research on rubberized concrete has shown that as the amount of rubber particles incorporated into a concrete mixture increases, the amount of air in the mixture also increases (Khatib and Bayomy 1999; Khaloo et al. 2008; Taha et al. 2008). As stated earlier, rubber particles may have a tendency to entrap air in their jagged surfaces. When rubber particles are introduced into a concrete mixture, they repel water and attract air (Khaloo et al. 2008). The air entrapped by the surfaces of the particles remains in the mixture and therefore produces a concrete with a high air content. The air entrapping theory can be described by examining the specific gravity of the rubber particles. The specific gravity of the particles used in the experiment by Taha et al. (2008) was 1.10, which suggests that the rubber particles are heavier than water and therefore should sink. However, the rubber particles floated in water, suggesting that the particles contained air around its surfaces that prevented it from sinking (Taha et al. 2008). High air contents can reduce unit weight, and cause a significant reduction in concrete compressive strength.

2.2.3 Hardened Rubber Concrete Properties

2.2.3.1 Compressive Strength

One of the reasons concrete is used widely as a construction building material is due to its ability to withstand large compressive loads. Therefore, it is important that this property be investigated to understand what happens when rubber particles are added to a conventional concrete mixture.

Eldin and Senouci (1993) conducted experiments using tire chips and crumb rubber. The tire chips retrieved either through mechanical grinding or cryogenic grinding had maximum sizes ranging from 1.50 in. to 0.24 in (38 mm to 6 mm). The crumb rubber also retrieved from a cryogenic grinding process had a maximum size less than 0.08 in (2 mm). The coarse aggregate was replaced by the tire chips while the sand was replaced by the crumb rubber in increments of 25 percent by volume. Compressive strengths decreased up to 85 percent for varying amounts of coarse rubber replacement and up to 65 percent for crumb rubber replacement. The strength gain from 7 to 28 days also decreased as the amount of rubber in the mixture increased (Eldin and Senouci 1993). This smaller reduction in compressive strength with crumb rubber as compared to coarse rubber becomes a common characteristic of rubberized concrete as further research proves.

Eldin and Senouci (1993) also discuss the decrease in compressive strength with the addition of rubber particles. One reason focused on the low modulus of elasticity of rubber. When the rubber particle is added to concrete, it replaces stronger aggregate such as limestone or sand and acts as a pore rather than a solid load-bearing material. With this in mind, the greater the volume of rubber added to a conventional concrete mix, the more pores are introduced. More pores means less load bearing material and therefore less compressive strength (Eldin and Senouci 1993). Another reason for the reduction in compressive strength was determined from the mathematical model constructed by Popovics (1987). Eldin and Senouci (1993) used the model from this investigation and found that the addition of rubber particles to concrete causes high stress concentrations at the boundaries of the rubber particles. The high stress concentrations cause a weakening effect and therefore results in a lower compressive strength.

Topçu (1995) conducted an experiment replacing mineral aggregates with different amounts of fine and coarse rubber chips. Between 15 and 45 percent of the conventional aggregates by volume were replaced with the rubber. Like Eldin and Senouci (1993), Topçu (1995) also reported losses in compressive strength with the addition of rubber and a larger reduction in strength due to the addition of coarse rubber particles in comparison to fine rubber particles. For specimens containing coarse rubber, compressive strength decreased by 60 percent for cylinder specimens and 80 percent for cube specimens. In specimens containing fine rubber, compressive strength decreased by 50 percent for both cylinder and cube specimens. Topçu (1995) stated that the reduction in compressive strength could be caused by the weak bond existing between the tire chips and the cement paste.

Biel and Lee (1996) examined the idea of creating a better bond between the rubber particles and the cement paste. An experiment was conducted in which Portland cement rubber concrete (PCRC) was compared to magnesium oxychloride cement rubber concrete (MOCRC) to see if the magnesium oxychloride cement would provide a better bond between the rubber particles and cement. When 25 percent rubber by aggregate volume was incorporated into the mix, a 90 percent reduction in compressive strength for both PCRC and MOCRC was observed. But the results also proved that using magnesium oxychloride cement increased the compressive strength 2.5 to 3 times in comparison to the concrete with Portland cement. Observations of failed specimens showed that the rubber particles themselves failed. This research concluded that the bond between the cement and rubber was increased by using magnesium oxychloride cement (Biel and Lee 1996).

Other processes of pretreatment to rubber particles in order to increase the compressive strength of the rubberized concrete were examined by later researchers. One of

these pretreatments is the simple process of washing the rubber aggregates with water (Khaloo et al. 2008). Another process involves soaking the rubber particles in a NaOH solution (Segre and Joekes 2000). These processes aim at improving the bond between the rubber particles and the cement paste. Further research demonstrated that the compressive strength did not dramatically increase when the aggregates are pretreated with NaOH and Silone solutions (Albano et al. 2005). With this much contradiction, it seems further research is needed to fully understand if pretreatment is worth the effort and cost.

Researchers performing other experiments throughout the years have come to different conclusions about how much or in what way rubber affects compressive strength but all have found that it does indeed cause a decrease in compressive strength. Toutanji (1996) described the relationship between strength reduction and rubber content as "not linear" while Ghaly and Cahill IV (2005) suggested the relationship is "almost linear". Khatib and Bayomy (1999) suggested there is a "systematic reduction" in concrete compressive strength as the amount of rubber particles in the mixture increases. In one experiment, specimens containing coarse rubber particles replaced for coarse mineral aggregate exhibited slightly higher compressive strengths up to 25 percent replacement of rubber by aggregate volume than those containing fine rubber particles in place of fine mineral aggregates. The results were different for larger than 25 percent replacement levels. The reason for the higher compressive strength is due to the presence of fibers in the coarse rubber particles (Khaloo et al. 2008). Others (Huang et al. 2004; Taha et al. 2008; Zheng et al. 2008; Aiello and Leuzzi 2010) reported similar results to Eldin and Senouci (1993) and Topçu (1995), stating that the replacement of large mineral aggregates by coarse rubber

particles decreases the compressive strength more than the replacement of fine mineral aggregates by fine rubber particles.

2.2.3.2 Tensile Strength

One of the major disadvantages of conventional concrete is its low tensile strength. Therefore, it is also important to understand the influence of rubber particles on the tensile strength of concrete. As stated previously, Eldin and Senouci (1993) performed an experiment using crumb rubber and tire chips, varying the percentage of aggregates replaced. Just as the compressive strength decreased, the tensile strength also decreased with increasing amounts of rubber. Specimens with tire chips and specimens with crumb rubber both exhibited up to a 50 percent decrease in tensile strength. Other research by Topçu (1995) also displayed a decrease in tensile strength with the addition of rubber particles when compared to conventional concrete. Specimens containing fine rubber particles exhibited tensile strength losses of 64 percent while specimens containing coarse rubber particles exhibited tensile strength losses up to 74 percent. Just as the coarse rubber particles affect the compressive strength more than the fine rubber particles, the tensile strength is affected in a similar manner. Comparable to the reasons for the decrease in compressive strength, the decrease in tensile strength can be attributed to an increase in pores, increase in stress concentration at the boundaries of rubber particles, and the poor bond between the cement paste and the rubber particles (Eldin and Senouci 1993; Topçu 1995).

Biel and Lee (1996) also provided information on the tensile performance of rubberized concrete during their investigation aiming to improve the bond between rubber particles and cement paste. Overall, it was concluded that tensile strength does decrease with the addition of rubber particles. The magnesium oxychloride cement rubber concrete

(MOCRC), however, did improve the tensile strength when compared to Portland cement rubber concrete (PCRC). The results show that the MOCRC retained 14 percent more tensile strength than the PCRC. This further supports the conclusion that the bond between the rubber and the cement paste was increased when magnesium oxychloride cement was used (Biel and Lee 1996). Though the bond strength was shown to increase with the use of magnesium oxychloride cement, the main conclusion drawn from this research is that the overall tensile performance decreases with increasing amounts of rubber particles added to conventional concrete.

2.2.3.3 Flexure

Toutanji (1996) conducted an experiment in which tire chips were incorporated into concrete mixtures by replacement of mineral aggregates by volume percentages of 25, 50, 75, and 100. A four-point bending test was performed on flexural specimens with dimensions of 4 x 4 x 14 in. (102 x 102 x 355.6 mm). The results show a decrease in flexural strength of up to 35 percent, depending on the rubber content, when compared with conventional concrete. It was noted that the flexural strength decreased less than the compressive strength. Again, similar to the results from the compressive tests, the relationship between the reduction in strength of the flexural specimens and the percentage of rubber introduced into the mix was "not linear" (Toutanji 1996).

Khatib and Bayomy (1999) performed an experiment using both tire chips and crumb rubber particles to replace conventional aggregates. They cast beam specimens with dimensions of 6 x 6 x 20 in. (152.4 x 152.4 x 508 mm) and performed a standard three point flexural bending test. Documented results show a "systematic" decrease in the flexural strength with increasing amounts of rubber particles. It was noted that the initial rate of

flexural strength reduction was much more significant when compared with the compressive strength. The beam specimens containing rubber particles did however exhibit deflections which were larger than those observed in specimens cast from conventional concrete (Khatib and Bayomy 1999). Though this research did not state whether the coarse rubber or fine rubber affected the flexural strength more, it is believed that the coarse rubber will have a greater effect based on the way it affects the compressive strength.

Aiello and Leuzzi (2010) conducted an experiment in which two types of specimens were cast; those containing crumb rubber particles and those containing coarse rubber particles. The crumb rubber replaced the fine aggregate, and the coarse rubber replaced the coarse aggregate. The percentages that were replaced by volume include 25, 50, and 75 percent. The results showed that the flexural strength did decrease with the addition of rubber particles. The results also showed that the coarse rubber particles affected the flexural strength more than fine rubber particles (Aiello and Leuzzi 2010). This information suggests that coarse rubber particles have a much higher impact on compressive, tensile, and flexural strength of rubberized concrete.

2.2.3.4 Toughness

One of the desired properties of construction materials that could be subjected to dynamic loadings is toughness. Toughness is the ability of a material to absorb energy. Increasing the toughness of concrete has been researched for many years. Investigations pertaining to the addition of rubber particles to conventional concrete in order to alter the toughness properties have been performed.

Eldin and Senouci (1993) stated that tough materials generate mostly plastic energy upon fracture while brittle materials generate mostly elastic energy upon fracture. Fracture

toughness was computed by calculating the area under the plastic portion on the stress strain diagram. The elastic energy was subtracted from the total energy in order to get the plastic energy. During Eldin and Senouci's (1993) investigation into rubberized concrete, it was found that most of the total energy generated upon fracture was plastic energy. Thus, the material was described as having a high toughness, or great capability of absorbing energy (Eldin and Senouci 1993).

Topçu (1995) found similar results to Eldin and Senouci (1993) in an investigation of rubberized concrete. It was noted that the toughness values decreased with the addition of rubber since the elastic energy capacity decreases with the addition of rubber. However, the rubberized concrete exhibited higher plastic energy capacities with an increase in rubber content. This allowed the material to reach higher strains before fracture of the material occurred. It also resulted in the material exhibiting ductile behavior.

Toutanji (1996) computed the toughness differently than previous researchers. It was derived based on the ratio between 85 percent of the total load withstood by a flexural specimen and the elastic limit on the load deflection diagram. Up to 50 percent replacement with tire chips, the toughness ratio of the rubberized concrete was equal to 1.21 which is higher than the ratio of 1 for conventional concrete. No change in toughness was recognized past 50 percent replacement of mineral aggregates. Thus, the rubberized concrete possesses a higher material toughness than the conventional concrete for up to 50 percent replacement levels (Toutanji 1996). Other researchers used a ratio between 80 percent of the ultimate stress and 100 percent of the ultimate stress to determine the toughness values of rubberized concrete. These results show the toughness of rubberized concrete is higher than conventional concrete up to replacement levels of 25 percent of mineral aggregates. Past 50

percent replacement level the toughness values decrease due to a decrease in the compressive strength of rubberized concrete (Khaloo et al. 2008).

Further research validates that the additon of rubber particles up to 50 percent replacement by volume of mineral aggregates enhances the toughness or energy absorbing capabilties of the concrete (Huang et al. 2004; Taha et al. 2008; Zheng et al. 2008). Taha et al. (2008) described how the rubberized concrete improved impact resistance and flexibility. Zheng et al. (2008) discussed how adding rubber particles to concrete helps convert concrete from a brittle material to a more ductile, energy absorbing material. From the research presented, it seems that adding rubber particles to concrete is a viable method of increasing the toughness of the material.

2.2.3.5 Modulus of Elasticity

Another important property of concrete is its modulus of elasticity. The modulus of elasticity is a measurement of the ability of a material to behave in an elastic manner. Little investigation has been performed on the impact of adding rubber particles to concrete has on the modulus of elasticity. Zheng et al. (2008) presented results on the effects of rubber particles in concrete with respect to its elastic modulus. Important factors affecting the modulus of elasticity of concrete are "the property of the cement paste, the stiffness of the selected aggregates, and also the method of determining the modulus". Since some of the stiffer mineral aggregates are replaced with softer rubber aggregates in rubberized concrete, differences in the modulus of elasticity are expected when it is compared to conventional concrete. Variations in coarse and fine rubber replacement for the experiment ranged from 15 to 45 percent. Reduction in static modulus varied between 14.8 to 29.9 percent for fine rubber specimens and between 27.4 to 49.4 percent for coarse rubber specimens. Reduction

in dynamic modulus varied between 5.7 to 28.6 percent for fine rubber specimens and between 16.5 to 25 percent for coarse rubber specimens. The general trend is that both the static and dynamic modulus of elasticity decreases with increasing amounts of rubber particles whether those particles be coarse or fine. However, the coarse rubber particles reduce the elastic modulus more than the fine rubber particles following previous trends (Zheng et al. 2008).

2.2.4 Failure Mode

Failure mode of conventional concrete versus the failure mode of rubberized concrete has been compared numerous times. It has been observed that rubberized concrete tends to display a more gradual, ductile failure mode instead of the brittle, explosive behavior seen in conventional concrete (Eldin and Senouci 1993; Topçu 1995; Biel and Lee 1996; Toutanji 1996; Khatib and Bayomy 1999). The failure of convenetional concrete is rather explosive and tends to leave the tested specimen in many pieces with no capability of carrying futher load (Biel and Lee 1996). To understand the failure of concrete specimens containing rubber particles, it is important to understand how that particle behaves in its surrounding matrix. Particles of rubber in hardened concrete are like elliptic-shaped voids capable of withstanding large tensile deformation before failure. Failure of rubberized concrete will initiate in the cement paste since the paste in tension will undergo a smaller deformation before cracking than will the rubber. Once the cracks form in the paste, they travel until coming into contact with rubber particles. The rubber particles tend to act as springs and keep the specimen from fully disintegrating. As more load is applied, more cracks form and widen until the bond between the cement paste and the rubber aggregate fails. Once the bond fails, the concrete begins to fall apart as the rubber no longer holds the tensile forces present in the

concrete specimen (Eldin and Senouci 1993). Huang et al. (2004) expanded on this concept by stating that if the bond between the rubber aggregate and the cement paste is enhanced, the rubber aggregate will give the concrete even more deformability or toughness as its full tensile strength and large deformation capabilities will be utilitized.

Eldin and Senouci (1993) characterized the failure mode of rubberized concrete depending on the type of rubber used. Tire chips containing steel wires or fibers made from the mechanical grinding process are known as Edgar chips. Preston rubber was produced by the cryogenic grinding process and is free of wires or fibers. For compressive failure, specimens containing Edgar chips tended to fail by gradually splitting while withstanding postfailure compression loads and significant displacement without full disintegration. Specimens containing Preston rubber tended to fail by a gradual shearing effect. The shear failure occurred because the shear stress exceeded the shear strength of the cement paste, and the tensile stress remained below the tensile strength of the cement paste. For tensile failure, the specimens also withstood measureable post-failure loads and underwent signifcant deformation. Unlike conventional concrete during a split tensile test, the specimens never seperated into two halves (Eldin and Senouci 1993). This could be due to the rubber particles bridging the cracks and holding the concrete matrix together.

2.3 Summary

In summary, research shows that fiber-reinforced concrete and composites have increased ductility and toughness, and with proper fiber concentrations, positive effects on compressive and tensile strengths compared to conventional concrete mixes. Like fiber-reinforced concrete, concrete containing recycled tire particles, although somewhat unconventional, also has an increased toughness compared to conventional concrete mixes. However, the inclusion of recycled tire particles shows negative effects on compressive and tensile strengths. While the two materials have both shown an increased toughness compared to conventional concrete, the two materials have not been used together as constituents in concrete mixes. A realistic potential exists for the development of a composite material through the proper combination of fiber concentration and recycled tire particles. The development of the composite material will use the positive characteristics of each constituent to potentially combat any negative characteristics. The material is expected to have high toughness and ductility while the use of fibers will likely reduce the tendency of compressive and tensile strengths to decrease with increases in rubber content.

CHAPTER 3: Methodology

3.1 Introduction

This investigation included 22 different mixes from which cylinder specimens and beam specimens were cast. Fresh concrete tests including slump, air content, and unit weight tests were performed. Hardened concrete tests performed on cylinders at standard time intervals included compression tests, split tensile tests, and modulus tests. Finally, a four point bending test was performed on flexural beam specimens.

3.2 Preliminary Mix Design

Certain desired parameters were set for the concrete mixes used in this investigation. These parameters included a minimum, worst-case concrete compressive strength of 5000 psi while maintaining a reasonable workability when incorporating both rubber particles and fibers. Based upon literature, it was assumed that the largest decrease in compressive strength would occur from a mixture which contained the largest percentage of coarse rubber. Fifteen percent replacement by volume of the total aggregate was selected as the maximum amount of rubber replacement due to compressive strength decreases observed by previous researchers. Mixes containing 15 percent coarse rubber in place of coarse aggregate by volume in a conventional concrete mix were tested. The ratio of sand cement and water was adjusted until a mix design achieved a minimum compressive strength of 5000 psi at 28 days in compression.

Once this was achieved, various percentages of hooked end steel fibers were incorporated into the mix to observe how fiber and rubber particles interacted in the mix. It was observed that the workability of the mix decreased dramatically when fibers were introduced, especially at higher percentages such as 1.5 to 2 percent. In order to compensate

for this reduction in workability, super plasticizer was used in various amounts. During these preliminary experiments, it was noticed that the aggregates and fibers may be settling to the bottom of the cylinders during casting due to the high amounts of water reducer. In mixes in which a large amount of super plasticizer was used, several 4 in. x 8 in. cylinders were cut in half along their length in order to visually inspect aggregate settlement. It was observed that in mixes where large amounts of superplasticizer was used, the larger aggregates and fibers settled to the bottom while fine aggregates remained at the top. Different water reducers were used to determine if the segregation issue could be resolved. From these experiments, an optimal superplasticizer was chosen and limits were placed on its usage in order to prevent aggregate segregation.

Other parameters for the final experiment such as final mix ingredient proportions and aggregate sizes were also determined. Based upon a mix which would achieve 5000 psi 28-day concrete compressive strength as well as dealing with the segregation issue, the volume of fine particles and coarse particles were set equal to one another. Also, the maximum coarse aggregate size was selected as ⅜ in. since it was very similar to the maximum coarse rubber size.

After evaluating a variety of different mixes including combinations of fibers, water reducers, and rubber, a comparison was made amongst different fiber types in the same matrix. Observations were made in order to determine which fibers performed the best in the final matrix, while not affecting the workability of the mix to a point requiring excessive amounts of water reducer. Based off of literature reviewed and knowledge of which fibers may perform the best for the designed matrix, five fiber types were chosen. The fibers along

with some of their properties can be found in Table 1. Using these five fiber types, a total of six mixes were tested, including a control mix which contained no fibers.

Table 1. Fibers selected for preliminary investigation

Properties of Fibers Selected for Preliminary Investigation					
Fiber Name	Material	Type	SG	Tensile Strength (psi)	Length
PVA RECS 15	Polyvinyl Alcohol	PVA	1.3	240,000	8 mm (0.375 in)
PVA RECS 100	Polyvinyl Alcohol	PVA	1.3	180,000	13 mm (0.5 in)
Helix 5-25	High Tensile Steel Wire	Twisted	7.8	246,000 (min)	25 mm (1 in) or cut to length
Hooked End Steel Fiber	Low-Carbon Steel	Hooked	7.8	165,000	25 mm (1 in) 38 mm (1.5 in)
Straight Steel Fiber	Low-Carbon Steel	Needles	7.8	285,000	13 mm (0.5 in)

The purpose of these test mixes was to select a fiber that performed the best in terms of both strength and workability. In order to ensure the minimum 5000 psi compressive strength goal was met, 15 percent coarse rubber was added to the mixes since this was determined to be the maximum percentage to be experimented with in the final mixes. This allowed observation of the potential worse case to be tested in terms of strength and workability and determine if the parameters were realistic. The only variation in mix composition was the type of fiber used. The fiber percentage was held constant at 1 percent since larger percentages in addition to 15 percent coarse rubber would not be practical due to severe workability problems.

The PVA RECS 15 and PVA 100 fibers performed similarly in that they tended to clump together forming balls. The balls decreased the workability dramatically even with the use of high amounts of water reducer. There was little bonding between the concrete matrix and the fibers especially where the balls of fibers existed. During compression testing, it was noticed that some fibers failed to come into contact with the matrix due to the clumping of fibers.

The Helix twisted fibers exhibited better workability during mixing and produced a concrete with an overall higher compressive strength when compared to the PVA fibers. Acceptable workability was noticed with the use of water reducer and no clumping of fibers was observed. However, after placement of the concrete in the cylinders, it was noticed that the concrete in the cylinders rose out of the cylinders up to ¼ of an inch. It was theorized that there was potentially a reaction occurring between the coating on the fibers and the rubber in the mix. Once the concrete hardened, many small bubbles around the fibers were observed. The bubbles around the fibers potentially resulted in decreased bond between the fibers and the matrix and created weak zones in the concrete leading to lower compressive strengths than anticipated. The air bubbles were also why the concrete appeared to expand.

Similar results were observed between the hooked end fibers and the steel needle fibers. Both exhibited acceptable workability, and no clumping of fibers was observed. Comparison of strength gain for up to 28 days between the five fiber mixes and the control mix can be found in Table 2. Overall, the mixture containing the steel needle fibers exhibited the highest compressive strength.

Table 2. Compressive strengths of preliminary mixes

Compressive Results of Preliminary Mixes (psi)					
Fiber Type	1-Day	4-Day	7-Day	14-Day	28-Day
PVA RECS 15	1210	2243	2845	2981	3211
PVA RECS 100	1207	2975	3184	3432	3773
Helix 5-25	1619	3403	3883	4194	4297
Hooked End	3238	4888	5179	5821	5891
Steel Needles	3377	5792	6180	6709	7036
Control Mix	3254	4767	4966	5613	5772

*Each value is average of 3 compression tests.

With the understanding that there are many factors that affect the performance of a certain fiber in a given concrete matrix, the steel needle fibers were selected for the research being performed due to acceptable workability and high compressive strength. Any of the

fibers mentioned could potentially work for this research but more tailoring of the mix would be required. The idea was to keep the mix as traditional as possible and be both practical and economical. Given the concrete matrix previously determined, the steel needle fibers seem to provide the most effective results for the goals of the experiment.

3.3 Final Mixes

Based on the results and observations from all preliminary mixes, the following matrix of mixes shown in Table 3 was chosen for the investigation. A nomenclature was created for the mixes for simplification. This nomenclature is found in Table 4.

Table 3. Mix matrix

Mix Matrix	Rubber Gradation			# of mixes
	Coarse	Fine	Coarse & Fine	
No Fiber	0%	0%	0%	2
	5%	5%	5%	3
	10%	10%	10%	3
	15%	15%	15%	3
1% Fiber	0%	0%	0%	2
	5%	5%	5%	3
	10%	10%	10%	3
	15%	15%	15%	3
Total Number of Mixes =				22

Table 4. Nomenclature for final mixes

LEGEND		
Mix #	Composition	Name
1	Plain concrete	PL1
2	Plain concrete	PL2
3	1% Fiber, No Rubber	F1
4	1% Fiber, No Rubber	F2
5	1% Fiber, 5% CoarseRubber	F5C
6	1% Fiber, 5% Fine Rubber	F5F
7	1% Fiber, 5% Coarse + Fine Rubber	F5CF
8	1% Fiber, 10% Coarse Rubber	F10C
9	1% Fiber, 10% Fine Rubber	F10F
10	1% Fiber, 10% Coarse + Fine Rubber	F10CF
11	1% Fiber, 15% Coarse Rubber	F15C
12	1% Fiber, 15% Fine Rubber	F15F
13	1% Fiber, 15% Coarse + Fine Rubber	F15CF
14	No Fiber, 5% Coarse Rubber	5C
15	No Fiber, 5% Fine Rubber	5F
16	No Fiber, 5% Coarse + Fine Rubber	5CF
17	No Fiber, 10% Coarse Rubber	10C
18	No Fiber, 10% Fine Rubber	10F
19	No Fiber, 10% Coarse + Fine Rubber	10CF
20	No Fiber, 15% Coarse Rubber	15C
21	No Fiber, 15% Fine Rubber	15F
22	No Fiber, 15% Coarse + Fine Rubber	15CF

3.4 Constituents of the Mixes

3.4.1 Aggregate

Limestone was used as the coarse aggregate in all mixtures with a maximum aggregate size of ⅜ in. The absorption value for limestone calculated using ASTM C127, was determined to be 1.27 percent. The bulk specific gravity calculated following ASTM C127 is 2.61 (ASTM 2012a). A typical sample of limestone is shown in Figure 1(a).

Sand was used as the fine aggregate. The fineness modulus was calculated from a sieve analysis and was determined to be 2.4. The absorption value for sand was calculated using ASTM C128 was 0.73 percent. Bulk specific gravity was calculated following ASTM C128 and is 2.6 (ASTM 2012b). A typical sample of sand is shown in Figure 1(b).

(a) (b)

Figure 1. (a) Limestone and (b) Sand

3.4.2 Rubber

Two sizes of rubber particles were used. The coarse rubber aggregates shown in Figure 2(a) are chipped tire particles which have the strings from the tires still in the rubber pieces as shown. The pieces vary in geometry but have a fairly uniform size averaging ⅜ in. The fine rubber aggregates shown in Figure 2(b) are ground tire particles that are free of tire

strings. The fine rubber has a fairly uniform size that passes a No. 8 sieve. The approximate specific gravity of both sizes of rubber particles is 1.05. The absorption value is negligible.

3.4.3 Fibers

The fibers used are NYCON-SF TYPE I (NEEDLES) High Performance Steel Fiber, conforming to ASTM A820 (ASTM 2011a). These fibers are shown in Figure 2(c). They have a length of 0.5 in. (13mm) and a diameter of 0.008 in. (0.2mm). The specific gravity of the fibers is 7.8. The tensile strength is 285ksi (1900MPa). The absorption value is negligible.

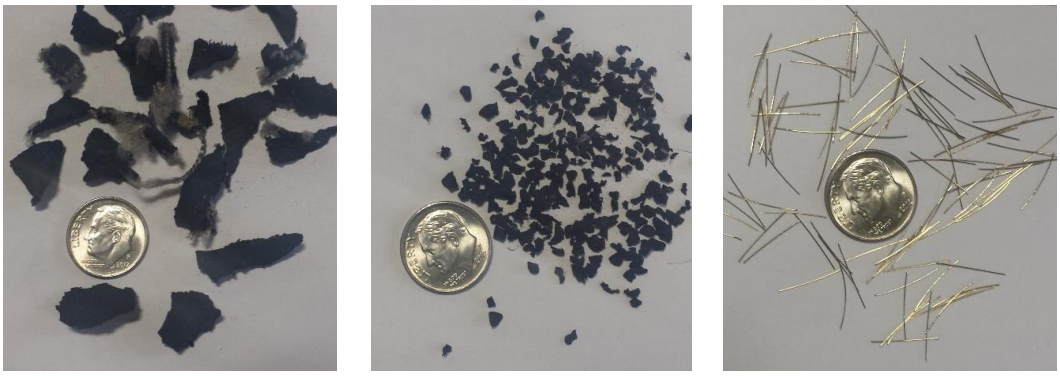

(a) (b) (c)

Figure 2. (a) Coarse rubber particles, (b) Fine rubber particles, and (c) Steel needle fibers

3.4.4 Water Reducer

The water reducer used was ADVA ® 190 High-range water-reducing admixture conforming to standard ASTM C494 (ASTM 2013a) Type A and F, and ASTM C1017 (ASTM 2013b) Type I (Grace 2014).

3.4.5 Cement

Portland Cement Type I, II produced by Holcim was used in all concrete mixes. The specific gravity of the cement is 3.15.

3.5 Mix Design

Each of the 22 mixes designed for the experiment were done so on a volumetric basis. Demonstration of the entire mix design process for a single mix will be shown in a step by step calculation for mix F5C. This mix incorporates both rubber and fibers into conventional concrete. From the preliminary mixes, it was determined that a 0.4 water cement ratio would be used. Based on the desired compressive strength, 750 pounds per cubic yard of cement was used.

Step 1: Cement

$$Cement\ (lbs/yd^3) = 750$$

$$Cement\ (ft^3/yd^3) = (lbs/yd^3) \div (specific\ gravity\ of\ cement \times density\ of\ water\ lbs/ft^3)$$

$$Cement\ (ft^3/yd^3) = (750\ lbs/yd^3) \div (3.15 \times 62.4\ lbs/ft^3)$$

$$Cement\ (ft^3/yd^3) = 3.82$$

Step 2: Water

$$Water\ (lbs/yd^3) = (w:c) \times (cement\ lbs/yd^3)$$

$$Water\ (lbs/yd^3) = (0.4) \times (750\ \ lbs/yd^3)$$

$$Water\ (lbs/yd^3) = 300$$

$$Water\ (ft^3/yd^3) = (lbs/yd^3) \div (density\ of\ water\ lbs/ft^3)$$

$$Water\ (ft^3/yd^3) = (300\ lbs/yd^3) \div (62.4\ lbs/ft^3)$$

$$Water\ (ft^3/yd^3) = 4.81$$

Step 3: Air

All mixes were designed with 1 percent air by volume. This is not designed as an air entrained mix, but all concrete will naturally have some volume of air which should be accounted for.

$$Air\ (ft^3/yd^3) = (1\%) \times (27\ ft^3/yd^3)$$

$$Air(ft^3/yd^3) = \ 0.27$$

Step 4: Sand and Limestone

$$Sand + Limestone\ (ft^3/yd^3) = (27\ ft^3/yd^3) - [Cement\ +\ Water\ +\ Air](ft^3/yd^3)$$

$$Sand + Limestone\ (ft^3/yd^3) = 27 - 3.82 - 4.81 - 0.27$$

$$Sand + Limestone\ (ft^3/yd^3) = 18.1$$

At this point, the volume of sand and the volume of limestone will be made equal.

$$Sand(ft^3/yd^3) = Limestone\ (ft^3/yd^3) = (Sand + Limestone\ (ft^3/yd^3))/2$$

$$Sand(ft^3/yd^3) = Limestone\ (ft^3/yd^3) = 18.1/2$$

$$Sand(ft^3/yd^3) = Limestone\ (ft^3/yd^3) = 9.05$$

Up to this point each of the 22 mixes are designed exactly the same.

Step 5: Rubber

Based on literature reviewed, the fine rubber will replace the fine aggregate (sand) and the coarse rubber will replace the coarse aggregate (limestone). In this sample calculation, 5 percent coarse rubber is replacing 5 percent of the total coarse aggregate volume in the mix. Since it is coarse rubber, 5 percent by volume of limestone will be removed from the mix.

$$Coarse\ Rubber\ (ft^3/yd^3) = \left(Sand + Limestone\ (ft^3/yd^3)\right) \times (rubber\ replacement\ \%)$$

$$Coarse\ Rubber\ (ft^3/yd^3) = 18.1 \times 5\%$$

$$Coarse\ Rubber\ (ft^3/yd^3) = 0.905$$

Step 6: Adjusted Limestone and/or Sand

Once the volume of rubber is determined, that volume must be subtracted from either the limestone if it is coarse rubber, the sand if it is fine rubber, or the limestone and sand if it is a combination of coarse and fine rubber. For this sample calculation, coarse rubber is being used so the volume of coarse rubber will subtracted from the previously calculated volume of limestone.

$$Adjusted\ Limestone\ (ft^3/yd^3) = \ Limestone\ (ft^3/yd^3) - \ Coarse\ Rubber\ (ft^3/yd^3)$$

$$Adjusted\ Limestone\ (ft^3/yd^3) = 9.05 - 0.905$$

$$Adjusted\ Limestone\ (ft^3/yd^3) = 8.15$$

Step 7: Convert units to Pounds per Cubic Foot

$$(lbs/ft^3) = (ft^3/yd^3) \times (specific\ gravity \times density\ of\ water\ (lbs/ft^3) \times\ (1\,yd^3/27\ ft^3)$$

$$Cement\ (lbs/ft^3) = 3.82 \times 3.15 \times 62.4 \times (1/27) = 27.8$$

$$Water\ (lbs/ft^3) = 4.81 \times 1 \times 62.4 \times (1/27) = 11.1$$

$$Sand\ (lbs/ft^3) = 9.05 \times 2.60 \times 62.4 \times (1/27) = 54.38$$

$$Coarse\ Rubber\ (lbs/ft^3) = 0.905 \times 1.05 \times 62.4 \times (1/27) = 2.2$$

$$Adjusted\ Limestone\ (lbs/ft^3) = 8.15 \times 2.61 \times 62.4 \times (1/27) = 49.16$$

Step 8: Absorption Water

Before each of the mixes were performed, the moisture content of the sand and limestone was determined so that the appropriate absorption water could be calculated and added or subtracted as needed. For mix F5C, the moisture contents were 1.84 percent and 0.29 percent for the sand and limestone, respectively.

$$for\ Sand = ((Absorption\ Value\ \%) - (Moisture\ Content\ \%)) \times\ Sand\ (lbs/ft^3)$$

$$Absorption\ for\ Sand\ (lbs/ft^3) = (0.73\% - 1.84\%) \times 54.4$$

$$Absorption\ for\ Sand\ (lbs/ft^3) = -0.60$$

$$for\ Limestone$$

$$= ((Absorption\ Value\ \%) - (Moisture\ Content\ \%))$$

$$\times\ Limestone\ (lbs/ft^3)$$

$$Absorption\ for\ Limestone\ (lbs/ft^3) = (1.27\% - 0.29\%) \times 49.2$$

$$Absorption\ for\ Limestone\ (lbs/ft^3) = 0.48$$

$$Total\ Absorption\ Water\ (lbs/ft^3)$$

$$= Absorption\ for\ Sand\ +\ Absorption\ for\ Limestone$$

$$Total\ Absorption\ Water\ (lbs/ft^3) = -0.60 + 0.48$$

$$Total\ Absorption\ Water\ (lbs/ft^3) = -0.12$$

The negative sign is due to the sand being saturated beyond its absorption value. For the cases in which the total absorption water yielded a negative value, this amount of water was taken out of the mix water calculated in Step 2.

Step 9: Fibers

For those mixes that contained fibers, the fibers were incorporated based upon the total volume of the mix. All fiber mixes contained 1 percent fibers.

$$Fibers\ (lbs/ft^3)$$

$$= (1\%) \times (specific\ gravity\ of\ fibers) \times (density\ of\ water(lbs/ft^3))$$

$$Fibers\ (lbs/ft^3) = (1\%) \times 7.8 \times 62.4$$

$$Fibers\ (lbs/ft^3) = 4.87$$

Step 10: Predicted Unit Weight

$$Total\ Volume\ (ft^3) = 1\ ft^3 + 1\%\ fibers\ by\ volume$$

$$Total\ Volume\ (ft^3) = 1\ ft^3 + 0.01 ft^3$$

$$Total\ Volume\ (ft^3) = 1.01$$

$$Constituents\ = Cement + Water + Sand + Rubber + Limestone +$$

$$Absorption\ Water + Fibers$$

$$Constituents\ (lbs/ft^3) = 27.8 + 11.1 + 54.38 + 2.2 + 49.16 - 0.12 + 4.87 = 149.39$$

$$Predicted\ Unit\ Weight\ (lbs/ft^3)$$

$$= \left(Constituents\ (lbs/ft^3) \div Total\ Volume\ (lbs/ft^3)\right) \times 1\ ft^3$$

$$Predicted\ Unit\ Weight\ (lbs/ft^3) = (149.39/1.01) \times 1\ ft^3$$

$$Predicted\ Unit\ Weight\ (lbs/ft^3) = 148$$

All of the calculations shown above were carried out using Microsoft Excel. A summary of mix design results including the pounds per cubic foot of each constituent and the predicted unit weight for each mix can be found in Table 5.

Table 5. Constituents of Mixes

Constituents of Mixes in lbs/cuft											
Mix #	Name	Cement	Water	Sand	Limestone	Coarse Rubber	Fine Rubber	Fibers	Absorption Water	Water Reducer (oz per 100lbs cement)	Predicted Unit Weight
1	PL1	27.78	11.11	54.46	54.71	0.00	0.00	0.00	-0.83	3.0	147.22
2	PL2	27.78	11.11	54.46	54.71	0.00	0.00	0.00	0.28	1.5	148.33
3	F1	27.78	11.11	54.46	54.71	0.00	0.00	4.87	0.28	3.0	151.68
4	F2	27.78	11.11	54.46	54.71	0.00	0.00	4.87	0.32	3.0	151.73
5	F5C	27.78	11.11	54.46	49.24	2.20	0.00	4.87	-0.13	2.0	148.04
6	F5F	27.78	11.11	49.01	54.71	0.00	2.20	4.87	-0.39	2.0	147.80
7	F5CF	27.78	11.11	51.73	51.98	1.10	1.10	4.87	0.06	2.0	148.25
8	F10C	27.78	11.11	54.46	43.77	4.39	0.00	4.87	-0.02	2.0	144.91
9	F10F	27.78	11.11	43.57	54.71	0.00	4.39	4.87	-0.23	3.0	144.75
10	F10CF	27.78	11.11	49.01	49.24	2.20	2.20	4.87	0.06	2.5	145.02
11	F15C	27.78	11.11	54.46	38.30	6.59	0.00	4.87	-0.12	2.0	141.57
12	F15F	27.78	11.11	38.12	54.71	0.00	6.59	4.87	-0.33	5.0	141.44
13	F15CF	27.78	11.11	46.29	46.51	3.30	3.30	4.87	0.24	5.0	141.96
14	5C	27.78	11.11	54.46	49.24	2.20	0.00	0.00	-0.89	5.0	143.90
15	5F	27.78	11.11	49.01	54.71	0.00	2.20	0.00	-0.34	5.0	144.47
16	5CF	27.78	11.11	51.73	51.98	1.10	1.10	0.00	-0.04	4.0	144.76
17	10C	27.78	11.11	54.46	43.77	4.39	0.00	0.00	0.02	4.0	141.53
18	10F	27.78	11.11	43.57	54.71	0.00	4.39	0.00	-0.22	4.5	141.34
19	10CF	27.78	11.11	49.01	49.24	2.20	2.20	0.00	0.16	5.0	141.70
20	15C	27.78	11.11	54.46	38.30	6.59	0.00	0.00	0.05	6.0	138.29
21	15F	27.78	11.11	38.12	54.71	0.00	3.30	0.00	0.10	5.5	138.41
22	15CF	27.78	11.11	46.29	46.51	3.30	3.30	0.00	0.38	4.5	138.66

*For negative absorption water values, the amount should be taken out from the mix water.

3.6 Flexure Beam Design

The initial thoughts and considerations made for the design of the flexure beam intended to ensure that the section would fail due to flexure rather than shear without the use of stirrups in the beam and accounting for the variability of compressive strengths between mixes. The compressive strengths of the 22 mixes vary due to the variation in rubber and fiber content. The size and amount of rebar in the beam was selected to ensure that the steel would yield under flexural loading so that a ductile, tension controlled failure would occur.

The test frame that was used had the capability to perform a 4 point bending test on a specimen with a 48 in. span between supports. The beam was made 54 in. long so that 3 in.

of the beam would overhang the supports at each end. The two applied point loads (P/2) were located 4 in. on either side of the center of the beam. This created an 8 in. region over which a constant moment would exist. Figure 3 shows a schematic of the flexure beam.

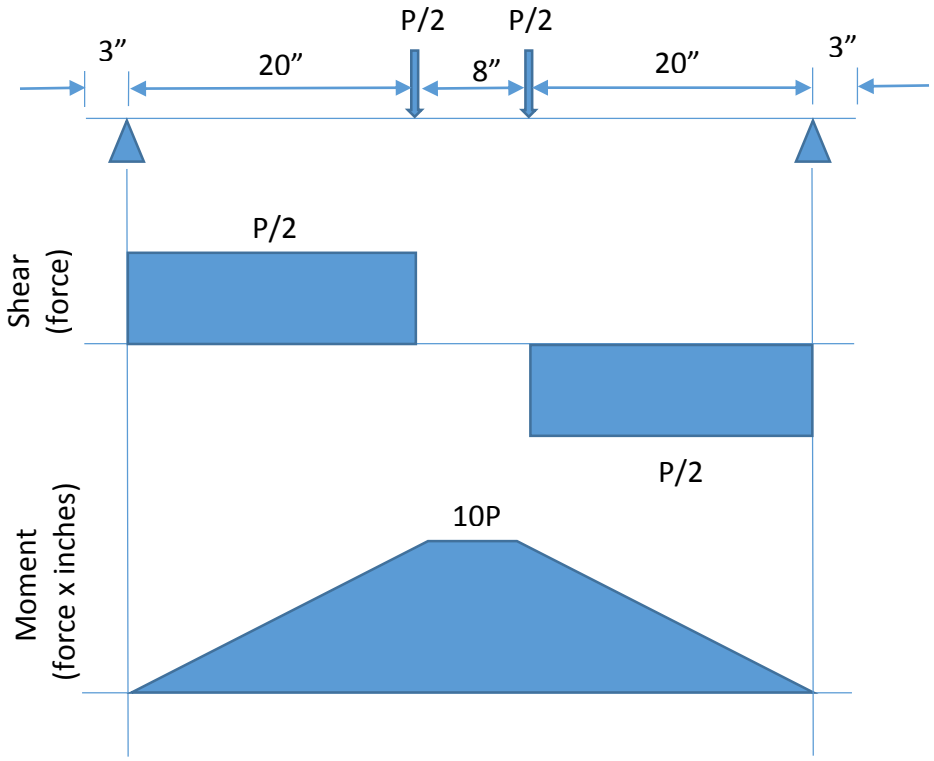

Figure 3. Shear and moment diagram for flexure beam

As seen in the shear and moment diagrams in Figure 3 above, the maximum shear force in the beam specimen will be the total load applied divided by two and the maximum moment applied will be ten times the total load applied.

Before designing the cross section, several ACI code requirements were considered. ACI 318-11 (ACI 2011) chapter 7.7.1 states that the concrete cover for non-prestressed reinforcement in cast in place concrete not exposed to weather or in contact with the ground should be ¾ in for No. 11 bars and smaller. ACI 318-11 chapter 7.6.1 states that the

minimum spacing between parallel bars in the same layer shall be equal to the diameter of the bar but not less than 1 inch (ACI 2011).

The beam cross section selected was 4 in. by 8 in. with 2 No. 4 rebar to ensure a flexural failure. The beam was chosen to be at least 4 in. deep so that the compression region at the top of the beam was sufficiently large enough to visualize. Figure 4 shows the cross section.

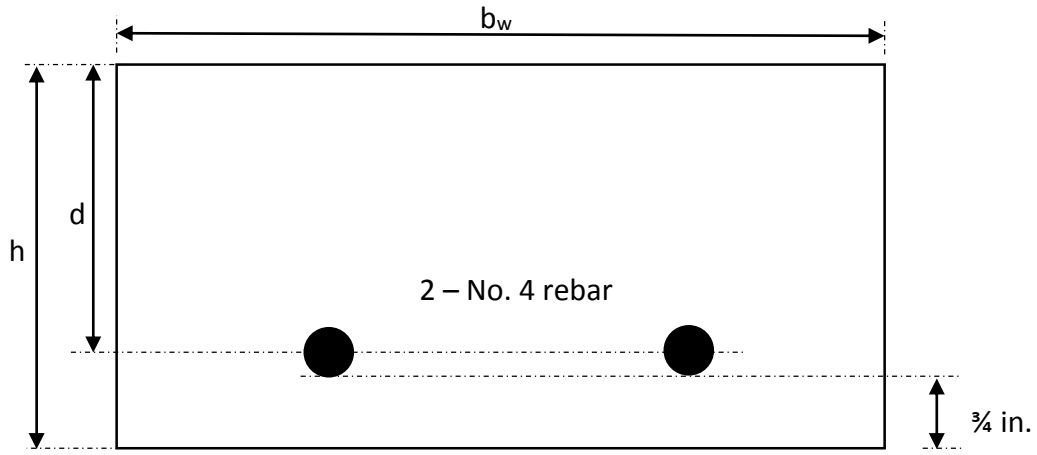

Figure 4. Cross-section of flexure beam

Table 6 shows the calculations for checking shear and flexure for a various range of compressive strengths for the cross section selected. The lowest compressive strength checked was 4500 psi because this is the lowest anticipated 28-day compressive strength out of the 22 different mixes.

Table 6. Shear capacity of the flexure beams for different concrete strengths

4" Height x 8" Width										
d (in)	b_w (in)	f'_c (psi)	β_1	A_s(2-#4's) (in2)	a (in)	c (in)	M (k-in)	P (kips)	Max Shear in Beam (kips)	Vc (kips)
3	8	4500	0.85	0.4	0.78	0.92	62.59	6.26	3.13	3.22
3	8	5000	0.8	0.4	0.71	0.88	63.53	6.35	3.18	3.39
3	8	5500	0.775	0.4	0.64	0.83	64.30	6.43	3.21	3.56
3	8	6000	0.75	0.4	0.59	0.78	64.94	6.49	3.25	3.72
3	8	6500	0.725	0.4	0.54	0.75	65.48	6.55	3.27	3.87
3	8	7000	0.7	0.4	0.50	0.72	65.95	6.59	3.30	4.02
3	8	7500	0.675	0.4	0.47	0.70	66.35	6.64	3.32	4.16
3	8	8000	0.65	0.4	0.44	0.68	66.71	6.67	3.34	4.29
3	8	8500	0.625	0.4	0.42	0.66	67.02	6.70	3.35	4.43
3	8	9000	0.6	0.4	0.39	0.65	67.29	6.73	3.36	4.55
3	8	9500	0.85	0.4	0.37	0.44	67.54	6.75	3.38	4.68
3	8	10000	0.55	0.4	0.35	0.64	67.76	6.78	3.39	4.80
3	8	10500	0.85	0.4	0.34	0.40	67.97	6.80	3.40	4.92

As shown in Table 6, the maximum available shear strength provided by the concrete (V_c) is greater than the maximum shear developed in the beam due to the applied load (P). Therefore, the beam should not fail in shear and should instead fail in flexure at a moment (M) equal to 10P. Additionally, the term $2\sqrt{f'_c}b_w d$ used in calculations is a considered a lower bound or conservative.

In order to ensure that the beam failed in flexure before the steel reinforcement pulled out of the concrete, the required development length was checked. Formulas (12-1) and (12-2) from ACI 318-11 chapter 12.2 were used to calculate the required development length for the lowest and highest anticipated compressive strengths (ACI 2011). All of the required development lengths for the No. 4 rebar were less than the 23 in. of available development length in the beam. Therefore, development length was satisfied.

3.7 Formwork

The forms for the flexure beam are shown in Figure 5(b). The beam forms were made from 2 in. x 4 in. lumber and ¾ in. ply form. The dimensions of pieces of the beam form are as follows:

1 – 55 ½" x 16 ½" of ¾" Ply form for base
2 – 54" x 4" of ¾" Ply form for sides
2 – 54" of 2" x 4" lumber for sides
4 – 2" of 2" x 4" lumber for sides (studs)
2 – 16 ½" x 4" ¾" Ply form for ends

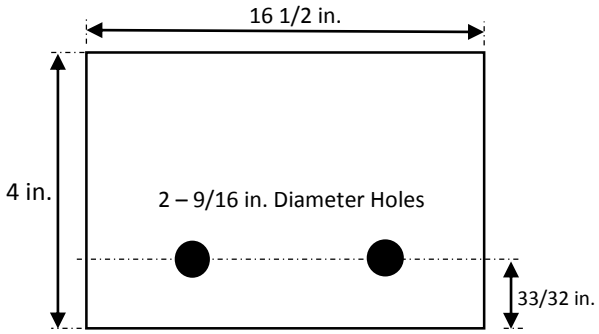

(a)

(b)

Figure 5. (a) End piece on flexure beam formwork and (b) Flexure beam formwork

The two 9/16 in. diameter holes shown in Figure 5(a) were drilled on the end pieces so that the rebar could slide through and be supported by the end pieces. Though the rebar size is ½ in., the holes were cut a 1/16 in. bigger in order to easily slide the rebar through. The rebar used to reinforce the concrete beams was aquired from a local distributor. A tensile test was performed on the rebar in order to determine the stress strain relationship needed for the strain compatibiltiy analysis. The stress strain curve of the steel rebar is shown in Appendix B.

3.8 Mix Procedure

The mix procedure for each of the 22 mixes is as follows. First, the sand and limestone were put into the mixer. The mixer used for this experiment is shown in Figure 6. The limestone and sand were mixed for 2 minutes. At this time, the cement and water was added and mixed for an additional 4 minutes. After 6 minutes of total mixing time, water reducer was added.

Figure 6. Concrete mixer

Variation between mixes with and without fibers exist after 8 minutes of mixing. For mixes containing fibers, the fibers were sprinkled in after 8 minutes of mixing time while the mixer continued mixing. After 16 minutes of total mixing time, the rubber was sprinkled in while the mixer continued mixing. For rubber mixes without fibers, after 8 minutes of mixing time the rubber particles were sprinkled in while the mixer continued mixing. For mixes with rubber and fibers, mixing was continued for an additional 4 minutes after the rubber was added. Thus, the total mixing time for a mix containing fibers was about 20 minutes while a mix without fibers had a mixing time of about 12 minutes. All of these times were plus or minus 1 minute depending on the consistency of the mixture observed during mixing.

The water reducer added to each mix varied depending on the amount and type of rubber and whether the mix contained fibers. The amount of water reducer for each mix, shown in Table 7, was estimated based on preliminary mixes and on an understanding of how rubber and fibers would affect the mix. The desired workability after all the constituents were added was a slump value between 4 in. and 6 in. Due to the fact that the water reducer was added before the addition of fibers and rubber, it was important to achieve a workability much higher than the goal and have an understanding of how much it would decrease when the fibers and rubber were added so that the final workability would be in the desired range.

Table 7. Amount of water reducer (Superplasticizer) added to each mix

Water Reducer (oz/100 lbs cement)			
Mix	Water Reducer	Mix	Water Reducer
PL1	3	F1	5
5C	1.5	F5C	5
5F	3	F5F	5
5CF	3	F5CF	5
10C	2	F10C	4
10F	2	F10F	4
10CF	2	F10CF	4.5
15C	2	F15C	5
15F	3	F15F	6
15CF	2.5	F15CF	5.5
PL2	2	F2	4.5

During the preliminary mixes, it was noticed that adding the rubber after all the other constituents are added, including the water reducer, decreased the amount of air entrapped by the rubber particles in the concrete mixture. Air voids in the hardened concrete mixture makes the concrete weaker, which is not desired. Therefore, rubber was the last constituent to be added during the mixing process.

3.9 Specimen Casting

3.9.1 Cylinders

For each of the 22 mixes, 24 – 4 in. x 8 in. cylinders were cast per ASTM C192 (ASTM 2014). To begin, the cylinders were filled half way then tamped 25 times, and tapped for consolidation 3 times on each quarter point of the cylinder. Then the cylinders were filled to the top and the process of tamping and tapping was repeated. The cylinders were finished with a tamping rod by sliding the rod horizontally back and forth across the top of the cylinders to create a smooth finish. Figure 7 shows a set of fresh concrete cylinders immediately after placement.

Figure 7. Fresh concrete cylinders

3.9.2 Beams

For each of the 22 mixes, 1 flexure beam was cast. The beams were cast in two layers and vibrated. The first layer was placed, then a vibrator was used to consolidate the concrete in the forms. Then the second layer was placed and again vibrated. The beams were finished with a trowel and hooks were placed in the ends of the beams for ease of moving the beams once the concrete hardened. A finished beam is shown in Figure 8(a) and hooks used in the beam ends are shown in Figure 8(b).

(a) (b)

Figure 8. (a) Finished flexure beam and (b) Hooks placed in beam ends

3.10 Fresh Concrete Tests

3.10.1 Slump

The workability of the concrete was measured by performing a slump test per ASTM C143 (ASTM 2012c). The slump cone was attached to the base plate, and the cone was filled with fresh concrete by thirds of its volume. After each third was filled, the concrete was tamped 25 times. Once the cone was filled, the excess concrete protruding from the top of the cone was scraped off. The latches holding the slump cone to the base plate were removed while downward force was applied to the slump cone to ensure the cone did not move. Then the slump cone was slowly raised off of the base plate allowing the cone of fresh concrete to stand alone. The handle attached to the base plate was raised to a vertical position over the fresh cone of concrete. The distance from the bottom of the handle to the top of the center of the concrete on the base plate was recorded as the slump value for that concrete mix. This is shown in Figure 9.

Figure 9. Slump test

3.10.2 Unit Weight

The unit weight of the fresh concrete was obtained by using a calibrated cast iron container, shown in Figure 10, which had a volume of one-tenth of a cubic foot. The container was filled in three layers, or three equal volumes similar to the process for filling the slump cone. After each layer, the concrete was tamped 25 times and the container was tapped 3 times on each of its quarter points around the container using a rubber mallet. Once the third layer was placed, tamped, and tapped, the excess concrete was removed from the top of the container using a striking plate. The container was weighed on a digital scale. The weight of the empty container was subtracted from the weight of the container with the fresh concrete in it. The resulting weight is the weight of one-tenth a cubic foot of the fresh concrete. Thus, to obtain the unit weight of the fresh concrete, the weight obtained should be multiplied by a factor of 10. This process was used to calculate the unit weight for each of the 22 mixes.

Figure 10. Unit weight container filled with fresh concrete

3.10.3 Air Content

The amount of air trapped in the fresh concrete was measured by a percentage by volume of concrete. ASTM Standard C231/C231M was followed (ASTM 2010a). The device, shown in Figure 11, consisted of a container and a lid. The container had a volume of 0.25 cubic feet. The lid, when placed on the container, created an air and water tight seal and was equipped with valves to allow compressed air into the volume of fresh concrete. To begin the process, the container was first filled with fresh concrete. The process of filling, tamping, and tapping the concrete in the container is the same as the unit weight test. Once the container was filled and the excess scrapped off, the rim of the container was carefully cleaned to ensure that the lid would create a good seal when placed on the container. The lid was placed on the container and clamped down to create the seal. Small red valves on either side of the lid were opened, and using a water dropper, water was forced carefully into the open valves until it exited through the valve on the opposite side of the lid. Adding the water at this point filled all the voids between the top of the fresh concrete in the container and the lid. These air voids must be removed since the air trapped in the space is not air trapped inside of the concrete. A small cylindrical air pump attached to the lid was pressurized by

hand-pumping the cylinder with the attached ram rod. The valves were then closed. Once pressurized to the calibrated value required by the device, the air was injected into the fresh concrete in the container via the red valve located on top of the cylindrical pump. The value that the needle on the gauge pointed to after the air was injected into the concrete was recorded as the percentage of air trapped in the fresh concrete. The concrete in the container was then discarded since the water cement ratio was altered when the water was added to it.

Figure 11. Air content test setup

3.11 Moist Curing

All test specimens were moist-cured for 28-days. About two hours after the fresh concrete was placed, wet burlap was placed on top of all the concrete specimens, then covered with visqueen to prevent moisture loss. The burlap was wet continuously for the 28 days of curing. The specimens were stored in a laboratory where room temperature was slightly affected by outside temperature changes. After 28 days of curing, the specimens were removed from beneath the wet burlap and stored in the laboratory to await testing. In order to remain consistent, all cylinders and beams were removed from their molds and forms three days after casting.

3.12 Hardened Concrete Tests

3.12.1 Compression Tests

Compression tests on the 4 x 8 cylinders were performed per ASTM C873 (ASTM 2010b) using an ELE International testing machine as shown in Figure 12(a). Neoprene pads were inserted into the cylinder caps to ensure even loading across the cylinder surface. The caps were placed on the cylinder specimen to be tested and the capped cylinder was placed in the compression machine as shown in Figure 12(b). Using the machine, a constant load rate of 35 psi/sec (440 lbs/sec for the 4 x 8 cylinders) was applied to the cylinder until failure. The digital monitor displayed the failure load and failure stress for the specimen.

For each of the 22 mixes conducted, 3 cylinders were tested in compression on 1, 4, 7, 14, and 56 days. On the 28th after casting each mix, 6 cylinders were tested in compression. A total of 462 cylinders were tested in compression for this research experiment. The neoprene pads were changed after every 25 tests since the pads tend to break down and inconsistency among failures is noticed beyond this amount.

(a)

(b)

Figure 12. (a) ELE International test machine and (b) Compression test on cylinder

3.12.2 Split Tensile Tests

Split tensile tests were performed per ASTM C496 (ASTM 2011b) on 4 x 8 cylinders using the same testing machine that was used for compression testing. The cylinder to be tested was placed in the testing device shown in Figure 13(a & b). To ensure consistent bearing conditions on the top and bottom of the device, small wood strips were placed between the cylinder and the steel as shown in Figure 13(a & b). With the cylinder and the test device in the testing machine, a constant load rate of 110 lbs/sec was applied to the cylinder until the first crack appeared. The digital monitor displayed the failure load which was later used to calculate the failure stress.

The split tensile test was performed on 3 cylinders from each of the 22 mixes. A total of 66 split tensile tests were performed for this research project. The wooden strips used to create improved bearing and load distribution between the cylinder and the iron device were discarded after each test. This provided consistency between each test since the wood strips deformed under loading.

(a) (b)

Figure 13. (a & b) Spilt tensile test setup

3.12.3 Modulus Tests

The modulus tests were conducted in the same test machine as the compression and tension tests. To begin, the modulus ring, shown in Figure 14, was placed around the cylinder. Screws attached to the modulus ring that secure the ring onto the cylinder were hand-tightened. Then the caps with the neoprene pads were placed on the ends of the cylinder. The cylinder with the pads and modulus ring were placed in the test machine. Before applying any load, the digital gauge on the modulus ring was zeroed. Load was applied to the cylinder at a rate of 35 psi/sec (440 lbs/sec). At every 5000 lbs up to 40 percent of f'_c the displacement given by the digital gauge on the modulus ring was recorded. For example, if 40 percent of f'_c was determined to be 36,000 pounds. The displacement was recorded at increments of 5000 lbs up to 35,000 lbs. This displacement will later be used to calculate the strain and ultimately plotted against the stress to obtain the modulus.

Since concrete typically exhibits linear behavior up to 40 percent of f'_c, $0.4*f'_c$ was the maximum stress the cylinders would be loaded to during the modulus tests. As mentioned previously, there were 6 cylinders set aside to be tested in compression on 28 days. Of the 6 cylinders, 3 were tested in compression prior to the modulus tests. Forty percent of the average stress of these 3 cylinders was used as the upper limit for the modulus tests. The modulus test was conducted on 3 cylinders from each of the 22 mixes. A total of 66 modulus tests were performed for this research project.

Figure 14. Modulus test setup

3.12.4 Flexure Tests

The four point bending tests on the beam specimens were conducted on an MTS uniaxial load frame. The flexure test frame in the machine consisted of two wide flange sections stiffened with web stiffeners. From each wide flange, there was a welded rod to which the grips on the MTS could tightly clamp and hold the wide flange sections in place. Thick steel cylindrical tubing was used as roller supports on either end of the concrete beam specimens as shown in Figure 15(a). The rollers were placed 24 in. from either side of the center of the test frame. Two more rollers attached to the top wide flange, as shown in Figure 15(b), were used to create the two applied loadings at the center of the specimens. These rollers were placed 4 in. away from the center of the test frame. The four locations of rollers created the loading condition in which the flexure beams were designed for previously discussed in the flexure beam design section of the methodology.

In order to measure the displacement at mid-span of the beam specimens, a three inch potentiometer was attached to the center of both sides of the test frame as shown in Figure 15. The average movement recorded by the two potentiometers would be taken as the

displacement at mid-span. A potentiometer on either side also provided backup in case one potentiometer malfunctioned during testing.

The load was measured by the force transducer in the MTS machine and sent to a National Instruments machine where the load was recorded at a frequency of 1 Hz. The potentiometers were wired directly to the National Instruments machine where the voltage was converted to a displacement and also recorded at a frequency of 1 Hz.

Load was applied to the test frame and ultimately to the beam specimen at a rate of 0.05 in. per minute. As cracks appeared on the concrete specimens during testing, the load was periodically stopped, usually at increments of 1000 pounds, and cracks were traced with permanent markers to better visualize the crack pattern at various loads.

(a) (b) (c)

Figure 15. (a, b & c) Flexure beam test setup

Chapter 4: Results and Analysis

4.1 Material Properties

Material properties, including slump, air content, unit weight, modulus of elasticity, compressive strength, and tensile strength were determined for each test mix. The material properties determined for each of the 22 mixes performed and tested are shown in Table 8.

Table 8. Results of material properties for each mix

Material Properties							
Mix	Slump (inches)	Air (%)	Unit Weight (lb/ft^3)	Modulus, E (ksi)	f_r (psi)	$f_{c\ 28\ days}$ (psi)	$f_{c\ 56\ days}$ (psi)
PL1	7.75	2.5	147.77	5160	657	8672	9416
5C	6.5	2.4	143.55	4436	517	6112	6670
5F	4.75	3.1	144.19	4939	650	7190	8144
5CF	6.5	2.7	144.29	5202	577	7079	8121
10C	5	2.7	140.72	4353	544	5314	5720
10F	4	3.6	141.16	3884	522	5455	6440
10CF	7.25	2.8	140.88	4126	520	5228	5975
15C	5.5	2.7	136.52	3895	451	4149	4273
15F	6	4.3	136.79	3521	433	3988	4895
15CF	8	2.9	136.70	3858	469	4216	4636
PL2	8.25	2.2	146.90	5278	675	8049	9106
F1	6.5	2.4	150.11	5872	946	10193	11443
F5C	5.75	2.2	147.20	5037	814	7121	8341
F5F	5.5	2.6	147.40	4994	838	7973	9031
F5CF	6	2.3	146.84	5124	765	7279	8450
F10C	5.25	2.3	145.47	4881	674	5814	6293
F10F	3.5	2.8	143.95	4571	611	6353	6974
F10CF	4	2.4	145.15	4636	740	6205	6972
F15C	6.5	1.7	141.12	3932	630	4523	5344
F15F	6.25	2.4	142.82	4045	558	5606	6285
F15CF	7.25	2.2	143.37	4093	596	4377	5616
F2	6.25	2.1	151.07	5501	869	9720	10887

4.1.1 Workability

Slump was measured for each mix in order to ensure that the mix was of a reasonable workability. A reasonable slump value was considered any value of at least 4 inches. Since each mix had varied rubber types and concentrations and some mixes contained fibers while others did not, the workability was determined for each mix. In order to achieve a relatively constant workability between mixes, different amounts of super plasticizer was added based

on need. The initial amount of superplasticizer added for each mix was determined from preliminary mixes and additional superplasticizer was added based upon visual inspection while mixing. If additional superplasticizer was deemed necessary by visual inspection, it was added before the rubber was incorporated into the mix.

4.1.2 Unit Weight

Unit weight values were plotted against percentage of rubber in mix and were separated based upon type of rubber; fine, coarse, and coarse and fine. The unit weight values, given in Table 9, for mixes without fibers and mixes with fibers are plotted in Figures 16 and 17, respectively. It can be seen from the plots that unit weight decreased with increasing percentage of rubber replacement in both mixes with fibers and mixes without fibers. The fact that the unit weight of concrete decreases with the addition of rubber agrees with the literature reviewed. When replacing mineral aggregates such as sand and limestone with less dense rubber particles, it is expected that the unit weight will decrease. In the same fashion, adding dense fiber particles to a mix without taking anything out should result in an overall heavier unit weight. This is evident when comparing the unit weight of mixes which do not contain fibers to mixes which do when both contain the same amount and type of rubber particles.

Overall, the unit weight increased an average of 2.96 percent with the addition of 1 percent fibers by volume to the mix. As shown by the figures below, the decrease in unit weight with increasing percentages of rubber is nearly linear since the R^2 values are almost equal to 1. The decrease in unit weight from 0 to 15 percent addition of fine, coarse, and fine and coarse rubber for mixes without fibers is 7.16, 7.34, and 7.22 percent, respectively. The

decrease in unit weight from 0 to 15 percent addition of fine, coarse, and fine and coarse rubber for mixes with fibers is 5.16, 6.29, and 4.79 percent, respectively.

Table 9. Unit weight of mixes

Unit Weight (lb/ft^3)						
Rubber %	Without fibers			With fibers		
	Fine Rubber	Fine & Coarse Rubber	Coarse Rubber	Fine Rubber	Fine & Coarse Rubber	Coarse Rubber
0	147.34*	147.34*	147.34*	150.59**	150.59**	150.59**
5	144.19	144.29	143.55	147.40	146.84	147.20
10	141.16	140.88	140.72	143.95	145.15	145.47
15	136.79	136.70	136.52	142.82	143.37	141.12

*Average of PL1 and PL2

**Average of F1 and F2

1 lb/ft^3 = 16.018463 kg/m^3

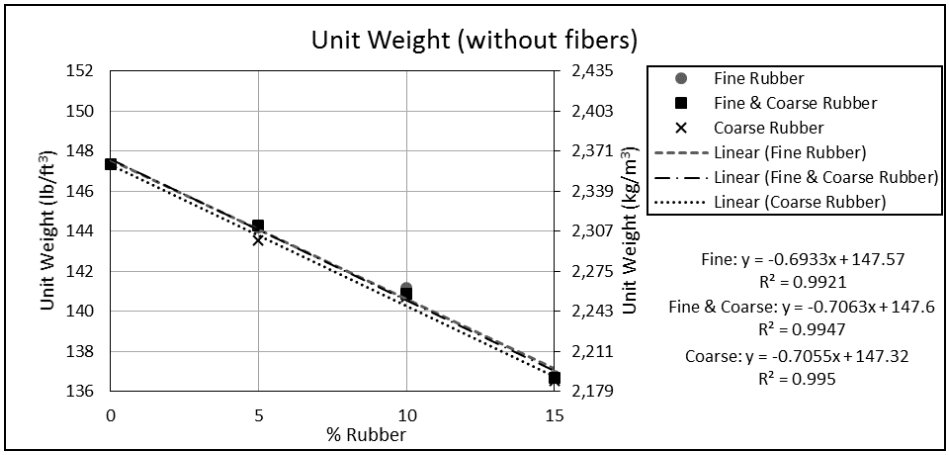

Figure 16. Unit weight of mixes without fibers

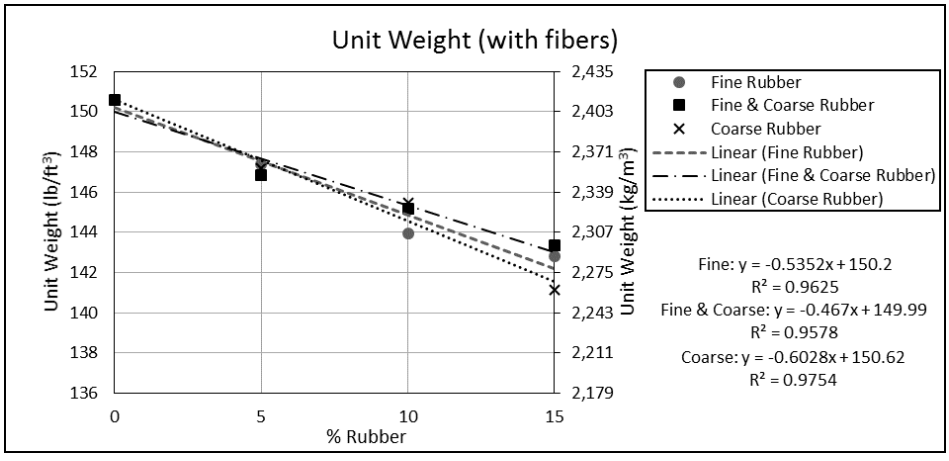

Figure 17. Unit weight of mixes with fibers

As shown in Table 10 and Figure 18, the predicted unit weights of the fresh concrete were very similar to the actual unit weight determined during the casting process. The actual unit weight for mixes without fibers was 0.59% less than the predicted unit weight values. The actual unit weight for mixes with fibers was 0.15% less than the predicted unit weight values.

Table 10. Predicted unit weight vs. actual unit weight

Predicted Unit Weight vs. Actual Unit Weight							
Mix	Without fibers			Mix	With fibers		
	Predicted (lb/ft^3)	Actual (lb/ft^3)	Actual / Predicted		Predicted (lb/ft^3)	Actual (lb/ft^3)	Actual / Predicted
PL1	147.22	147.77	1.0037	F1	151.68	150.11	0.9896
5C	143.90	143.55	0.9976	F5C	148.04	147.20	0.9943
5F	144.47	144.19	0.9981	F5F	147.80	147.40	0.9973
5CF	144.76	144.29	0.9968	F5CF	148.25	146.84	0.9905
10C	141.53	140.72	0.9943	F10C	144.91	145.47	1.0039
10F	141.34	141.16	0.9987	F10F	144.75	143.95	0.9945
10CF	141.70	140.88	0.9942	F10CF	145.02	145.15	1.0009
15C	138.29	136.52	0.9872	F15C	141.57	141.12	0.9969
15F	138.41	136.79	0.9883	F15F	141.44	142.82	1.0098
15CF	138.66	136.70	0.9859	F15CF	141.96	143.37	1.0099
PL2	148.33	146.90	0.9903	F2	151.73	151.07	0.9957
$1\ lb/ft^3 = 16.018463\ kg/m^3$		Average =	0.9941			Average =	0.9985

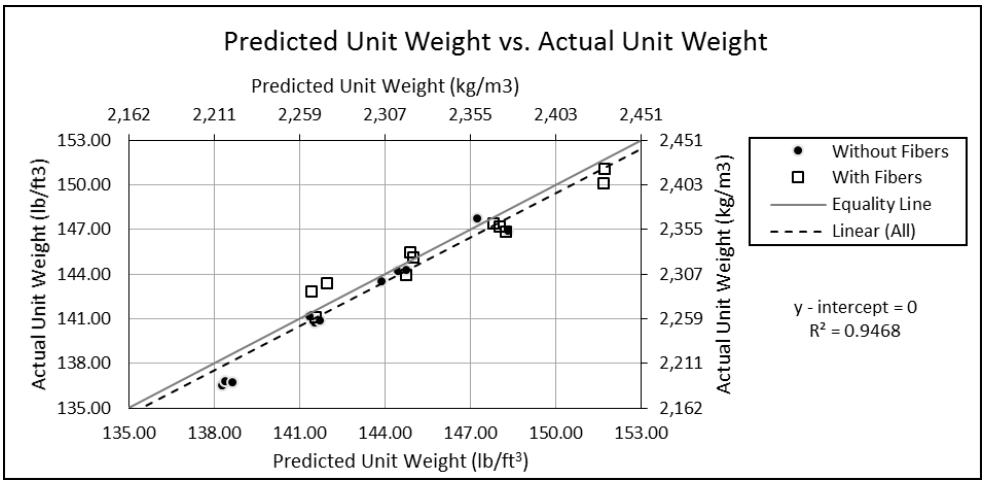

Figure 18. Predicted unit weight vs. actual unit weight

4.1.3 Air Content

The air content values, given in Table 11, for mixes without fibers and mixes with fibers are plotted in Figures 19 and 20, respectively. Past research indicates that the air content tends to increase with the addition of rubber particles. This trend can be seen more prominently in the mixes which do not contain fibers. There is a greater increase in air content with the addition of fine rubber as shown in both Figures 19 and 20. It can be seen that the air content is not greatly affected by the addition of rubber when fibers are present in the mix. This is evidenced by trend line slopes in Figure 20 which are very near zero. The change in air content with increasing percentages of rubber in mixes which do not contain fiber is nearly linear as evidenced by R^2 values greater than 0.85. However, when fibers are added to the mixes, the relationship becomes much more erratic. This could possibly be due to the fact that more water reducer was added to mixes with fibers making the mixes much more fluid.

The increase in air content from 0 to 15 percent addition of fine, coarse, and fine and coarse rubber for mixes without fibers is 83.0, 14.9, and 23.4 percent, respectively. The increase in air content from 0 to 15 percent addition of fine rubber for mixes with fibers is 6.67 percent while the decrease in air content from 0 to 15 percent addition of coarse and coarse and fine rubber is 24.4, and 2.22 percent, respectively.

Table 11. Air Content

Air Content (%)						
Rubber %	Without fibers			With fibers		
	Fine Rubber	Fine & Coarse Rubber	Coarse Rubber	Fine Rubber	Fine & Coarse Rubber	Coarse Rubber
0	2.35*	2.35*	2.35*	2.25**	2.25**	2.25**
5	3.10	2.70	2.40	2.60	2.30	2.20
10	3.60	2.80	2.70	2.80	2.40	2.30
15	4.30	2.90	2.70	2.40	2.20	1.70

*Average of PL1 and PL2

**Average of F1 and F2

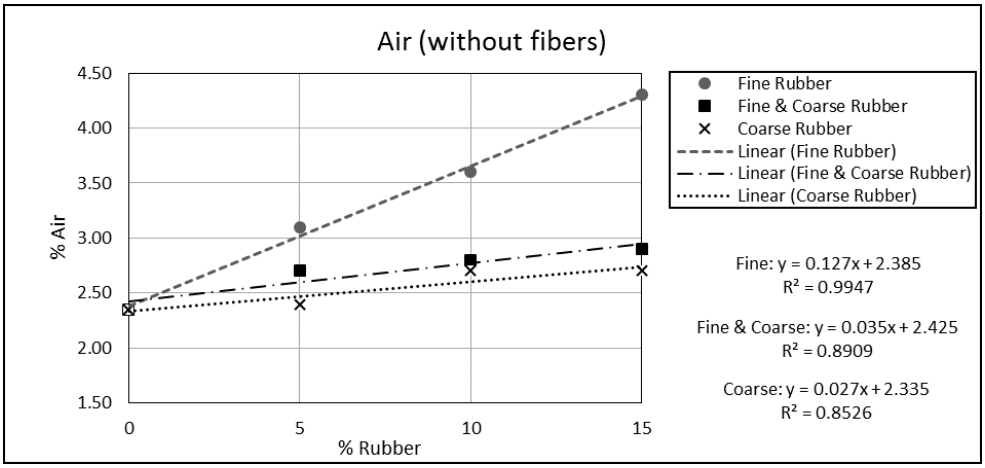

Figure 19. Air content of mixes without fibers

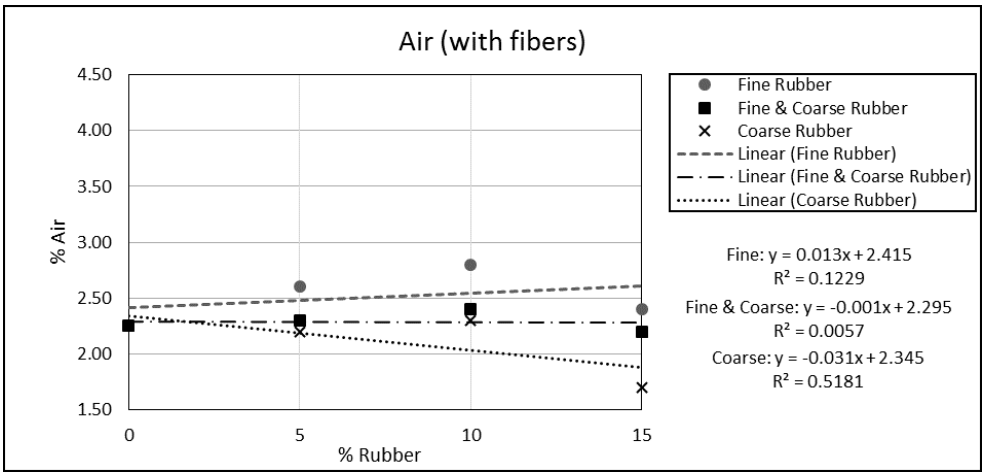

Figure 20. Air content of mixes with fibers

4.1.4 Compressive Strength

The 28-day average compressive strength values, given in Table 12, for mixes without fibers and mixes with fibers are plotted in Figures 21 and 22, respectively. The 56-day average compressive strength values, given in Table 13, are plotted in Figures 23 and 24, respectively. Full strength gain plots for each mix over 56 days can be found in Appendix A. Past research has found that compressive strength decreases with the addition of rubber. This trend is apparent in all four figures.

The decrease in 28-day compressive strength with the addition of rubber was analyzed with respect to rubber particle size. The decrease in compressive strength from 0 to 15 percent addition of fine, coarse, and fine and coarse rubber for mixes without fibers is 52.3, 50.4, and 49.6 percent, respectively. The decrease in 28-day compressive strength from 0 to 15 percent addition of fine, coarse, and fine and coarse rubber for mixes with fibers is 43.7, 54.6, and 56.0 percent, respectively. Though the 28-day compressive strength decreased more in mixes which contained fibers, the 28-day compressive strength value was still greater for mixes which contained fibers when compared to the mixes which did not. The increase in compressive strength due to the addition of fibers agrees with past research.

Table 12. 28-day compressive strength of concrete

f_c 28 days (psi)						
Rubber %	Without fibers			With fibers		
	Fine Rubber	Fine & Coarse Rubber	Coarse Rubber	Fine Rubber	Fine & Coarse Rubber	Coarse Rubber
0	8360*	8360*	8360*	9957**	9957**	9957**
5	7190	7079	6112	7973	7279	7121
10	5455	5228	5314	6353	6205	5814
15	3988	4216	4149	5606	4377	4523

*Average of PL1 and PL2

**Average of F1 and F2

1 MPa = 145.0377 psi

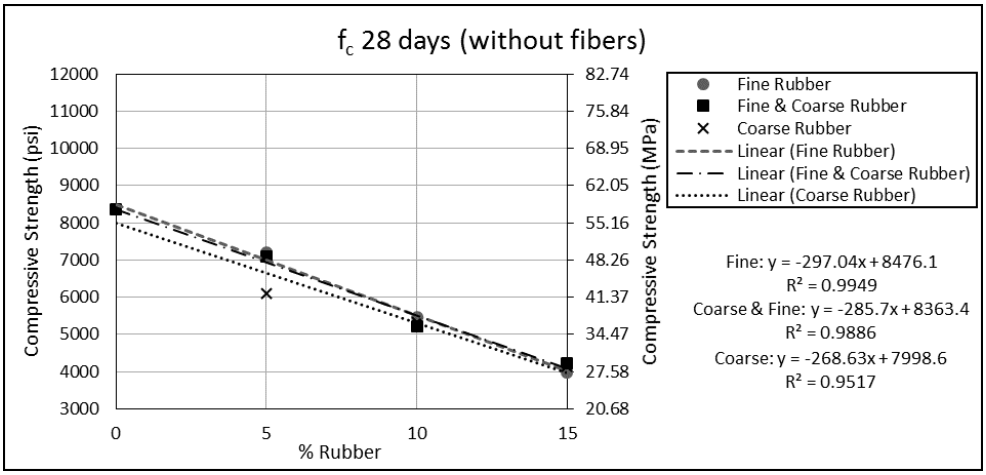

Figure 21. 28-day compressive strength of mixes without fibers

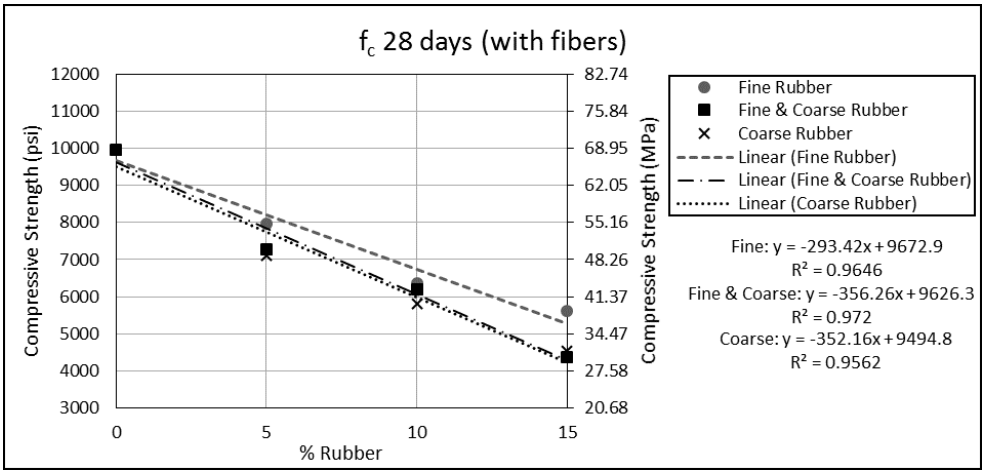

Figure 22. 28-day compressive strength of mixes with fibers

Table 13. 56-day compressive strength of concrete

f_c 56 days (psi)						
Rubber %	Without fibers			With fibers		
	Fine Rubber	Fine & Coarse Rubber	Coarse Rubber	Fine Rubber	Fine & Coarse Rubber	Coarse Rubber
0	9261*	9261*	9261*	11165**	11165**	11165**
5	8144	8121	6670	9031	8450	8341
10	6440	5975	5720	6974	6972	6293
15	4895	4636	4273	6285	5616	5344

*Average of PL1 and PL2

**Average of F1 and F2

1 MPa = 145.0377 psi

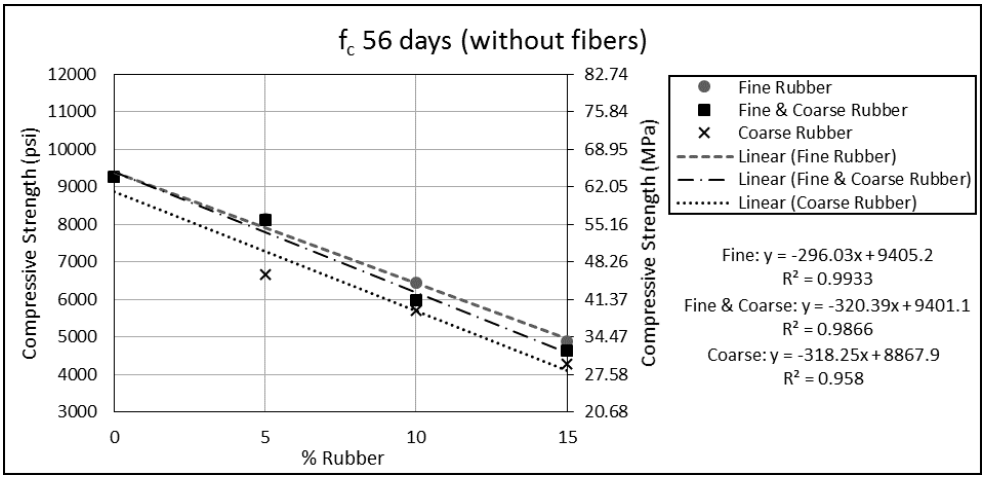

Figure 23. 56-day compressive strength of mixes without fibers

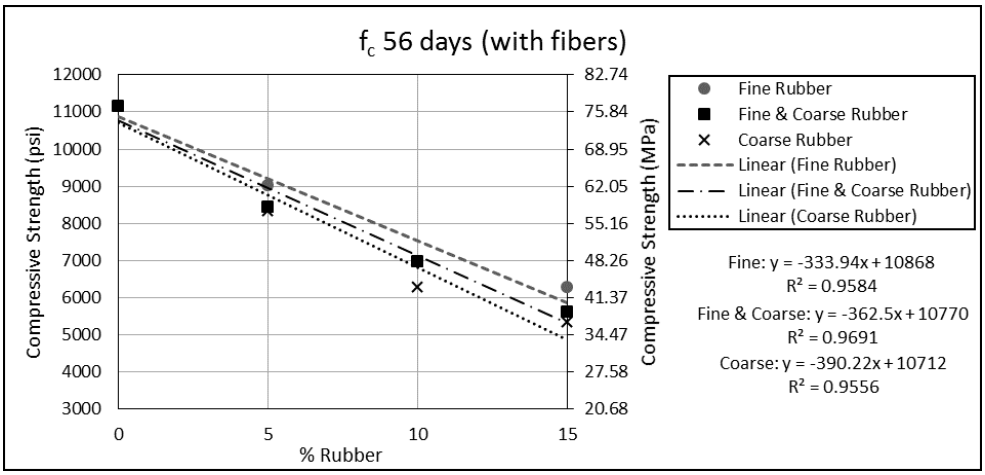

Figure 24. 56-day compressive strength of mixes with fibers

The increase in compressive strength was compared between mixes that contain fibers and mixes that did not contain fibers for both 28-day and 56-day average compressive strength. At 28-days, mixes that contained fibers had a 15.1 percent higher compressive strength compared to those that did not contain fibers. At 56-days, mixes that contained fibers had a 17.3 percent higher compressive strength compared to those that did not contain fibers. This comparison is shown in Table 14 and Figures 25 and 26.

Table 14. Ratio of compressive strength: with and without fibers for 28 and 56 days

Ratio of Compressive Strength Between Mixes With Fibers and Without Fibers for 28 and 56 days							
Mix	Without fibers		Mix	With fibers		$\frac{28w}{28wo}$	$\frac{56w}{56wo}$
	f_c 28 days (psi) *28wo*	f_c 56 days (psi) *56wo*		f_c 28 days (psi) *28w*	f_c 56 days (psi) *56w*		
PL1	8672	9416	F1	10193	11443	1.175	1.215
5C	6112	6670	F5C	7121	8341	1.165	1.250
5F	7190	8144	F5F	7973	9031	1.109	1.109
5CF	7079	8121	F5CF	7279	8450	1.028	1.041
10C	5314	5720	F10C	5814	6293	1.094	1.100
10F	5455	6440	F10F	6353	6974	1.165	1.083
10CF	5228	5975	F10CF	6205	6972	1.187	1.167
15C	4149	4273	F15C	4523	5344	1.090	1.251
15F	3988	4895	F15F	5606	6285	1.406	1.284
15CF	4216	4636	F15CF	4377	5616	1.038	1.211
PL2	8049	9106	F2	9720	10887	1.208	1.196
					Averages:	1.151	1.173

1 MPa = 145.0377 psi

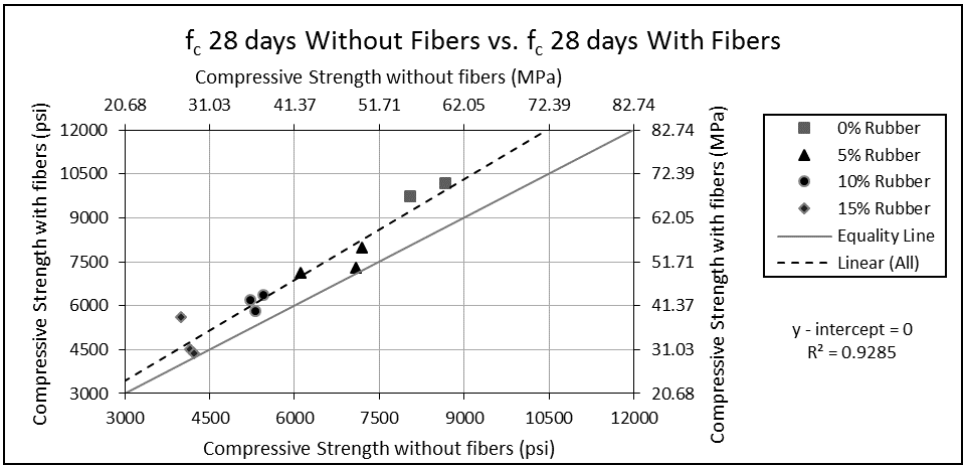

Figure 25. 28-day compressive strength without fibers vs with fibers

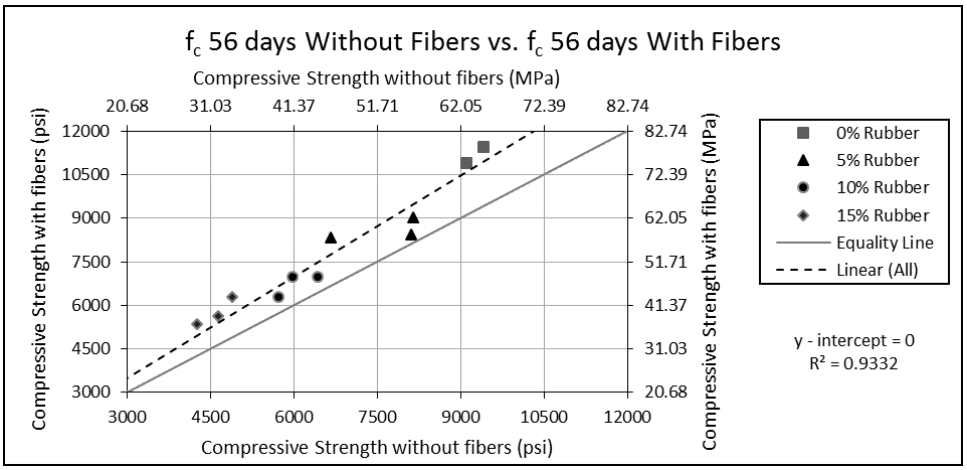

Figure 26. 56-day compressive strength without fibers vs with fibers

Table 15 shows the percent increase in compressive strength between 28-days and 56-days for mixes with and without fibers. The average compressive strength increase from 28-days to 56-days was 12.2 percent for mixes which did not contain fibers and 14.5 percent for mixes which did contian fibers.

Table 15. Increase in compressive strength: with and without fibers for 28-days and 56-days

Percent Increase in Compressive Strength Between 28 days and 56 days for Mixes With and Without Fibers							
Mix	Without fibers			Mix	With fibers		
	f_c 28 days (psi)	f_c 56 days (psi)	Percent Increase		f_c 28 days (psi)	f_c 56 days (psi)	Percent Increase
PL1	8672	9416	8.6%	F1	10193	11443	12.3%
5C	6112	6670	9.1%	F5C	7121	8341	17.1%
5F	7190	8144	13.3%	F5F	7973	9031	13.3%
5CF	7079	8121	14.7%	F5CF	7279	8450	16.1%
10C	5314	5720	7.6%	F10C	5814	6293	8.2%
10F	5455	6440	18.0%	F10F	6353	6974	9.8%
10CF	5228	5975	14.3%	F10CF	6205	6972	12.4%
15C	4149	4273	3.0%	F15C	4523	5344	18.2%
15F	3988	4895	22.8%	F15F	5606	6285	12.1%
15CF	4216	4636	10.0%	F15CF	4377	5616	28.3%
PL2	8049	9106	13.1%	F2	9720	10887	12.0%
1 MPa = 145.0377 psi		Average =	12.2%			Average =	14.5%

The manner in which cylinder specimens failed in compression was observed and compared based on presence of rubber and/or fibers. Pictures which show cylinder failure for each mix can be found in Appendix A. It was observed that control cylinder specimens without fibers, PL1 and PL2, tested in compression failed in an explosive and brittle manner. As rubber particles replaced mineral aggregates in the mixes, the failure became much less explosive and cylinders retained their shape. However, pieces of the cylinder did fall off or could easily be pulled away once removed from the machine. It was also observed that the mixes which contained only 5 percent rubber exhibited behavior closer to that of plain concrete in that they failed in a conical manner. The mixes containing 10 and 15 percent rubber showed longitudinal cracks along the length of the cylinder rather than cracking in a typical cone shape. Rubber particles caused the cylinders to fail in a more gradual manner.

Control cylinder specimens tested in compression that contained fibers, F1 and F2, failed explosively but all pieces remained part of the cylinder due to the fiber interaction. All specimens containing fibers, regardless of the presence of rubber, retained the majority of its cylindrical shape after failure. Large cracks were visible at failure and concrete appeared to expand away from the core in the center of the cylinder in some cases.

4.1.5 Split Tensile Strength

The average split tensile strength values, given in Table 16, for mixes without fibers and mixes with fibers are plotted in Figures 27 and 28, respectively. Literature has found that split tensile strength decreases with increasing amounts of rubber particles. This trend is apparent in Figures 27 and 28. Past research has also found that fibers tend to increase the split tensile strength.

The decrease in split tensile strength with the addition of rubber was analyzed with respect to rubber particle size. The decrease in split tensile strength from 0 to 15 percent addition of fine, coarse, and fine and coarse rubber for mixes without fibers is 35.0, 32.3, and 29.6 percent, respectively. The decrease in split tensile strength from 0 to 15 percent addition of fine, coarse, and fine and coarse rubber for mixes with fibers is 38.5, 30.6, and 34.3 percent, respectively. Similarly to compressive strength, though the split tensile strength decreased more in mixes that contained fibers, the individual split tensile strength values for mixes with fibers were much larger than those for the mixes without fibers. The split tensile strength values decreased nearly linearly with respect to the addition of rubber as exhibited by R^2 values very close to 1.0.

Table 16. Split tensile strength of concrete

Split Tensile Strength f_r (psi)						
Rubber %	Without fibers			With fibers		
	Fine Rubber	Fine & Coarse Rubber	Coarse Rubber	Fine Rubber	Fine & Coarse Rubber	Coarse Rubber
0	666*	666*	666*	908**	908**	908**
5	650	577	517	838	765	814
10	522	520	544	611	740	674
15	433	469	451	558	596	630

*Average of PL1 and PL2

**Average of F1 and F2

1 MPa = 145.0377 psi

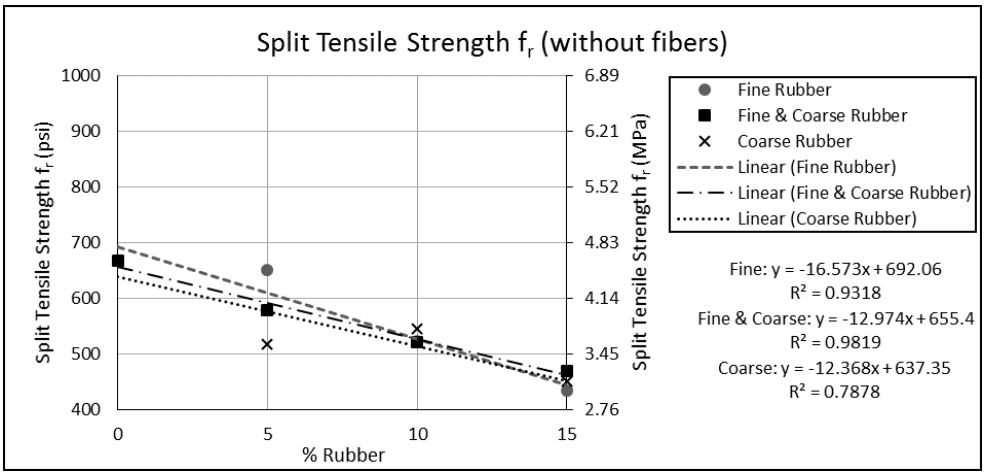

Figure 27. Split tensile strength of mixes without fibers

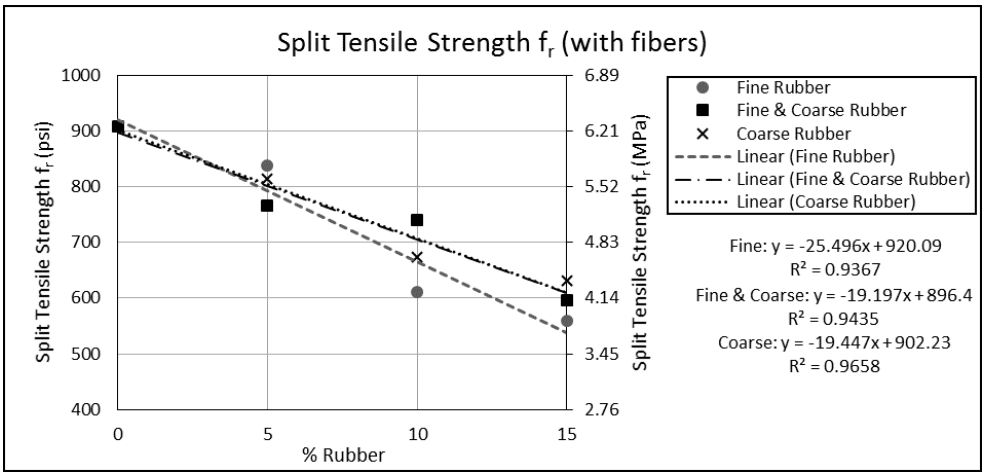

Figure 28. Split tensile strength of mixes with fibers

The increase in split tensile strength of mixes which contained fibers was compared to mixes which did not contain fibers. Table 17 and Figure 29 show this comparison. Mixes that contained fibers had an average split tensile strength 33.7 percent higher than that of mixes that did not contain fibers.

Table 17. Ratio of split tensile strength between mixes with fibers and without fibers

Ratio of Split Tensile Strength Between Mixes With Fibers and Without Fibers				
Mix	f_r (psi) f_rwo	Mix	f_r (psi) f_rw	$\frac{f_rw}{f_rwo}$
PL1	657	F1	946	1.440
5C	517	F5C	814	1.573
5F	650	F5F	838	1.288
5CF	577	F5CF	765	1.326
10C	544	F10C	674	1.238
10F	522	F10F	611	1.172
10CF	520	F10CF	740	1.423
15C	451	F15C	630	1.398
15F	433	F15F	558	1.290
15CF	469	F15CF	596	1.272
PL2	675	F2	869	1.288
1 MPa = 145.0377 psi			Averages:	1.337

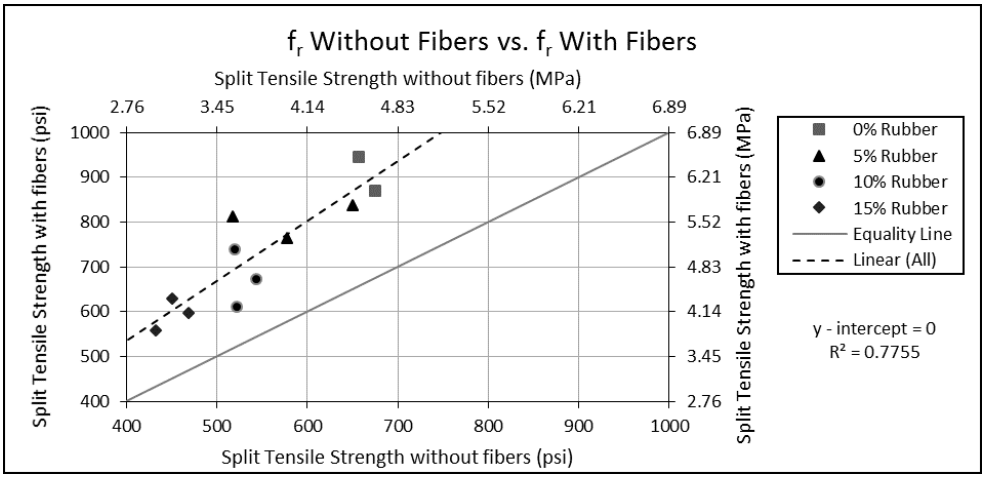

Figure 29. Split tensile strength of mixes without fibers vs. with fibers

Figures 30 and 31 show the relationship between split tensile strength and the square root of f'_c. Table 18 gives the values which are plotted in the two figures. Per ACI, 7.5 times square root of f'_c is defined as the tensile strength of normal concrete (ACI 318-11 Eq. 9-10) (ACI 2011). The value given by ACI is a standard value which can be used as an estimate but a coefficient which defines the actual material tested can be found from a plot of tensile strength versus the square root of f'_c of each mix. A linear trend line is then found from this data, and the slope of the line is the coefficient which can be used in place of the 7.5 in the ACI formula to calculate the tensile strength of the material. Figures 30 and 31 show a fairly strong correlation between the square root of f'_c and f_r as indicated by the R^2 values. From Figure 30, for mixes which do not contain fibers, the ACI equation can be modified to $f_r = 7.16\sqrt{f'_c}$. This equation is similar to that given by ACI for conventional concrete. From Figure 31, for mixes which contain fibers, the ACI equation can be modified to $f_r = 8.94\sqrt{f'_c}$. The higher coefficient for the mixes that contained fibers suggests that the split tensile strength increased with the addition of fibers, which agrees with past research.

Table 18. Split Tensile strength per ACI

Square Root of f_c 28 days vs. f_r					
Mix	Without fibers		Mix	With fibers	
	Square root f_c 28 days (psi)	f_r (psi)		Square root f_c 28 days (psi)	f_r (psi)
PL1	93.1	657	F1	101.0	946
5C	78.2	517	F5C	84.4	814
5F	84.8	650	F5F	89.3	838
5CF	84.1	577	F5CF	85.3	765
10C	72.9	544	F10C	76.3	674
10F	73.9	522	F10F	79.7	611
10CF	72.3	520	F10CF	78.8	740
15C	64.4	451	F15C	67.3	630
15F	63.1	433	F15F	74.9	558
15CF	64.9	469	F15CF	66.2	596
PL2	89.7	675	F2	98.6	869

1 MPa = 145.0377 psi

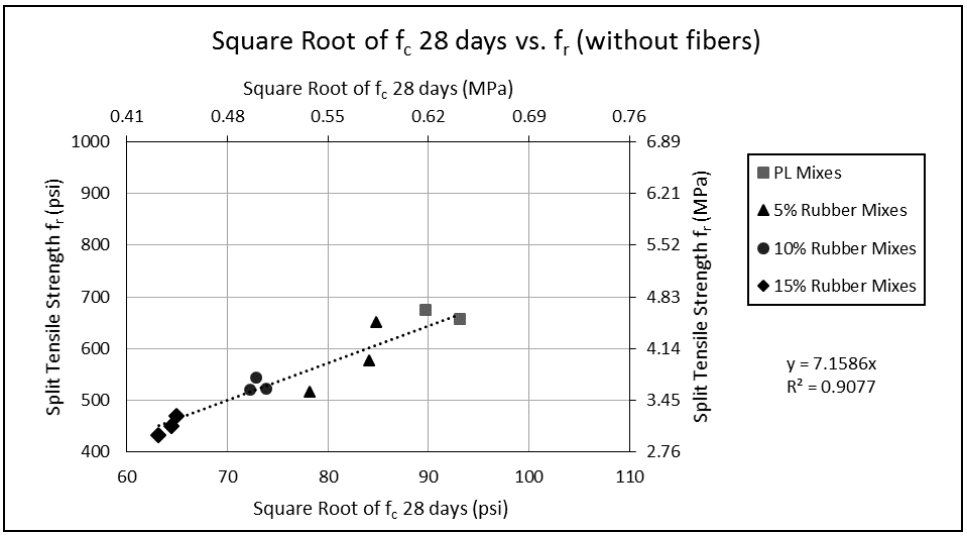

Figure 30. Split Tensile strength per ACI without fibers

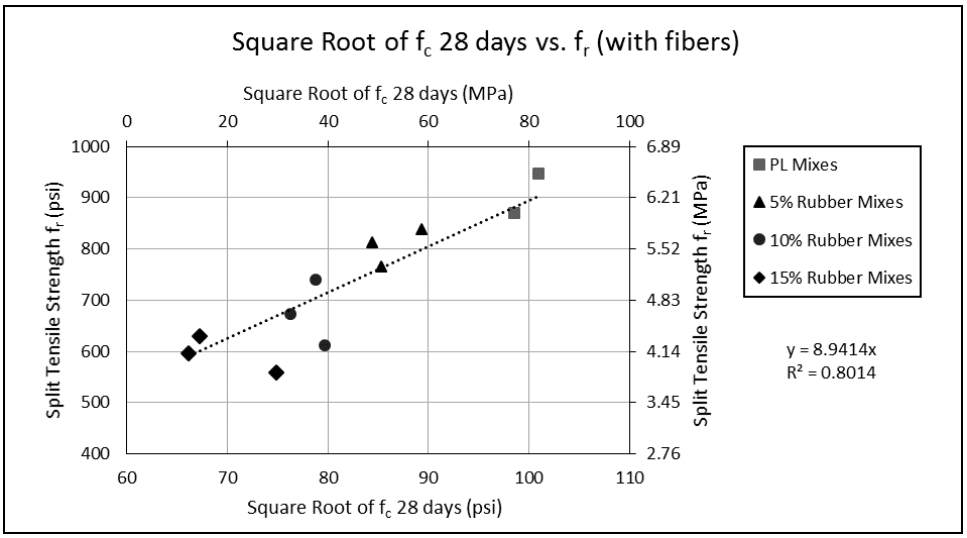

Figure 31. Split Tensile strength per ACI with fibers

Experimental split tensile strength was plotted against the ACI 318 -11 tensile strength value of 7.5 times the square root of f'$_c$ at 28 days (ACI 2011). An equality line, a line representing points at which the ACI value is equal to the experimental value, was then plotted to show the deviation of experimental values from the ACI values. This data is shown in Table 19 and plotted in Figures 32 and 33. For mixes with no fibers, it can be seen that the experimental data is much closer to the ACI value than for mixes with fibers. Additionally,

the equations for the trend lines of the data represent the average difference between experimental values and the ACI value. For mixes without fibers, the experimental values are an average of 4.82 percent less than the ACI values. For mixes with fibers, the experimental values are an average of 18.7 percent greater than the ACI values.

Table 19. Split Tensile strength: ACI vs. Experimental

ACI f_r vs. Experimental f_r							
Mix	Without fibers			Mix	With fibers		
	ACI, f_r (ksi)	Exp., f_r (ksi)	Exp. f_r / ACI f_r		ACI, f_r (ksi)	Exp., f_r (ksi)	Exp. f_r / ACI f_r
PL1	698	657	0.9409	F1	757	946	1.250
5C	586	517	0.8820	F5C	633	814	1.286
5F	636	650	1.0229	F5F	670	838	1.251
5CF	631	577	0.9148	F5CF	640	765	1.196
10C	547	544	0.9951	F10C	572	674	1.178
10F	554	522	0.9417	F10F	598	611	1.023
10CF	542	520	0.9591	F10CF	591	740	1.253
15C	483	451	0.9336	F15C	504	630	1.250
15F	474	433	0.9139	F15F	562	558	0.994
15CF	487	469	0.9630	F15CF	496	596	1.202
PL2	673	675	1.0033	F2	739	869	1.176
1 MPa = 145.0377 psi		Average =	0.9518			Average =	1.187

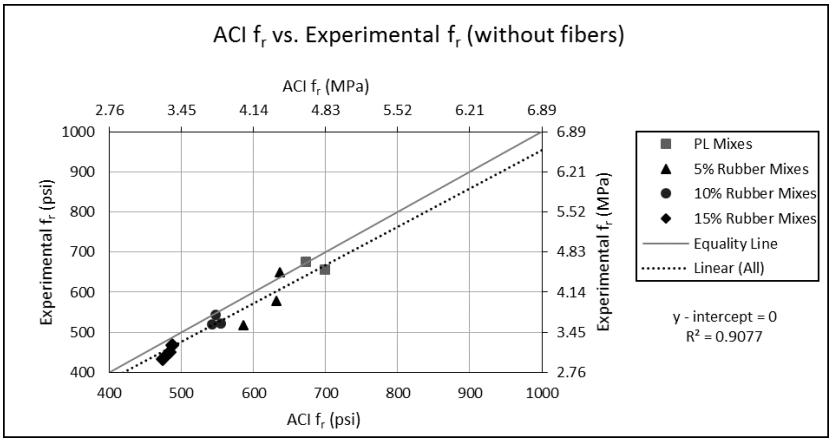

Figure 32. Split Tensile strength without fibers (ACI vs. Experimental)

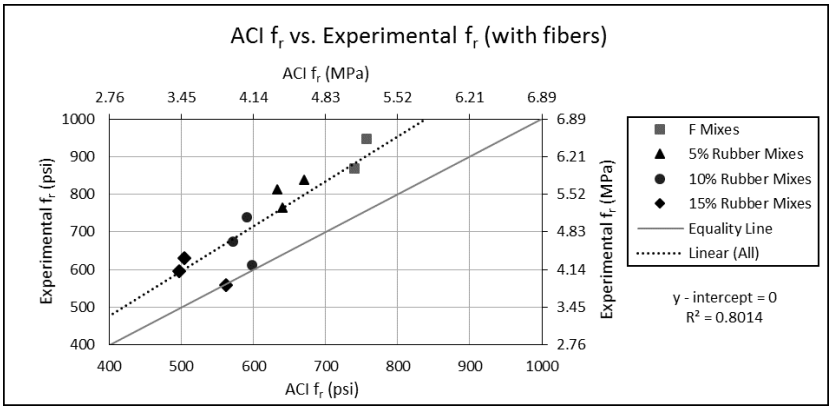

Figure 33. Split Tensile strength with fibers (ACI vs. Experimental)

As with compression tests, the failure mode of the cylinder specimens were observed for each split tensile test. For plain concrete mixes, PL1 and PL2, and mixes with 5 percent rubber without fibers, the cylinder split into two pieces as in conventional split cylinder tests. The cylinders which contained 10 and 15 percent rubber without fibers formed a crack but did not break into two pieces. For the mixes which contained fibers, a much smaller crack formed, and when load was removed, the crack width closed and became difficult to see.

4.1.6 Modulus of Elasticity

The average modulus of elasticity, given in Table 20, for mixes without fibers and mixes with fibers are plotted in Figures 34 and 35, respectively. Literature has shown that the modulus of elasticity tends to decrease with the addition of rubber. Figures 34 and 35 agree with this trend. Literature suggests that the addition of fibers has little effect on the modulus of elasticity.

The decrease in modulus of elasticity values from 0 to 15 percent addition of fine, coarse, and fine and coarse rubber for mixes without fibers is 32.5, 25.4, and 26.1 percent, respectively. The decrease in modulus of elasticity values from 0 to 15 percent addition of fine, coarse, and fine and coarse rubber for mixes with fibers is 28.9, 30.9, and 28.0 percent, respectively.

Table 20. Modulus of elasticity of concrete

Modulus of Elasticity, E (ksi)						
Rubber %	Without fibers			With fibers		
	Fine Rubber	Fine & Coarse Rubber	Coarse Rubber	Fine Rubber	Fine & Coarse Rubber	Coarse Rubber
0	5219*	5219*	5219*	5686**	5686**	5686**
5	4939	5202	4436	4994	5124	5037
10	3884	4126	4353	4571	4636	4881
15	3521	3858	3895	4045	4093	3932

*Average of PL1 and PL2

**Average of F1 and F2

1 GPa = 145.0377 ksi

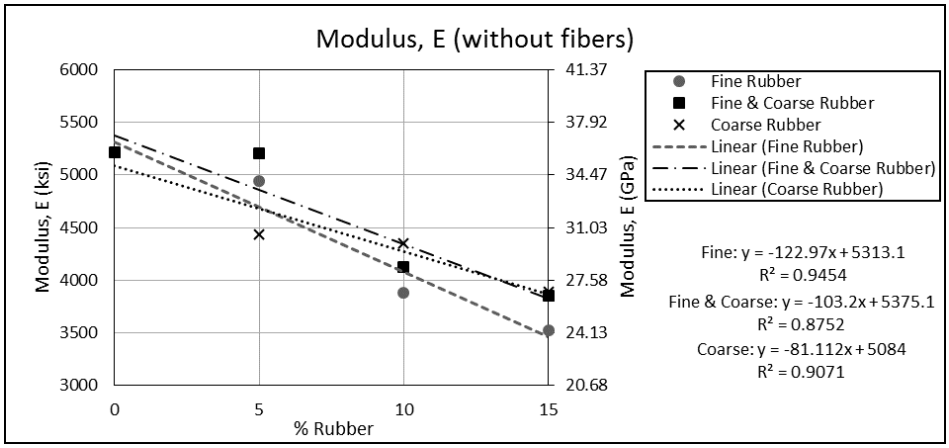

Figure 34. Modulus of Elasticity of concrete without fibers

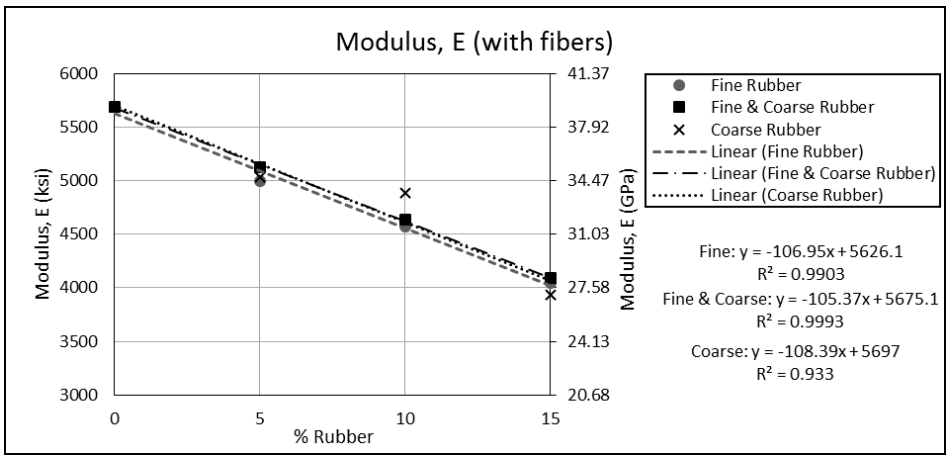

Figure 35. Modulus of Elasticity of concrete with fibers

A comparison was made between the modulus of elasticity of mixes that contain fibers to mixes that do not contain fibers. This comparison can be seen in Table 21 and

Figure 36. The results show that the modulus of elasticiy increased an average of 8.70 percent with the addition of fibers. This is a relatively small increase, but in almost all cases the modulus values are consistently larger with the adition of fibers.

Table 21. Ratio of modulus of elasticity between mixes with fibers and without fibers

Ratio of Modulus of Elasticity Between Mixes With Fibers and Without Fibers				
Mix	Modulus (ksi) E *wo*	Mix	Modulus (ksi) E *w*	$\frac{E\,w}{E\,wo}$
PL1	5160	F1	5872	1.138
5C	4436	F5C	5037	1.135
5F	4939	F5F	4994	1.011
5CF	5202	F5CF	5124	0.985
10C	4353	F10C	4881	1.121
10F	3884	F10F	4571	1.177
10CF	4126	F10CF	4636	1.124
15C	3895	F15C	3932	1.009
15F	3521	F15F	4045	1.149
15CF	3858	F15CF	4093	1.061
PL2	5278	F2	5501	1.042
1 GPa = 145.0377 ksi			Averages:	1.087

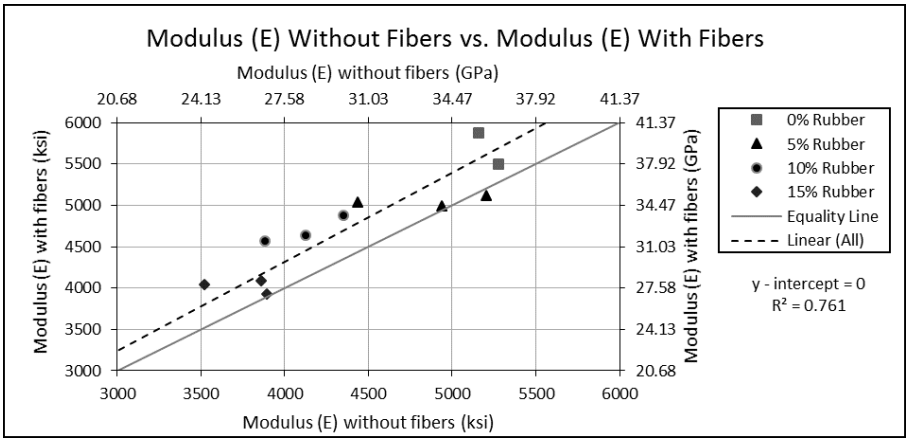

Figure 36. Modulus of elasticity of concrete without fibers vs. with fibers

The values shown in Tables 22 and plotted in Figures 37 and 38 show that for both mixes that contain fibers and those without, as compressive strength increases, the modulus of elasticity of the material also increases. The modulus of elasticity is plotted against the square root of f_c since concrete strength and modulus are generally related in this fashion with a coefficient in front of the square root that adjusts for concrete unit weight.

Table 22. Concrete strength vs modulus of elasticity

Square Root of f_c 28 days vs. Modulus					
Mix	Without fibers		Mix	With fibers	
	Square root f_c 28 days (psi)	Modulus (ksi)		Square root fc 28 days (psi)	Modulus (ksi)
PL1	93.1	5160	F1	101.0	5872
5C	78.2	4436	F5C	84.4	5037
5F	84.8	4939	F5F	89.3	4994
5CF	84.1	5202	F5CF	85.3	5124
10C	72.9	4353	F10C	76.3	4881
10F	73.9	3884	F10F	79.7	4571
10CF	72.3	4126	F10CF	78.8	4636
15C	64.4	3895	F15C	67.3	3932
15F	63.1	3521	F15F	74.9	4045
15CF	64.9	3858	F15CF	66.2	4093
PL2	89.7	5278	F2	98.6	5501

1 MPa = 145.0377 psi and 1 GPa = 145.0377 ksi

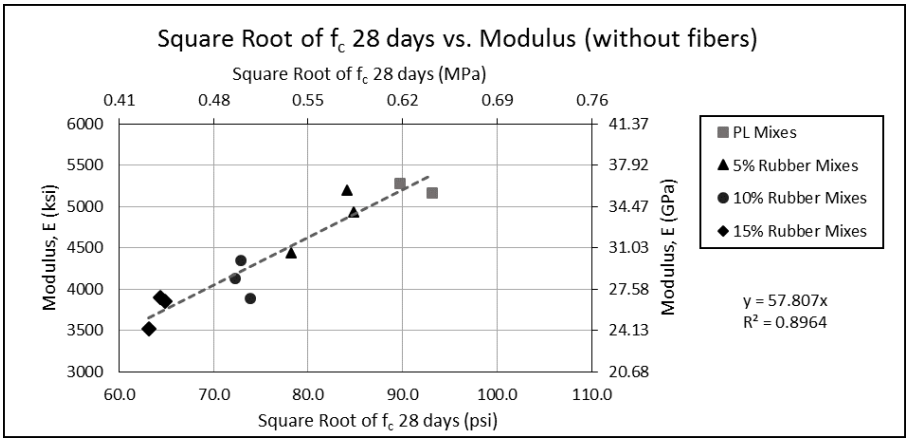

Figure 37. Concrete strength vs. modulus of elasticity without fibers

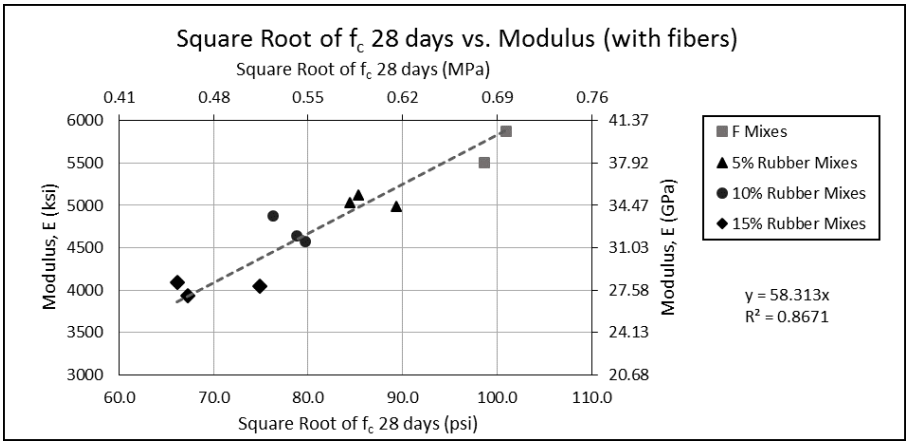

Figure 38. Concrete strength vs. modulus of elasticity with fibers

Experimental modulus of elasticity values were plotted against the value of modulus of elasticity calculated from ACI 318-11 Section 8.5.1 (ACI 2011). The experimental values and the ACI values are shown in Tables 23 and plotted in Figures 39 and 40. An equality line, a line representing points at which the ACI value is equal to the experimental value, was then plotted to show the deviation of experimental values from the ACI value. For mixes that contain fibers, it can be seen that the experimental data is closer to the ACI value than for mixes without fibers. For mixes without fibers, the experimental values are an average of 3.96 percent larger than the ACI values. For mixes with fibers, the experimental values are an average of 0.83 percent greater than the ACI values.

Table 23. Modulus of elasticity: Experimental values vs ACI values

ACI Modulus vs. Experimental Modulus							
Mix	Without fibers			Mix	With fibers		
	ACI, E (ksi)	Exp., E (ksi)	Exp./ACI		ACI, E (ksi)	Exp., E (ksi)	Exp./ACI
PL1	5520	5160	0.9348	F1	6127	5872	0.9583
5C	4437	4436	0.9997	F5C	4973	5037	1.0128
5F	4845	4939	1.0194	F5F	5273	4994	0.9470
5CF	4812	5202	1.0809	F5CF	5010	5124	1.0227
10C	4016	4353	1.0839	F10C	4415	4881	1.1057
10F	4088	3884	0.9502	F10F	4543	4571	1.0062
10CF	3990	4126	1.0341	F10CF	4546	4636	1.0200
15C	3391	3895	1.1488	F15C	3721	3932	1.0568
15F	3334	3521	1.0562	F15F	4217	4045	0.9591
15CF	3424	3858	1.1265	F15CF	3748	4093	1.0920
PL2	5271	5278	1.0013	F2	6041	5501	0.9106
1 GPa = 145.0377 ksi		Average =	1.0396			Average =	1.0083

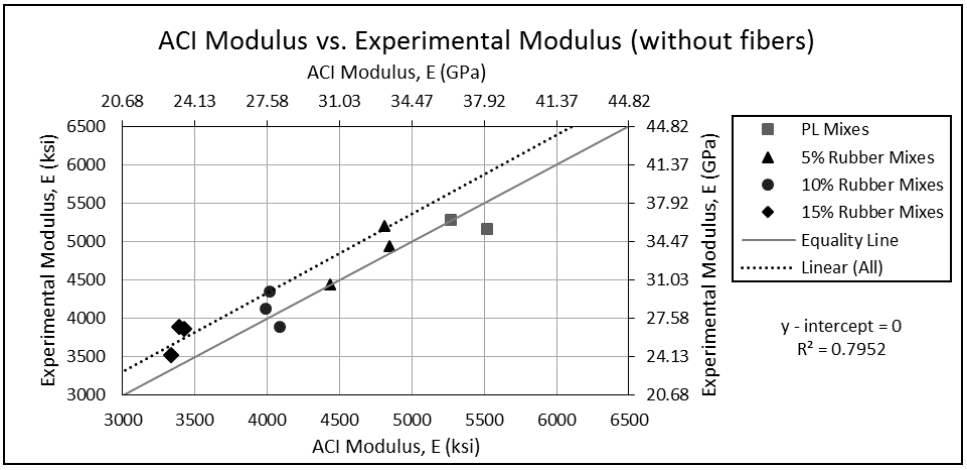

Figure 39. Modulus of elasticity: Experimental vs. ACI without fibers

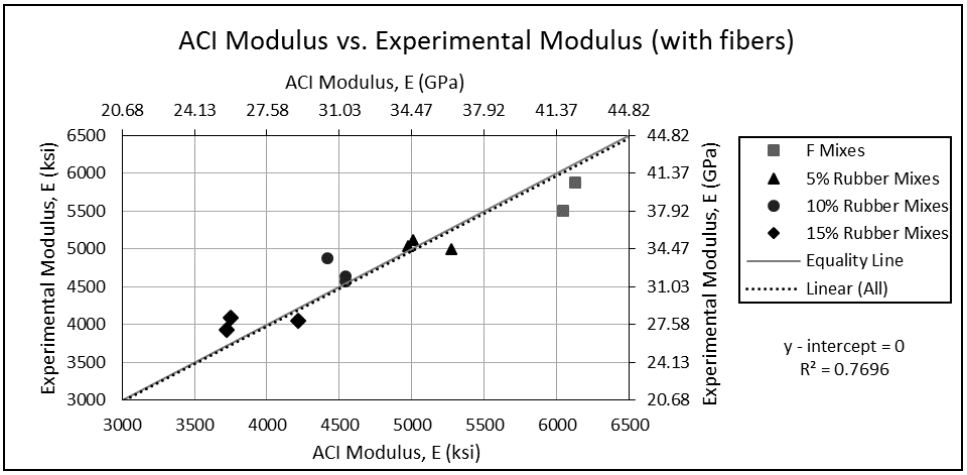

Figure 40. Modulus of elasticity: Experimental vs. ACI with fibers

4.2 Flexural Properties

Flexural properties were determined from flexural tests, including ultimate load, toughness indices, and displacement ductility ratios for each test mix. The properties and values determined for each of the 22 mixes performed and tested are shown in Table 24.

Table 24. Flexure properties of concrete with and without fibers

Flexure Properties									
Mix	P_n ACI (kips)	P_u Actual (kips)	P_u Theoretical (kips)	% Error (Actual vs. Theoretical)	Total Energy up to $P_{95\%}$ (kip-in)	Toughness Index 95	Toughness Index 90	Displacement Ductility Ratio	Displacement Ductility Ratio 95
PL1	7.60	8.30	8.98	8.27%	9.578	1.0058	-	5.7874	5.8154
5C	7.36	8.93	8.25	-7.64%	6.637	1.1343	-	2.6192	2.8881
5F	7.50	8.94	8.82	-1.32%	6.720	1.0491	-	2.7983	2.9045
5CF	7.50	9.53	8.75	-8.12%	8.039	1.0422	-	3.0288	3.1277
10C	7.22	8.76	7.71	-11.96%	5.619	1.0285	-	2.4885	2.5421
10F	7.33	7.49	8.26	10.29%	6.539	1.0932	-	4.2088	4.5291
10CF	7.26	8.23	7.90	-4.01%	5.838	1.1971	-	2.3524	2.7002
15C	6.90	7.03	7.01	-0.25%	4.697	1.2074	-	3.0574	3.5387
15F	7.06	6.98	7.41	6.18%	4.298	1.2089	-	2.9651	3.4376
15CF	7.00	8.27	7.20	-12.93%	4.250	1.1815	-	1.8196	2.0570
PL2	7.58	8.86	8.93	0.79%	6.694	1.0030	-	3.0498	3.0571
F1	7.70	10.74	9.97	-7.19%	13.84	1.2155	1.3733	4.6927	5.5382
F5C	7.52	9.85	9.07	-7.93%	11.22	1.5950	2.2741	2.9748	4.4235
F5F	7.57	10.41	9.35	-10.20%	8.084	1.0666	1.9867	2.9496	3.1006
F5CF	7.53	10.44	9.08	-13.03%	11.07	1.3534	1.5729	3.0469	3.9091
F10C	7.31	8.50	8.05	-5.25%	12.56	1.8534	2.2963	3.7625	6.4916
F10F	7.39	10.38	8.50	-18.15%	10.78	1.2916	1.2979	3.1608	3.8874
F10CF	7.39	10.44	8.51	-18.46%	9.780	1.2466	1.6377	2.9201	3.5211
F15C	7.15	9.10	7.71	-15.19%	7.685	1.5603	2.5208	2.4190	3.4988
F15F	7.31	7.55	8.20	8.64%	8.504	1.6072	1.9012	3.7610	5.6517
F15CF	7.20	7.48	7.83	4.59%	7.210	1.7920	2.5327	2.6502	4.3444
F2	7.67	11.68	9.83	-15.84%	11.64	1.1164	1.4319	4.1779	4.5727

4.2.1 Ultimate Capacity

The ultimate capacity was determined for each beam specimen, experimentally and theoretically, and was then compared to ACI code provisions. The methodology and calculations performed to determine the theoretical curves as well as full theoretical and experimental load deflection curves can be found in Appendix B and C respectively.

Once the full theoretical curves were developed, the theoretical ultimate load was compared to the experimental ultimate load. Figures 41 and 42 show the relationship between theoretical values and experimental values given in Table 25. The solid gray line represents a line of equality or the points at which the theoretical value would be equal to the

experimental value. For the mixes without fibers, the experimental values are an average of 2.52 percent larger than the theoretical values. This is a very small difference and suggests that the model used resulted in relatively accurate theoretical values. For the mixes that contain fibers, all data points fell above the equality line except two corresponding to 15 percent rubber mixes. Excluding these two exceptions, the data would resemble that of the mixes with no fibers. However, when a trendline was plotted for all data, the experimental values were an average of 10.7 percent larger than the theoretical value as can be seen in Figure 42. This suggests that there could be more fiber contribution than accounted for by the theoretical model.

Table 25. Ultimate Flexural Load: Experimental vs. Theoretical

Theoretical P_u vs. Experimental P_u							
Mix	Without fibers			Mix	With fibers		
	Experimental P_u (kips)	Theoretical P_u (kips)	Experimental / Theoretical		Experimental P_u (kips)	Theoretical P_u (kips)	Experimental / Theoretical
PL1	8.30	8.98	0.9236	F1	10.74	9.97	1.0775
5C	8.93	8.25	1.0827	F5C	9.85	9.07	1.0861
5F	8.94	8.82	1.0134	F5F	10.41	9.35	1.1136
5CF	9.53	8.75	1.0884	F5CF	10.44	9.08	1.1498
10C	8.76	7.71	1.1358	F10C	8.50	8.05	1.0554
10F	7.49	8.26	0.9067	F10F	10.38	8.50	1.2217
10CF	8.23	7.90	1.0418	F10CF	10.44	8.51	1.2264
15C	7.03	7.01	1.0025	F15C	9.10	7.71	1.1791
15F	6.98	7.41	0.9418	F15F	7.55	8.20	0.9205
15CF	8.27	7.20	1.1485	F15CF	7.48	7.83	0.9561
PL2	8.86	8.93	0.9922	F2	11.68	9.83	1.1883
1 kilonewton = 0.224808943 kips		Average =	1.0252			Average =	1.1068

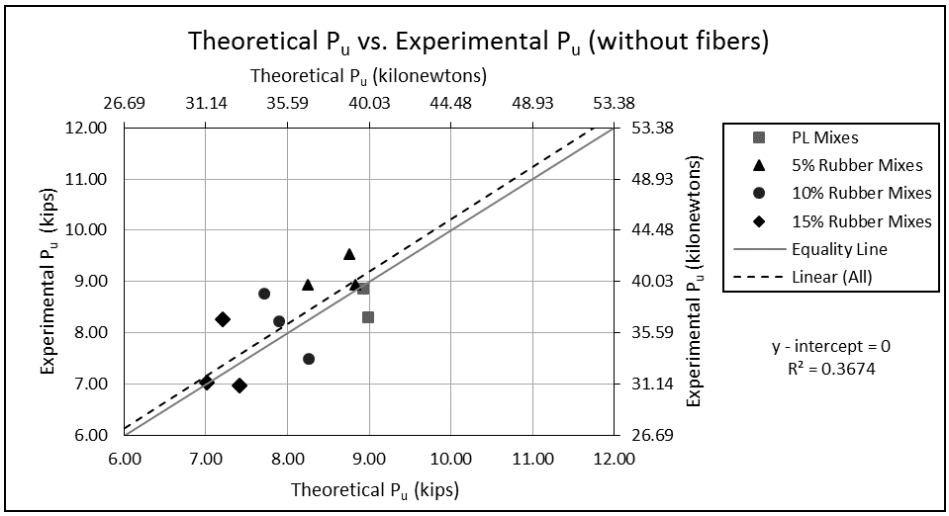

Figure 41. Ultimate Flexural Load: Experimental vs. Theoretical without fibers

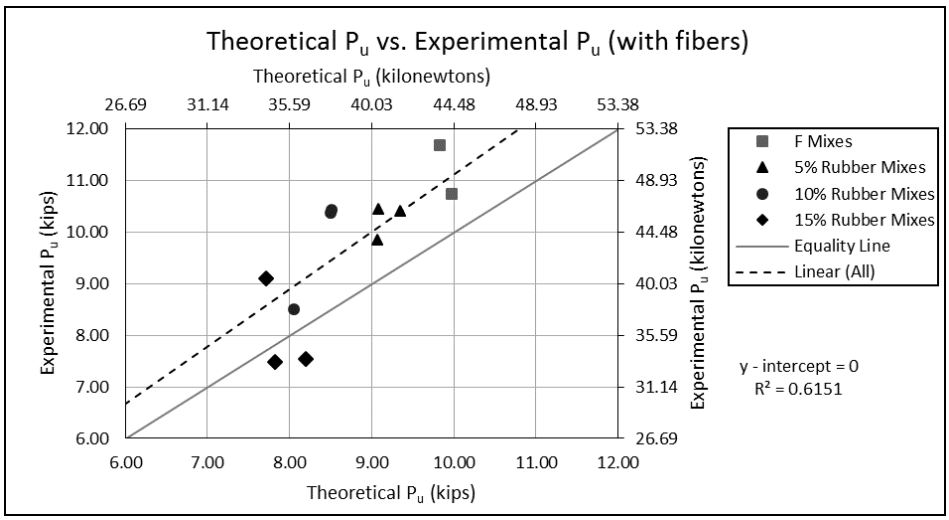

Figure 42. Ultimate Flexural Load: Experimental vs. Theoretical with fibers

As shown in Table 25, beams that contained fibers withstood higher loads than beams that did not have fibers. The reason for this can be attributed to the fibers in the compressive region of the flexure beam. These fibers confined the concrete during loading which allowed the beam to experience higher ultimate loads when compared to beams which did not contain fibers. When rubber was present in the beams, the beams failed in a more gradual manner especially with rubber percentages of 10 and 15 percent. The rubber in the concrete prevents sharp quick failures by altering the crack propagation in the matrix. The cracks, which cause

failure, must travel around the rubber particles in the concrete matrix rather than in a more direct path. This redirection results in a greater amount of energy absorption.

4.2.2 Toughness

Toughness is the ability of a material to absorb energy. There are many different methods to calculate toughness. Since flexural tests were performed and load deflection plots were obtained, toughness was represented as an area underneath the load deflection plot and presented as a toughness index rather than a unit of energy as is derived from the area under a stress-strain plot. The method used to determine the toughness index was based on the procedure presented by Toutanji (1996) and Khaloo et al. (2008).

Figure 43 represents the method used to define the toughness index. The area defined as A_1 represents the area under the load deflection plot up to the ultimate load ($P_{100\%}$). The area defined as A_2 represents the area under the load deflection plot from ultimate load ($P_{100\%}$) to 95 percent of the ultimate load ($P_{95\%}$) on the descending portion of the load deflection plot. The toughness index ($T_{95\%}$) represents the ratio of total area up to 95 percent ultimate load on the descending branch to the area up to ultimate load.

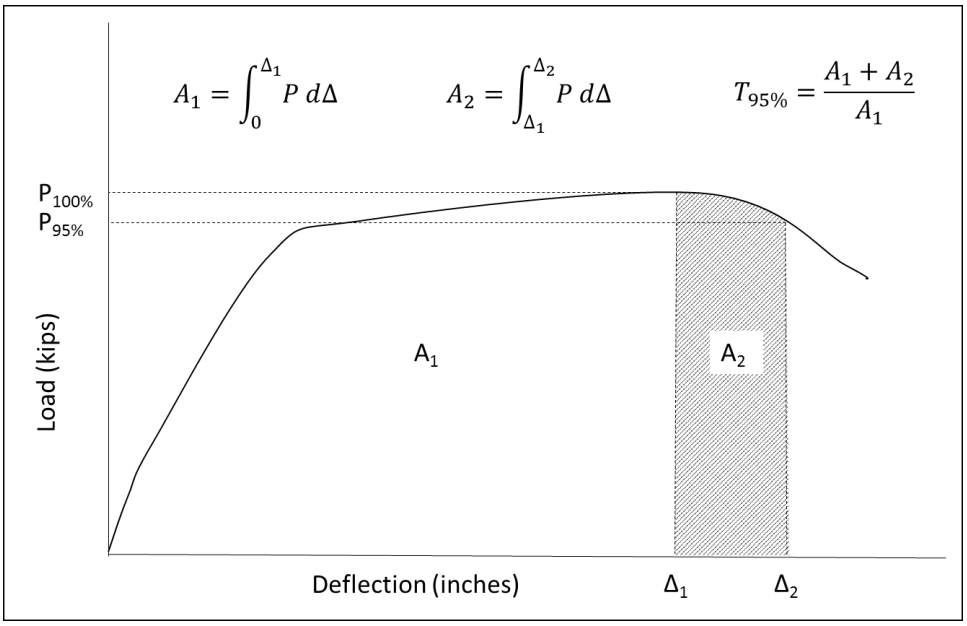

Figure 43. Method used to determine Toughness Indices

The relationship between the toughness indices and the percentage of rubber is shown in Figures 44 and 45 for mixes with and without fibers. Values corresponding to these figures are given in Table 26. The mixes which contained no fibers and no rubber (PL1 and 2) have a toughness index of nearly one. This indicates that the energy absorption capacity of these mixes is low and under flexural loading, the beam experience very little deflection before failure past ultimate load. As the percentage of rubber was increased for both mixes with and without fibers, the toughness index increased. For mixes which did not contain fibers, from 0 to 15 percent rubber, the toughness index increased by an average of 10.5 percent. For mixes which contained fibers, from 0 to 15 percent rubber, the toughness index increased an average of 42.7 percent. The toughness index 95 was compared for mixes which contain fibers to mixes which did not contain fibers. This comparison can be seen in Table 26 and Figure 46. Overall, mixes that contained fibers had a 29.2 percent larger toughness index value when compared to the mixes without fibers.

Table 26. Toughness Index 95

Toughness Index 95				
Mix	Index 95 without fibers	Mix	Index 95 with fibers	I 95 with / I 95 without
PL1	1.0058	F1	1.2155	1.2085
5C	1.1343	F5C	1.5950	1.4062
5F	1.0491	F5F	1.0666	1.0166
5CF	1.0422	F5CF	1.3534	1.2986
10C	1.0285	F10C	1.8534	1.8020
10F	1.0932	F10F	1.2916	1.1815
10CF	1.1971	F10CF	1.2466	1.0413
15C	1.2074	F15C	1.5603	1.2923
15F	1.2089	F15F	1.6072	1.3295
15CF	1.1815	F15CF	1.7920	1.5167
PL2	1.0030	F2	1.1164	1.1130
Average:	1.1047	Average:	1.4271	1.2915

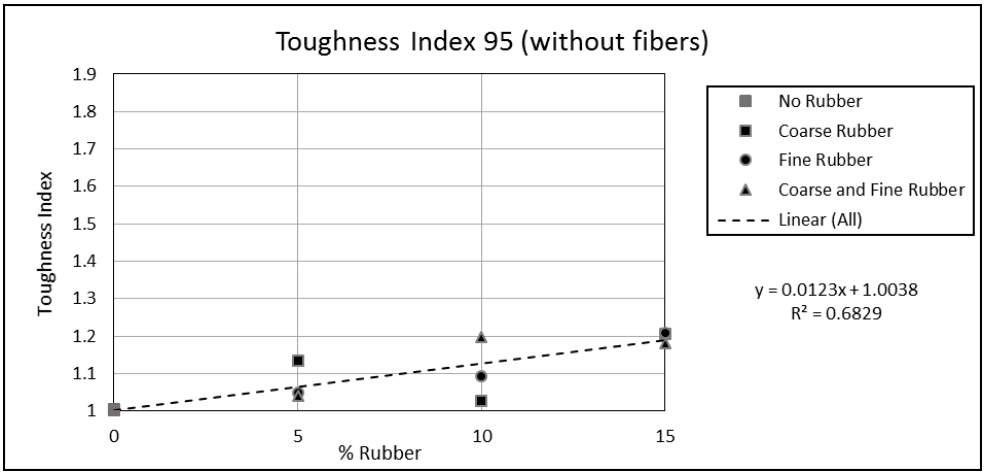

Figure 44. Toughness Index 95 without fibers

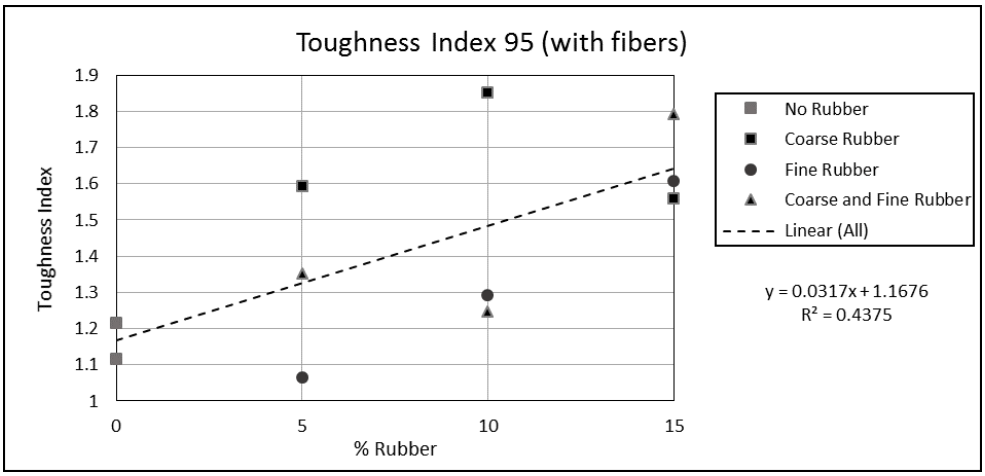

Figure 45. Toughness Index 95 with fibers

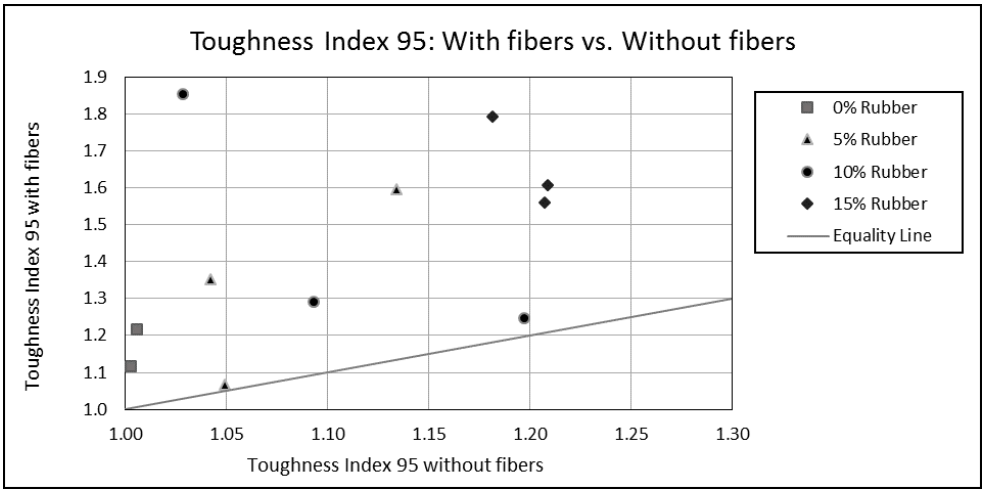

Figure 46. Toughness Index 95: with fibers vs. without fibers

For the purposes of comparison of mixes with fibers and without fibers, a load value of $P_{95\%}$ was chosen because all 22 load deflection plots had a point on the descending branch that corresponded to this value. After this point, beams that did not contain fibers failed and experienced a dramatic decrease in load carrying capacity, whereas mixes which contained fibers held a relatively high load for a longer period of time and reached higher deflections after ultimate load was reached. For comparison amongst beams that contain fibers only, it was possible to use a load value equal to 90 percent of ultimate load ($P_{90\%}$) because each plot contained a point on the descending branch of the curve that corresponded to this value.

Therefore in Figure 43, the value of A_2 represents the area under the load deflection plot from ultimate load ($P_{100\%}$) to 90 percent of the ultimate load on the descending branch ($P_{90\%}$). Here, the toughness index ($T_{90\%}$) represents the ratio of total area up to 90 percent ultimate load on the descending branch to the area up to ultimate load.

As expected, the toughness index ($T_{90\%}$) increased with increasing percentages of rubber as shown in Figure 47. Values corresponding to this figure are shown in Table 27. It can be seen from Figure 47 that the coarse rubber appears to increase the toughness more than the fine rubber. This is shown by the linear trend line representing each rubber type. Overall, the toughness index increase from 0 to 15 percent rubber is 65.3 percent. This shows a more dramatic increase in toughness, when compared to the toughness index 95, due to addition of rubber. This further confirms the fact that rubber increases the toughness of the material.

Table 27. Toughness Index 90 with fibers

Toughness Index 90 (with fibers)		
Mix	% Rubber	Index
F1	0	1.3733
5C	5	2.2741
5F	5	1.9867
5CF	5	1.5729
10C	10	2.2963
10F	10	1.2979
10CF	10	1.6377
15C	15	2.5208
15F	15	1.9012
15CF	15	2.5327
F2	0	1.4319

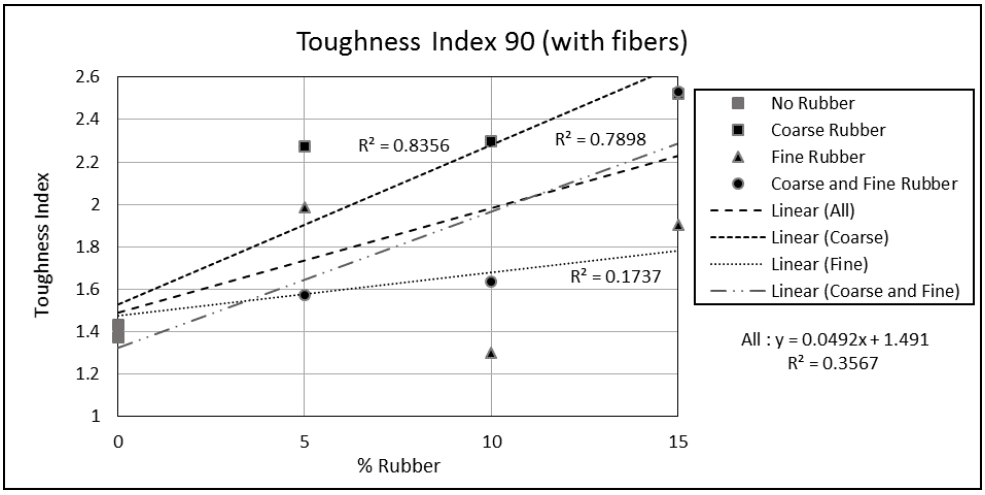

Figure 47. Toughness Index 90 with fibers

4.2.3 Displacement Ductility Factor

A different approach was used to determine the ductility ratio using the load deflection plots rather than moment curvature plots. Conventionally, the ductility ratio is φ_u/φ_y. Buyukozturk (2004) stated that the ductility of a structure may be defined as a ratio of Δ_u to Δ_y where Δ_u is the deflection at the end of the post-elastic range and Δ_y is the deflection at yielding. For this research, the displacement ductility factor is a ratio of the displacement corresponding to the ultimate load to the displacement corresponding to the yield point on the load deflection plot.

The displacement ductility factors, given in Table 28, are plotted with respect to percentage of rubber in Figures 48 and 49. Even though the data in the figures show a trend of decreasing ductility with increasing rubber percentages, since ductility is heavily related to compressive strength, we cannot say that the ductility decreases as the percentage of rubber is increased since the compressive strength of the concrete was decreased with the addition of rubber. Two mixes, one containing rubber and one free of rubber, with the same compressive strength could show different results. However, it can be concluded that if there exists two

mixes with the same base mix, one with rubber and one without rubber, the ductility of the concrete containing the rubber particles would be less since the compressive strength would be less as well. Overall, mixes which contained fibers had a 12.7 percent larger ductility displacement value when compared to the mixes without fibers. Figure 50 shows this trend as a majority of the points are above the equality line.

Table 28. Displacement Ductility Factor

Displacement Ductility Factor				
Mix	Factor without fibers	Mix	Factor with fibers	DDF with / DDF without
PL1	5.7874	F1	4.6927	0.8108
5C	2.6192	F5C	2.9748	1.1358
5F	2.7983	F5F	2.9496	1.0540
5CF	3.0288	F5CF	3.0469	1.0060
10C	2.4885	F10C	3.7625	1.5119
10F	4.2088	F10F	3.1608	0.7510
10CF	2.3524	F10CF	2.9201	1.2413
15C	3.0574	F15C	2.4190	0.7912
15F	2.9651	F15F	3.7610	1.2684
15CF	1.8196	F15CF	2.6502	1.4565
PL2	3.0498	F2	4.1779	1.3699
			Average:	1.1270

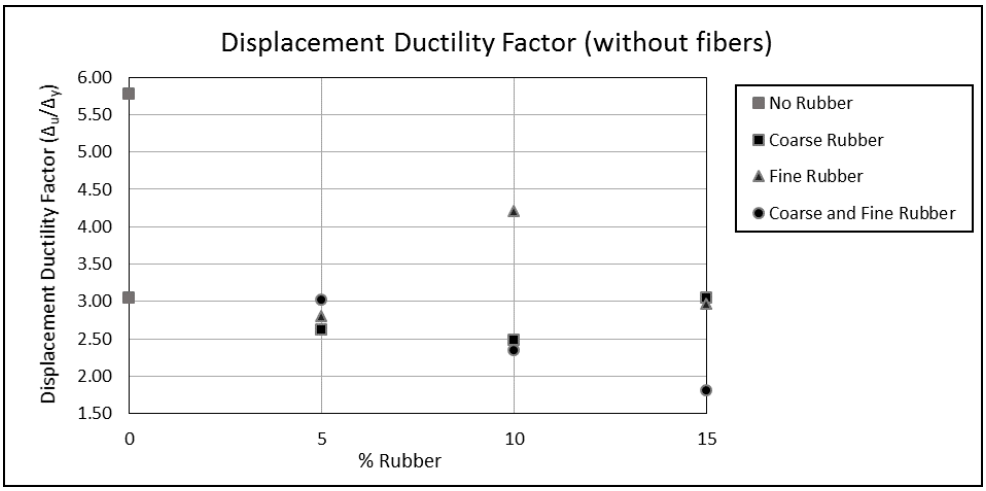

Figure 48. Displacement Ductility Factor without fibers

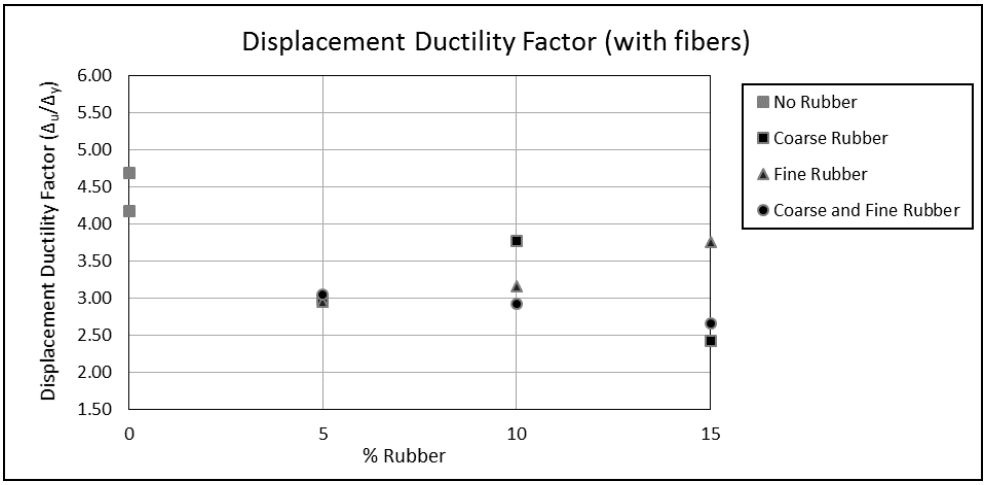

Figure 49. Displacement Ductility Factor with fibers

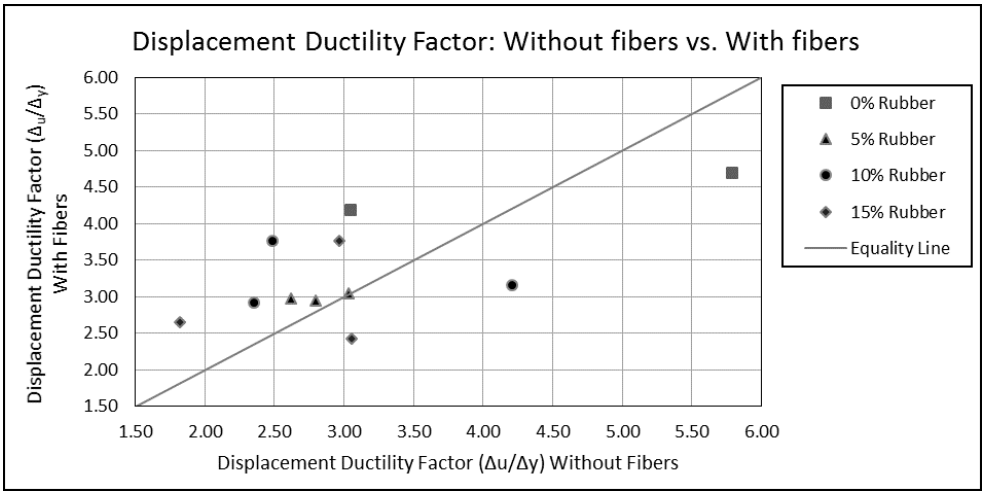

Figure 50. Displacement Ductility Factor: without fibers vs. with fibers

A second ductility displacement factor was also determined for further comparison of ductility between mixes with and without fibers. Recall that the first ductility displacement factor was based on the ratio of Δ_u/Δ_y. The second ductility displacement factor is based on the ratio of $0.95\Delta_u/\Delta_y$ where $0.95\Delta_u$ represents the deflection value corresponding to 95 percent of the ultimate load on the descending branch of the load deflection curves. This ratio is identified herein as displacement ductility factor 95. Again when displacement ductility factor 95 was plotted against increasing percentages of rubber, there is a slight decrease in

ductility with increasing percentages of rubber as shown in Figures 51 and 52. However, for the reasons mentioned previously, it cannot be said that the ductility decreases with increasing percentages of rubber for mixes with different compressive strengths. From the data provided in Table 29 and the plot in Figure 53, it is again apparent that when fibers are introduced into the rubber concrete mixture, the ductility of the composite material increases. Comparing displacement ductility factor 95 for mixes with fibers to mixes without fibers shows an increase of 43.3 percent in ductility when fibers exist in the mixture.

Table 29. Displacement Ductility Factor 95

Displacement Ductility Factor 95				
Mix	Factor without fibers	Mix	Factor with fibers	DDF with / DDF without
PL1	5.8154	F1	5.5382	0.9523
5C	2.8881	F5C	4.4235	1.5316
5F	2.9045	F5F	3.1006	1.0675
5CF	3.1277	F5CF	3.9091	1.2498
10C	2.5421	F10C	6.4916	2.5536
10F	4.5291	F10F	3.8874	0.8583
10CF	2.7002	F10CF	3.5211	1.3040
15C	3.5387	F15C	3.4988	0.9887
15F	3.4376	F15F	5.6517	1.6441
15CF	2.0570	F15CF	4.3444	2.1120
PL2	3.0571	F2	4.5727	1.4958
			Average:	1.4325

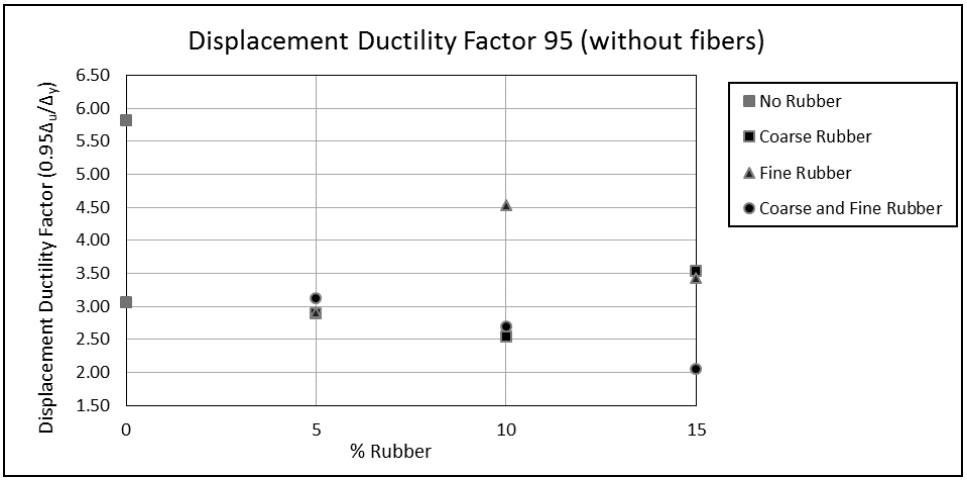

Figure 51. Displacement Ductility Factor 95 without fibers

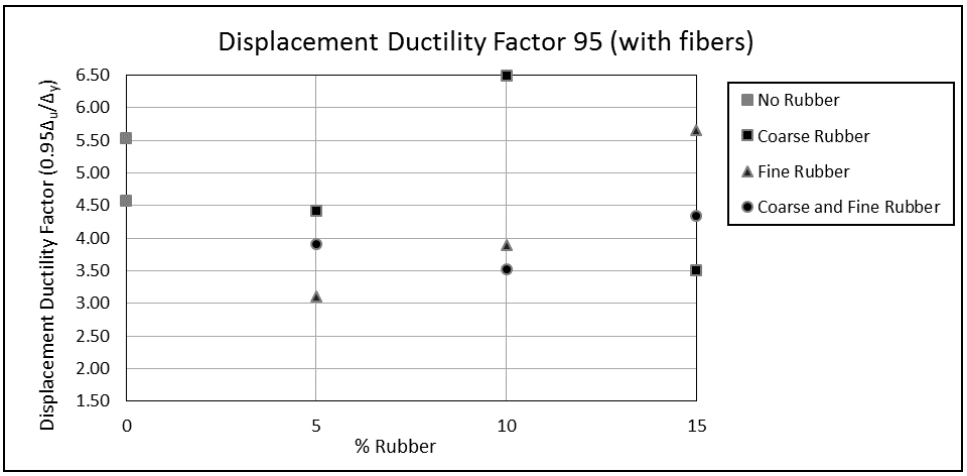

Figure 52. Displacement Ductility Factor 95 with fibers

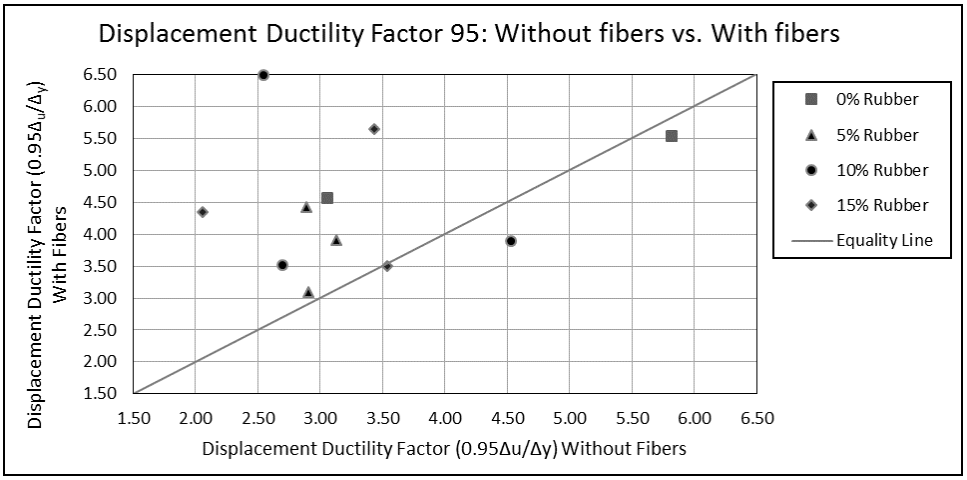

Figure 53. Displacement Ductility Factor 95: without fibers vs. with fibers

4.3 Summary of Results

4.3.1 Compressive Strength

Results show that compressive strength shows a definitive decrease with the addition of rubber, as expected. No matter the type of rubber, with the addition of larger percentages, the compressive strength appears to decrease at the same rate in a linear manner. The mixes which contained coarse rubber appear to have the lowest overall compressive strength while the mixes which contained fine rubber appear to have the highest overall compressive strength. However, close examination of the data shows that the difference in ultimate

compressive strengths reached is not statistically significant. Literature suggests that the coarse rubber particles should have negatively affected the compressive strength more than the fine rubber particles. The lack of significant difference could be attributed to differences in mix proportions of aggregates when comparing mixes tested from literature to mixes tested in this research. Overall, the compressive strength of mixes which contain fibers resulted in higher compressive strength than those without fibers.

From 28-day compressive strength to 56-day compressive strength, mixes which contained only rubber had a 12.2 percent increase in compressive strength. From 28-day compressive strength to 56-day compressive strength, in mixes which contained both rubber and fibers, there is a 14.5 percent increase in compressive strength. Figures A35, A37, A39, and A41 in Appendix A titled "Average Compressive Strength" show an interesting trend. The rate of compressive strength gain from 28 to 56 days was greater over this time interval than of the time interval from 14 to 28 days. This could have been due to significant temperature changes during concrete curing time. Even though specimens were cast and cured in a temperature controlled laboratory, the atypical climate experienced during the curing period altered the temperature of the laboratory.

4.3.2 Split Tensile Strength

Results show that tensile strength sharply decreases with an increase in rubber addition. The rate of decrease in tensile strength was the most dramatic with the addition of fine rubber. However, the rate of decrease in tensile strength in mixes with a combination of fine and coarse rubber and only coarse rubber were similar. Overall, the tensile strength of mixes with fibers was higher than mixes which did not contain fibers.

4.3.3 Modulus of Elasticity

The modulus of elasticity decreases with the addition of rubber. The difference in the modulus of elasticity values with respect to particle size was negligible. The modulus of elasticity in mixes that only contain rubber showed a relatively linear decrease with increasing rubber percentages. When fibers were added to the mix, the modulus of elasticity decreased in an almost perfect linear trend as shown by R^2 values very near 1. Overall, in mixes that contained fibers, the modulus of elasticity was higher.

4.3.4 Toughness

Toughness indices indicate that the flexural toughness increases with the addition of rubber. Mixes which contained fibers show a 42.7 percent increase in toughness with the addition of rubber while mixes which do not contain fibers show an increase of only 10.5 percent. One of the main benefits which the addition of rubber to concrete results in is a more ductile behavior of a very brittle material. The fact that the overall toughness increased with the addition of fiber and rubber demonstrates a degree of success in that increasing the ductility of a rubber concrete mixture was an overall goal. The fibers do not necessarily increase the ductility of the beam from yielding to $P_{100\%}$, but they do significantly enhance the post peak response to continued loading. This is evidenced by the decreased displacement ductility ratio but increase in toughness indices.

4.3.5 Ductility

As previously stated, it cannot be concluded that with increasing amounts of rubber, the ductility will decrease unless the concrete being compared has the same compressive strength. However, it can be concluded that if fibers are added to the rubber concrete mix, the ductility is enhanced.

4.3.6 Flexural Crack Distribution

When a concrete beam is subjected to flexural loading, more cracks forming indicate a more ductile behavior. The figures in Appendix C show the cracking behavior of the flexure beams tested. As indicated by the figures, there are generally the same number and distribution of cracks in mixes that contain fibers, fibers and rubber, and only rubber. This indicates that crack formation does not appear to be affected by the addition of rubber to the concrete mix.

CHAPTER 5: Conclusions and Recommendations

5.1 Summary

Numerous studies exist on both rubber concrete and fiber-reinforced concrete that show the effects of rubber and fibers on fresh and hardened concrete properties. Existing research shows that the addition of rubber results in decreased compressive strength and split tensile strength in concrete, while the addition of fibers results in increased compressive strength and tensile strength when compared to conventional concrete mixes. Both rubber and fiber addition have been shown to result in decreased workability but increased toughness. The primary objective of this research was to create a composite material, combining positive characteristics of both the addition of rubber particles and fiber reinforcement to conventional concrete for potential use in structural applications. This research found that the compressive and tensile strength of rubber concrete increased with the addition of fibers. The toughness of the rubber concrete was found to increase with the addition of rubber as well as with the addition of fibers.

5.2 Conclusions

1. The addition of fibers and rubber to conventional concrete decreases workability.
2. With increasing amounts of rubber, the unit weight is found to decrease. With the addition of fibers to rubber concrete, the unit weight is seen to increase.
3. With increasing amounts of rubber, the air content is found to increase. No conclusion can be drawn about the addition of fibers to rubber concrete and the relationship to air content.

4. With increasing amounts of rubber, the compressive strength is found to decrease, while the addition of fiber to rubber concrete is found to increase the compressive strength.
5. With increasing amounts of rubber, the split tensile strength is found to decrease, while the addition of fiber to rubber concrete is found to increase the split tensile strength.
6. With increasing amounts of rubber, the modulus of elasticity is found to decrease, while the addition of fiber to rubber concrete is found to increase the modulus of elasticity. Though the decrease in modulus of elasticity is not significant, there is a visible trend.
7. Increasing amounts of rubber is found to increase the toughness of conventional concrete. Adding fibers to rubber concrete increases the toughness even more.
8. No conclusion can be drawn with respect to increasing amounts of rubber and ductility since the compressive strength of the concretes compared are not the same. It can be concluded that if there exist two mixes with the same base mix, one with rubber and one without rubber, that the ductility of the concrete containing the rubber particles would be less since the compressive strength would be less as well. However, when fibers are added to rubber concrete, the ductility is found to increase.

5.3 Recommendations

It can be seen that the addition of fibers to rubber concrete results in an increase in material properties which were negatively affected by the addition of only rubber such as compressive strength and tensile strength. It is concluded that a strong correlation between

the addition of fibers to rubber concrete and the enhancement of the desired properties justifies the addition of fibers to rubber concrete.

The addition of fine rubber appears to have a slightly less negative impact on compressive strength but does not significantly increase flexural toughness when compared to the addition of coarse rubber. Depending on the desired material properties (i.e. increased flexural capacity or greater strength with slight increased flexural capacity), it is recommended that a mix with both fibers and 5 to 10 percent fine rubber be used in applications where strength is a concern and a mix with fibers and 5 to 10 percent coarse rubber be used in applications where flexural capacity is a concern. If both flexural capacity and strength are desired, this research has shown that a combination of coarse and fine rubber generally results in properties which lie between the two.

5.4 Future Research

This research used a conventional concrete mix as the base mix. It would be beneficial for future research to experiment with different mix proportions and mix design procedures in order to better tailor a mix specifically for rubber and fiber addition. Additionally, only one percentage of fibers was used when adding fibers to rubber concrete. Different percentages of fibers as well as different fiber types could be used in addition to rubber to better tailor the rubber concrete mix. Though there is a great deal of research that has been performed on both rubber concrete and fiber-reinforced concrete, this research indicates that it would be beneficial to better explore the addition of both fibers and rubber to conventional concrete.

BIBLIOGRAPHY

ACI Committee 318. (2001). *Building code requirements for structural concrete (ACI 318-11) and commentary*. American Concrete Institute, Farmington Hills, MI, 92-94.

Aiello, M., and Leuzzi, F. (2010). "Waste tyre rubberized concrete: Properties at fresh and hardened state." *Waste Management,* 30(8-9), 1696-1704.

Albano, C., Camacho, N., Reyes, J., Feliu, J.L., and Hernandez, M. (2005). "Influence of scrap rubber addition to Portland I concrete composites: destructive and non-destructive testing." *Compos. Struct.,* 71(3-4), 439-446.

ASTM. (2010a). "Standard test method for air content of freshly mixed concrete by the pressure method." *ASTM Standard C231*. ASTM International, West Conshohocken, PA, 2003, DOI: 10.1520/C0231_C0231M-10, www.astm.org.

ASTM. (2010b). "Standard test method for compressive strength of concrete cylinders cast in place in cylindrical molds." *ASTM Standard C873*. ASTM International, West Conshohocken, PA, 2010, DOI: 10.1520/C0873-C0873M-10A, www.astm.org

ASTM. (2011a). "Standard specifications for steel fibers for fiber-reinforced concrete." *ASTM Standard A820.* ASTM International, West Conshohocken, PA, 2011, DOI: 10.1520/A820_A0820M-11, www.astm.org

ASTM. (2011b). "Standard test method for splitting tensile strength of cylindrical concrete specimens." *ASTM Standard C496*. ASTM International, West Conshohocken, PA, 2011, DOI: 10.1520/C0496_C0496M-11, www.astm.org

ASTM. (2012a). "Standard test method for density, relative density (specific gravity), and absorption of coarse aggregate." *ASTM Standard C127*. ASTM International, West Conshohocken, PA, 2003, DOI: 10.1520/C0127-12, www.astm.org.

ASTM. (2012b). "Standard test method for density, relative density (specific gravity), and absorption of fine aggregate." *ASTM Standard C128*. ASTM International, West Conshohocken, PA, 2003, DOI: 10.1520/C0128-07A, www.astm.org.

ASTM. (2012c). "Standard test method for slump of hydraulic-cement concrete." *ASTM Standard C143*. ASTM International, West Conshohocken, PA, 2012, DOI: 10.1520/C0143-C0143M-12, www.astm.org

ASTM. (2013a). "Standard specification for chemical admixtures for concrete." *ASTM Standard C494*. ASTM International, West Conshohocken, PA, 2011, DOI: 10.1520/C0494_C0494M-13, www.astm.org

ASTM. (2013b). "Standard specification for chemical admixture for use in producing flowing concrete." *ASTM Standard C1017*. ASTM International, West Conshohocken, PA, 2011, DOI: 10.1520/C1017_C1017M, www.astm.org

ASTM. (2014). "Standard practice for making and curing concrete test specimens in the laboratory." *ASTM Standard C192*. ASTM International, West Conshohocken, PA, 2014, DOI: 10.1520/C0192-C0192M-14, www.astm.org

Balaguru, P., Narahari, R., and Patel, M. (1992). "Flexural toughness of steel fiber reinforced concrete." *ACI Mater. J.,* 89(6), 541-546.

Bencardino, F., Rizzuti, L., Spadea, G., and Swamy, R. N. (2008). "Stress-strain behavior of steel fiber-reinforced concrete in compression." *J. Mater. Civ. Eng.,* 20(3), 255-263.

Bhargava, P., Sharma, U. K., and Kaushik, S. K. (2006). "Compressive stress-strain behavior of small scale steel fibre reinforced high strength concrete cylinders." *J. Adv. Concr. Technol.*, 4(1), 109-121.

Biel, T. D., and Lee, H. (1996). "Magnesium Oxychloride Cement Concrete with Recycled Tire Rubber." *Transportation Research Record,* 1561, 6-12.

Buyukozturk, O. (2004). "Mechanics and Design of Concrete Structures, Outline 6 - Ductility and Deflections." *Massachusetts: Massachusetts Institute of Technology*. 1-9

Chandrangsu, K., and Naaman, A. E. (2003). "Comparison of tensile and bending response of three high performance fiber reinforced cement composites." *Proceeding pro 030: high performance fiber-reinforced cement composites (HPFRCC4), RILEM Publications*, 259-274.

Chao, S.H., Naaman, A. E., and Parra-Montesinos, G. J. (2006). "Bond behavior of strand embedded in fiber reinforced cementitious composites." *PCI Journal*, 51(6), 56-71.

Corinaldesi, V., and Moriconi, G. (2011). "Characterization of self-compacting concretes prepared with different fibers and mineral additions." *Cement and Concrete Composites, 33*(5), 596-601.

Cottrell, A. H. (1964). "Strong solids." *Proceedings of the Royal Society, Series A A282*, 2-9.

Dhonde, H. B., Mo, Y. L., Hsu, T. T., and Vogel, J. (2007). "Fresh and hardened properties of self-consolidating fiber-reinforced concrete." *ACI Mater. J.,* 104(5), 491-500.

Eldin, N. N., and Senouci, A. B. (1993). "Rubber-tire particles as concrete aggregate." *Journal of Materials in Civil Engineering,* 5(4), 478-496.

Environmental Protection Agency. (2013). *Wastes - Resource Conservation - Common Wastes & Materials - Scrap Tires*. Retrieved from U.S. Environmental Protection Agency Web Site: http://www.epa.gov/epawaste/conserve/materials/tires/faq.htm

Ezeldin, A. S., and Balaguru, P. N. (1992). "Normal and high-strength fiber reinforced concrete under compression." *J. Mater. Civ. Eng.,* 4(4), 415-429.

Ghaly, A. M., and Cahill(IV), J. D. (2005). "Correlation of strength, rubber content, and water to cement ratio in rubberized concrete." *Canada Journal of Civil Engineering,* 32(6), 1075-1081.

Grace. (2014). *ADVA 190: High-range water-reducing admixture* [Data Sheet]. Retrieved from https://grace.com/construction/en-us/Documents/DC-60A_ADVA_190_11_14_07.pdf

Hassoun, M. N., and Sahebjam, K. (1985) "Plastic hinge in two-span reinforced concrete beams containing steel fibers." *Proceedings of the Canadian Society for Civil Engineering*, 119-139.

Helfet, J. L., and Harris, B. (1972). "Fracture toughness of composites reinforced with discontinuous fibres." *J. Mater. Sci.,* 7(5), 494-498.

Hsu, L. S., and Hsu, C. T. (1994). "Stress-strain behavior of steel-fiber high-strength concrete under compression." *ACI Struct. J.,* 91(4), 448-457.

Huang, B., Li, G., Pang, S.-S., and Eggers, J. (2004). "Investigation into waste tire rubber-filled concrete." *Journal of Materials in Civil Engineering*, 16(3), 187-194.

Kanda, T., and Li, V. (1998). "Interface property and apparent strength of a high strength hydrophilic fiber in cement matrix." *ASCE Journal of Materials in Civil Engineering,* 10(1), 5-13.

Khaloo, A. R., Dehestani, M., and Rahmatabadi, P. (2008). "Mechanical properties of concrete containing a high volume of tire-rubber particles." *Waste Management,* 28(12), 2472-2482.

Khatib, Z. K., and Bayomy, F. M. (1999). "Rubberized portland cement concrete." *Journal of Materials in Civil Engineering*, 11(3), 206-213.

Kim, D. j., Naaman, A. E., and El-Tawil, S. (2008). "Comparitive flexural behavior of four fiber reinforced cementitious composites." *Cement and Concrete Composites,* 30(10), 917-928.

Li, V. C. (1992). "A simplified micromechanical model of compressive strength of fiber-reinforced cementitious composites." *Cement & Concrete Composites,* 14(2), 131-141.

Li, V. C., Wu, C., Wang, S., Ogawa, A., and Saito, T. (2002). Interface tailoring for strain-hardening polyvinyl alcohol-engineered cementitious composite (PVA-ECC)." *ACI Materials Journal*, 99(5), 463-472.

Mansur, M. A., Chin, M. S., and Wee, T. H. (1999). "Stress-strain relationship of high-strength fiber concrete in compression." *J. Mater. Civ. Eng.,* 11(1), 21-29.

Morton, J., and Groves, G. W. (1974). "The cracking of composites consisting of discontinuous ductile fibres in a brittle matrix-effect of fibre orientation." *Journal of Materials Science,* 9(9), 1436-1445.

Morton, J., and Groves, G. W. (1976). "The effect of metal wires on the fracture of a brittle-matrix composite." *Journal of Materials Science,* 11(4), 617-622.

Mydin, M. A., and Soleimanzadeh, S. (2012). "Effect of polypropylene fiber content on flexural strength of lightweight foamed concrete at ambient and elevated temperatures." *Adv. Appl. Sci. Res.,* 3(5), 2837-2846.

Naaman, A. E. (2003). "Engineered steel fibers with optimal properties for reinforcement of cement composites." *Journal of Advanced Concrete Technology,* 1(3), 241-252.

Naaman, A.E., and Reinhardt, H.W. (1996). "Characterization of high performance fiber reinforced cement composites-HPFRCC." *High Performance Fiber Reinforced Cement Composites 2, Proc., 2nd Int. RILEM Workshop,* A.E. Naaman and H.W. Reinhardt, eds., E and FN Spon, Ann Arbor Mich., 1-24

Nataraja, M. C., Dhang, N., and Gupta, A. P. (1999). "Stress strain curve for steel-fiber reinforced concrete under compression." *Cem. Concr. Compos.,* 21(5-6), 383-390.

Noushini, A., Samali, B., and Vessalas, K. (2013). "Effect of polyvinyl alcohol (PVA) fibre on dynamic and material properties of fibre reinforced concrete." *Construction and Building Materials,* 49, 374-383.

Nycon. (2014). *Nycon Type I – Steel Fiber Needles* [Data Sheet]. Retrieved from http://nycon.com/wp-content/uploads/2013/08/NyconSFTypeINeedlesSheet011012.pdf

Otter, D. E., and Naaman, A. E. (1988). "Properties of steel fiber reinforced concrete under cyclic loading." *ACI Materials Journal*, 85(4), 254-261.

Ou, Y.-C., Tsai, M.-S., Liu, K.-Y., and Chang, K.-C. (2012). "Compressive behavior of steel-fiber-reinforced concrete with a high reinforcing index." *Journal of Materials in Civil Engineering*, 24(2), 207-215.

Outwater, J. P., and Murphy, M. C. (1969). "On the fracture energy of unidirectional laminate", in proceedings of 24th Annual Technical Conference of Reinforced Plastic/Composites Division, The society of the Plastics Industry Inc., Composite Div., New York, Paper No. 11C.

Park, R., and Paulay, T. (1975). *Reinforced concrete structures*. Wiley, New York. Print.

Parra-Montesinos, G. J., and Chompreda, P. (2007). “Deformation capacity and shear strength of fiber-reinforced cement composite flexural members subjected to displacement reversals.” *Journal of Structural Engineering*, 133(3), 421-431.

Popovics, S. (1987). “A hypothesis concerning the effects of macro-porosity on mechanical properties of concrete.” *Proc., SEM/RELIM Int. Conf. on Fracture of Concrete and Rock*, 170-174.

Rubber Manufacturers Association. (2013). *U.S. Scrap Tire Management Summary 2005-2009.* Washington, DC. http://www.rma.org/download/scrap-tires/market-reports/US_STMarkets2009.pdf

Segre, N., and Joekes, I. (2000). “Use for tire rubber particles as addition to cement paste.” *Cement Concrete Res.,* 30(9), 1421-1425.

Shao, Y., and Shah, S. P. (1997). “Mechanical properties of PVA fiber reinforced cement composites fabricated by extrusion processing.” *ACI Materials Journal*, 94(6), 555-564.

Skripkiunas, Gintautas, Audrius Grinys, and Benjaminas Cernius. (2007). "Deformation properties of concrete with rubber waste additives." *Materials Science,* 13(3), 219-23.

Soranakom, Chote, and Barzin Mobasher. (2009). "Flexural design of fiber-reinforced concrete." *ACI Materials Journal*, 106(5), 461-69.

Soroushian, P., and Bayasi, Z. (1991). “Fiber type effects on the performance of steel fiber reinforced concrete.” *ACI Materials Journal,* 88(2), 129-134.

Soulioti, D. V., Barkoula, N. M., Paipetis, A., and Matikas, T. E. (2011). “Effects of fibre geometry and volume fraction on the flexural behaviour of steel-fibre reinforced concrete.” *Strain,* 47(s1), 534-541.

Swamy, R. N., and Al-Ta'an, S. A. (1981). "Deformation and ultimate strength in flexural of reinforced concrete beams made with steel fiber concrete," *ACI Structural Journal*, 78(5), 395-405.

Taha, M. M., El-Dieb, A. S., El-Wahab, M. A., and Abdel-Hameed, M. E. (2008). "Mechanical, fracture, and microstructural investigations of rubber concrete." *Journal of Materials in Civil Engineering*, 20(10), 640-649.

Thomas, J., and Ramaswamy, A. (2007). "Mechanical properties of steel fiber-reinforced concrete." *Journal of Materials in Civil Engineering,* 19(5), 385-392.

Topçu, I. B. (1995). "The properties of rubberized concretes." *Cement and Concrete Research,* 25(2), 304-310.

Toutanji, H. A. (1996). "The use of rubber tire particles in concrete to replace mineral aggregate." *Cement and Concrete Composites,* 18(12), 135-139.

Toutanji, H. A., Xu, B., and Gilbert, J. (2010). "Impact resistance of poly(vinyl alcohol) fiber reinforced high-performance organic aggregate cementitious material." *Cement and Concrete Research,* 40(2), 347-351.

Vandewalle, L. et al., (Oct. 2003). "Test and design methods for steel fibre reinforced concrete-σ-ε design method—final recommendation," *Materials and Structures*, 36(262), 560-567.

Wang, Y., Backer, S. (1989). "Toughness determination for fibre reinforced concrete." *The International Journal of Cement Composites and Lightweight Concrete,* 11(1), 11,18-19.

Ward, R., Yamanobe, K., Li, V., and Backer, S. (1989). "Fracture resistance of acrylic fiber reinforced mortar in shear and flexure." *In Fracture Mechanics: Application to Concrete,* V.C. Li and Z. Bazant, eds., *ACI SP-118*, 17-68.

Willie, K., and Naaman, A. E. (2012). "Pullout behavior of high-strength steel fibers embedded in ultra-high-performance concrete." *ACI Materials Journal*, 109(4), 479-487.

Wu, H.-C., and Li, V. C. (1994). "Trade-off between strength and ductility of random discontinuous fiber reinforced cementitious composites." *Cement and Concrete Composites,* 16(1), 23-29.

Zheng, L., Huo, X. S., and Yuan, Y. (2008). "Strength, modulus of elasticity, and brittleness index of rubberized concrete." *Journal of Materials in Civil Engineering*, 20(11), 692-699.

APPENDIX A

Mix PL1

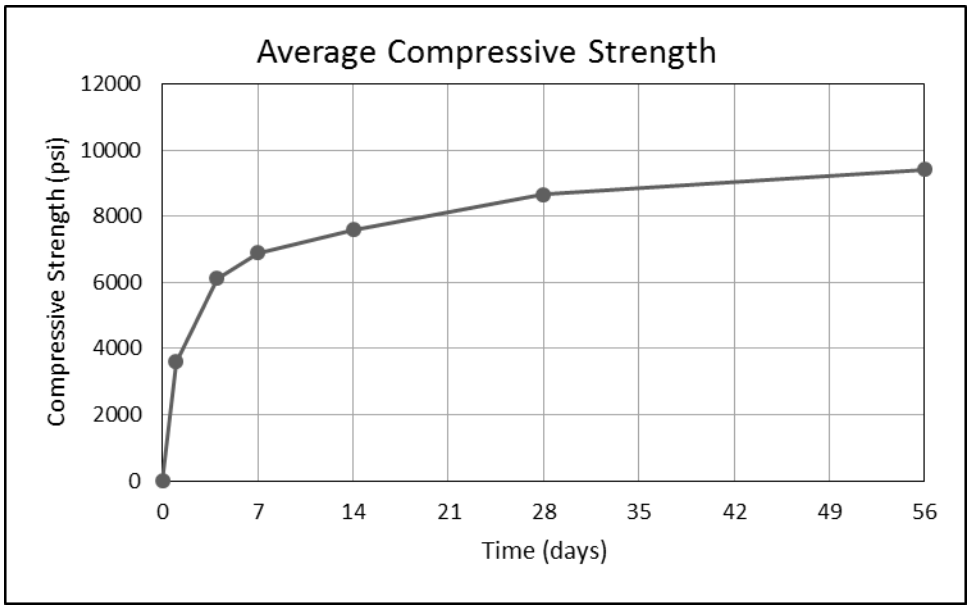

Figure A1. Average Compressive Strength for Mix PL1

Day	Test 1	Test 2	Test 3	Average
Compression, f_c (psi)				
1	3581	3574	3632	3596
4	5794	6509	6060	6121
7	6659	6893	7157	6903
14	7552	7847	7371	7590
28	8492 8733	8293 8711	8875 8927	8672
56	9223	9232	9792	9416
Split Tensile, f_r (psi)				
28	693	617	661	657
Modulus, E (ksi)				
28	5284	5082	5115	5160

Table A1. Properties of Mix PL1

Figure A2. Mix PL1 - 28-day Compressive Failure

Mix 5C

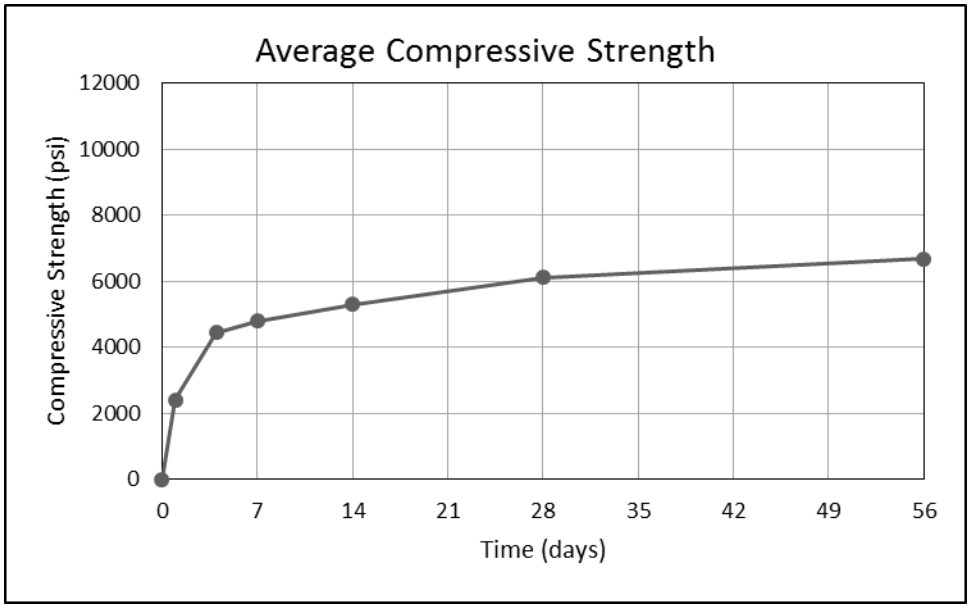

Figure A3. Average Compressive Strength for Mix 5C

Day	Test 1	Test 2	Test 3	Average
Compression, f_c (psi)				
1	2218	2596	2418	2411
4	4517	4126	4702	4448
7	4478	4662	5244	4795
14	5156	5427	5327	5303
28	5955 6080	5375 6443	6327 6493	6112
56	6642	6897	6472	6670
Split Tensile, f_r (psi)				
28	494	473	584	517
Modulus, E (ksi)				
28	4479	4508	4321	4436

Table A2. Properties of Mix 5C

Figure A4. Mix 5C - 28-day Compressive Failure

Mix 5F

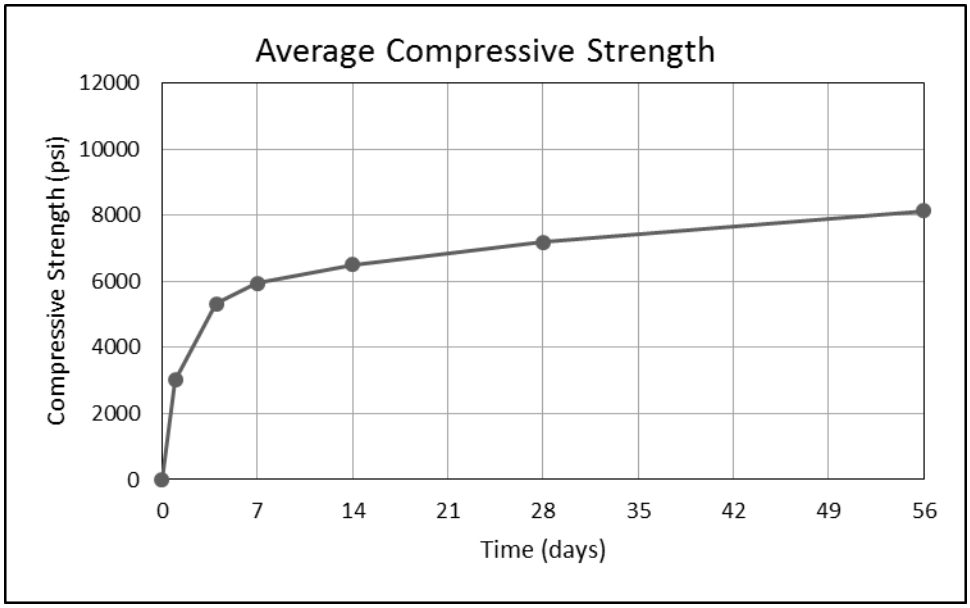

Figure A5. Average Compressive Strength for Mix 5F

Day	Test 1	Test 2	Test 3	Average
Compression, f_c (psi)				
1	2997	3003	3041	3014
4	5397	5429	5140	5322
7	6034	5765	6052	5950
14	6778	6350	6408	6512
28	7350 7416	6973 7064	7543 6793	7190
56	7774	8451	8208	8144
Split Tensile, f_r (psi)				
28	645	632	674	650
Modulus, E (ksi)				
28	4917	5077	4823	4939

Table A3. Properties of Mix 5F

Figure A6. Mix 5F - 28-day Compressive Failure

Mix 5CF

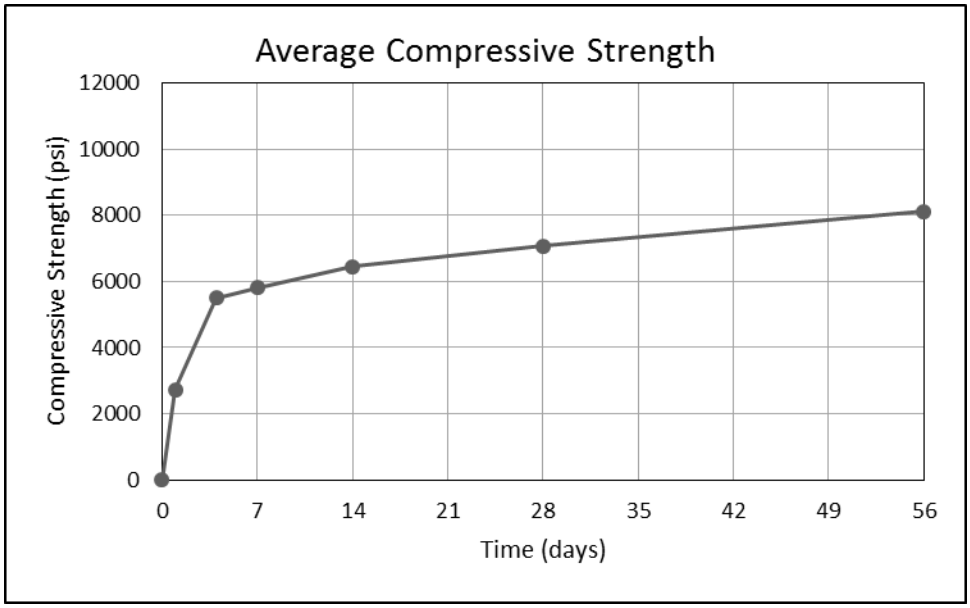

Figure A7. Average Compressive Strength for Mix 5CF

Day	Test 1	Test 2	Test 3	Average
Compression, f_c (psi)				
1	3184	2458	2572	2738
4	5544	5298	5641	5494
7	5765	5733	5952	5817
14	6587	6277	6488	6451
28	6931 6622	7345 6883	7150 7542	7079
56	7669	8369	8325	8121
Split Tensile, f_r (psi)				
28	617	564	550	577
Modulus, E (ksi)				
28	4726	5317	5562	5202

Table A4. Properties of Mix 5CF

Figure A8. Mix 5CF - 28-day Compressive Failure

Mix 10C

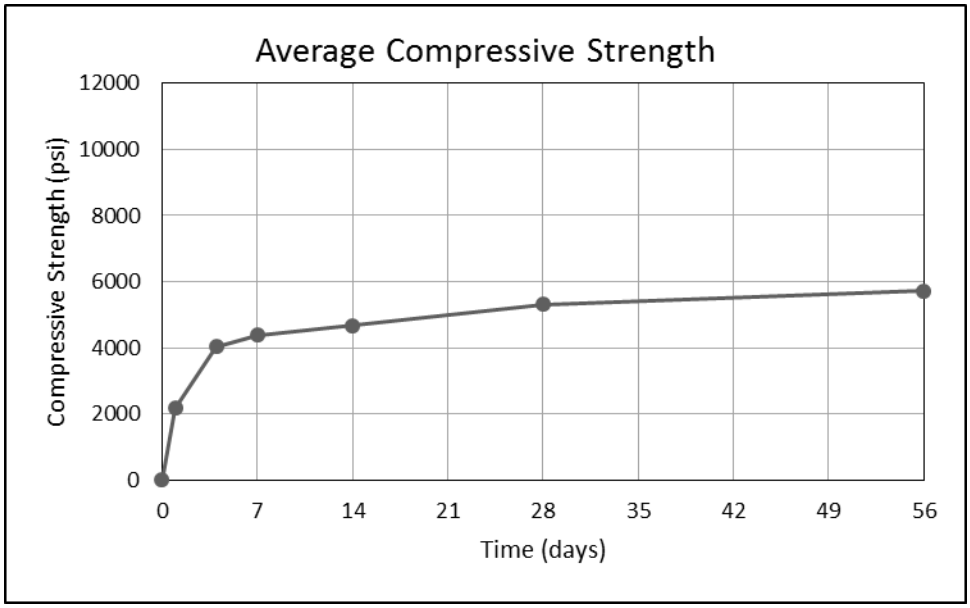

Figure A9. Average Compressive Strength for Mix 10C

Day	Test 1	Test 2	Test 3	Average
Compression, f_c (psi)				
1	2162	2192	2158	2171
4	3642	4122	4316	4027
7	4421	4451	4261	4378
14	4557	4666	4809	4677
28	5094 5558	5258 5358	5410 5206	5314
56	5762	6128	5270	5720
Split Tensile, f_r (psi)				
28	509	570	553	544
Modulus, E (ksi)				
28	4455	4560	4043	4353

Table A5. Properties of Mix 10C

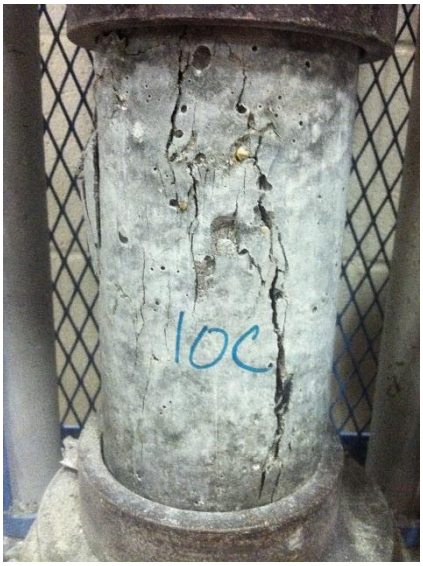

Figure A10. Mix 10C - 28-day Compressive Failure

Mix 10F

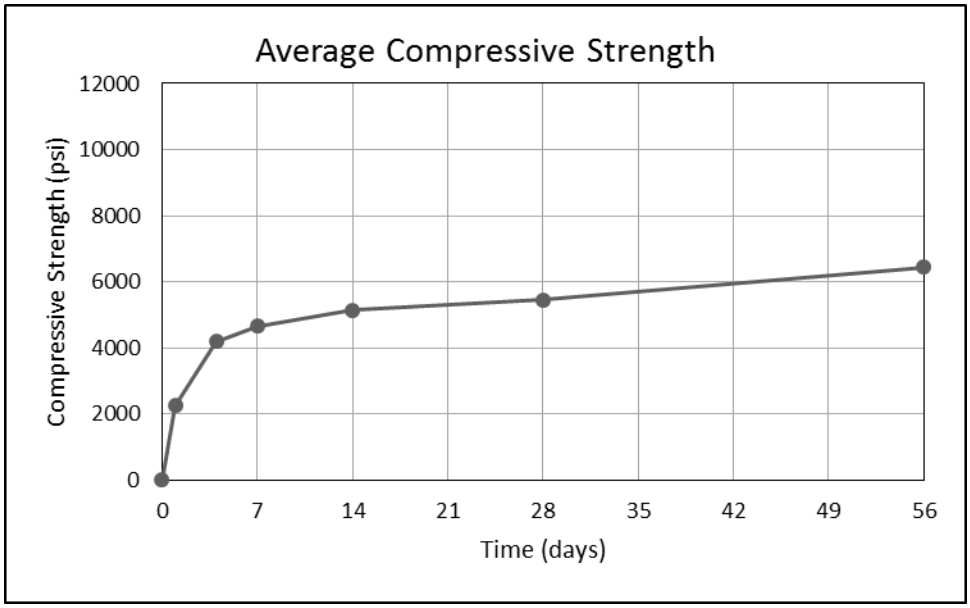

Figure A11. Average Compressive Strength for Mix 10F

Day	Test 1	Test 2	Test 3	Average
Compression, f_c (psi)				
1	2109	2248	2395	2251
4	4275	4097	4219	4197
7	4463	4829	4695	4662
14	5143	5123	5152	5139
28	5246 5396	5428 5531	5380 5751	5455
56	6459	6260	6600	6440
Split Tensile, f_r (psi)				
28	494	468	603	522
Modulus, E (ksi)				
28	4055	4268	3330	3884

Table A6. Properties of Mix 10F

Figure A12. Mix 10F - 28-day Compressive Failure

Mix 10CF

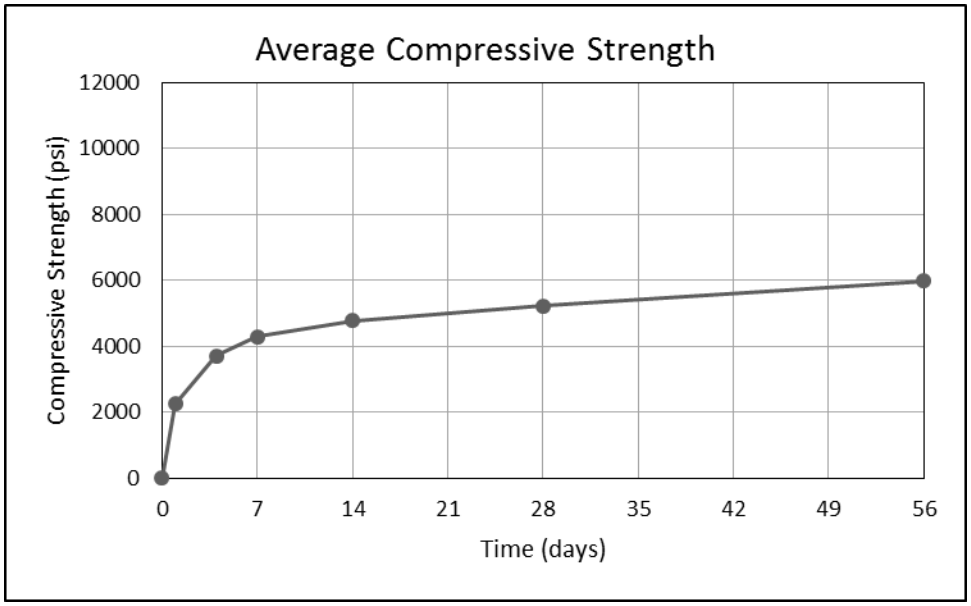

Figure A13. Average Compressive Strength for Mix 10CF

Day	Test 1	Test 2	Test 3	Average
Compression, f_c (psi)				
1	2223	2440	2123	2262
4	3463	3686	3970	3706
7	3840	4732	4318	4297
14	4645	4692	4992	4776
28	5059 5674	5516 5138	4916 5065	5228
56	6035	5766	6123	5975
Split Tensile, f_r (psi)				
28	585	425	551	520
Modulus, E (ksi)				
28	4365	4307	3705	4126

Table A7. Properties of Mix 10CF

Figure A14. Mix 10CF - 28-day Compressive Failure

Mix 15C

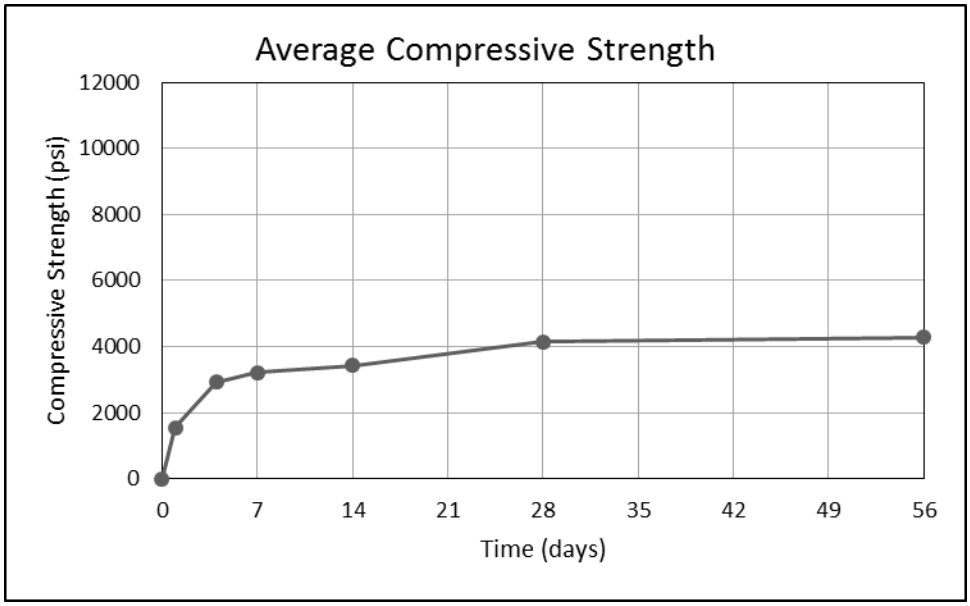

Figure A15. Average Compressive Strength for Mix 15C

Day	Test 1	Test 2	Test 3	Average
Compression, f_c (psi)				
1	1551	1522	1558	1544
4	2861	3065	2835	2920
7	3347	2718	3589	3218
14	3454	3290	3554	3433
28	3558 4465	4189 4002	4441 4239	4149
56	4144	4427	4249	4273
Split Tensile, f_r (psi)				
28	451	436	466	451
Modulus, E (ksi)				
28	3939	3741	4005	3895

Table A8. Properties of Mix 15C

Figure A16. Mix 15C - 28-day Compressive Failure

Mix 15F

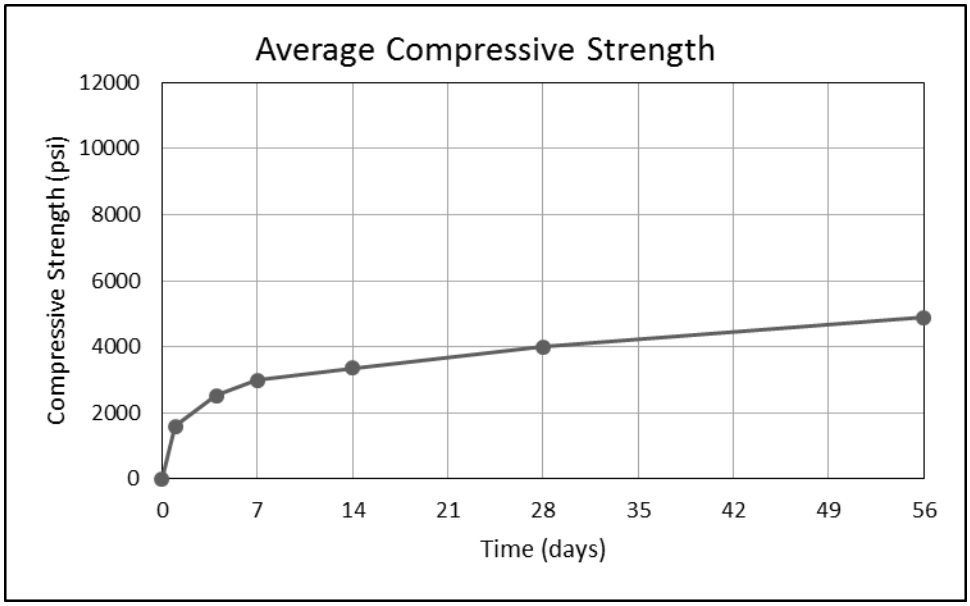

Figure A17. Average Compressive Strength for Mix 15F

Day	Test 1	Test 2	Test 3	Average
Compression, f_c (psi)				
1	1515	1602	1625	1581
4	2661	2567	2304	2511
7	2970	3057	2946	2991
14	3504	3274	3309	3362
28	3936 4173	4021 3990	3720 4086	3988
56	4946	4896	4843	4895
Split Tensile, f_r (psi)				
28	405	398	495	433
Modulus, E (ksi)				
28	3490	3481	3593	3521

Table A9. Properties of Mix 15F

Figure A18. Mix 15F - 28-day Compressive Failure

Mix 15CF

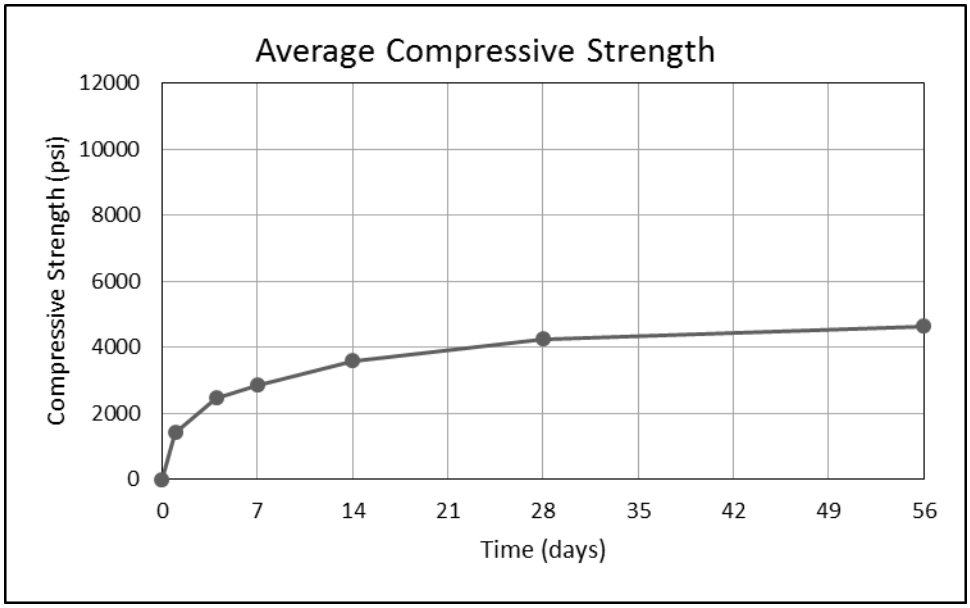

Figure A19. Average Compressive Strength for Mix 15CF

Day	Test 1	Test 2	Test 3	Average
Compression, f_c (psi)				
1	1436	1387	1426	1416
4	2432	2460	2533	2475
7	2906	3045	2640	2864
14	3601	3649	3517	3589
28	4035 4252	4022 4840	3580 4817	4258
56	4252	4840	4817	4636
Split Tensile, f_r (psi)				
28	505	482	420	469
Modulus, E (ksi)				
28	3739	4039	3794	3858

Table A10. Properties of Mix 15CF

Figure A20. Mix 15CF - 28-day Compressive Failure

Mix PL2

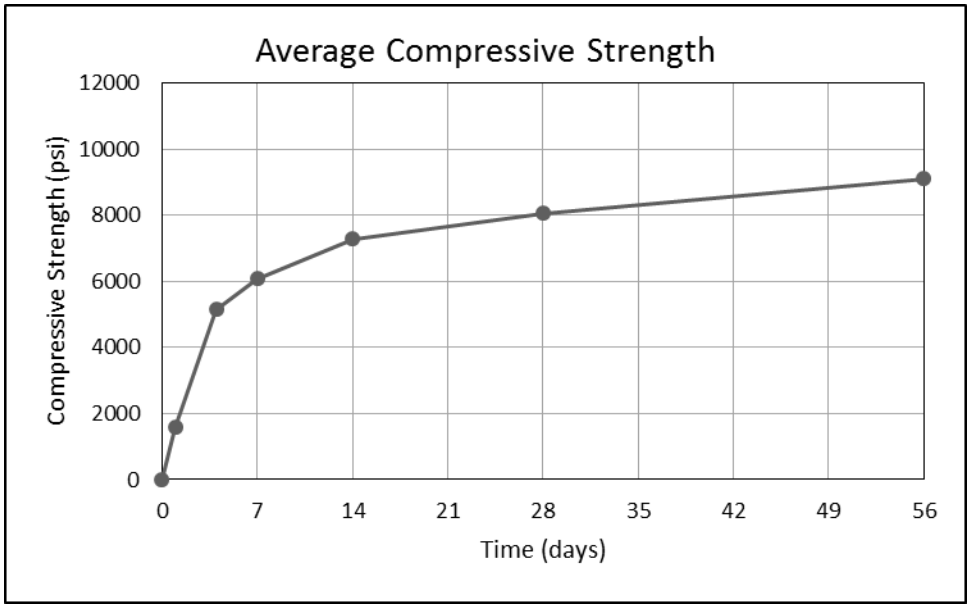

Figure A21. Average Compressive Strength for Mix PL2

Day	Test 1	Test 2	Test 3	Average
Compression, f_c (psi)				
1	1601	1644	1517	1587
4	5006	5074	5343	5141
7	6090	5929	6202	6074
14	7437	6936	7452	7275
28	8381 7953	8443 8287	7790 7437	8049
56	9096	9014	9207	9106
Split Tensile, f_r (psi)				
28	604	668	753	675
Modulus, E (ksi)				
28	4988	5449	5396	5278

Table A11. Properties of Mix PL2

Figure A22. Mix PL2 - 28-day Compressive Failure

Mix F1

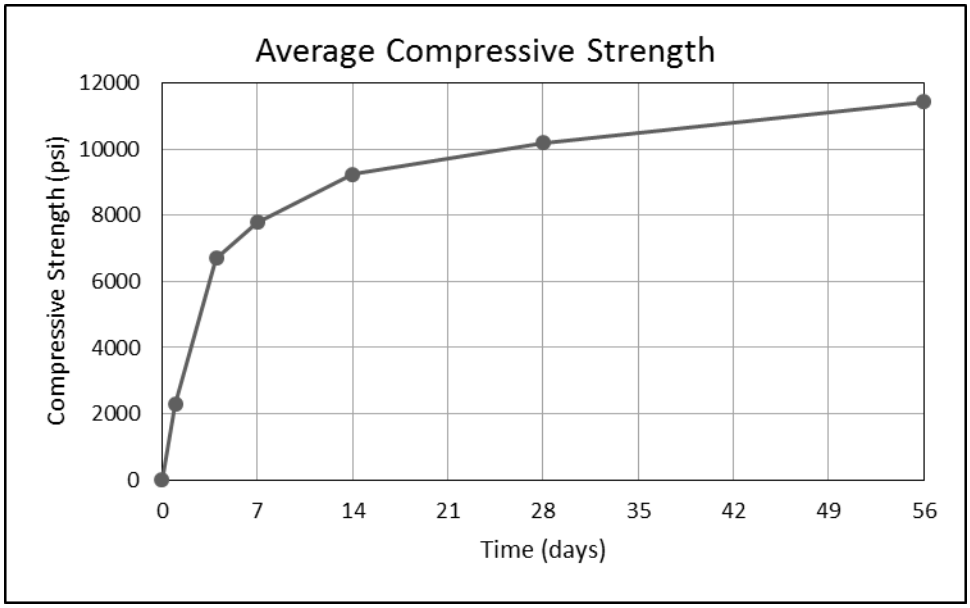

Figure A23. Average Compressive Strength for Mix F1

Day	Test 1	Test 2	Test 3	Average
Compression, f_c (psi)				
1	2416	2334	2102	2284
4	6512	6427	7153	6697
7	7581	7862	7928	7790
14	9479	9107	9154	9247
28	10450 10660	10130 10060	9658 10200	10193
56	11370	11270	11690	11443
Split Tensile, f_r (psi)				
28	903	946	991	946
Modulus, E (ksi)				
28	6029	5906	5682	5872

Table A12. Properties of Mix F1

Figure A24. Mix F1 - 28-day Compressive Failure

Mix F5C

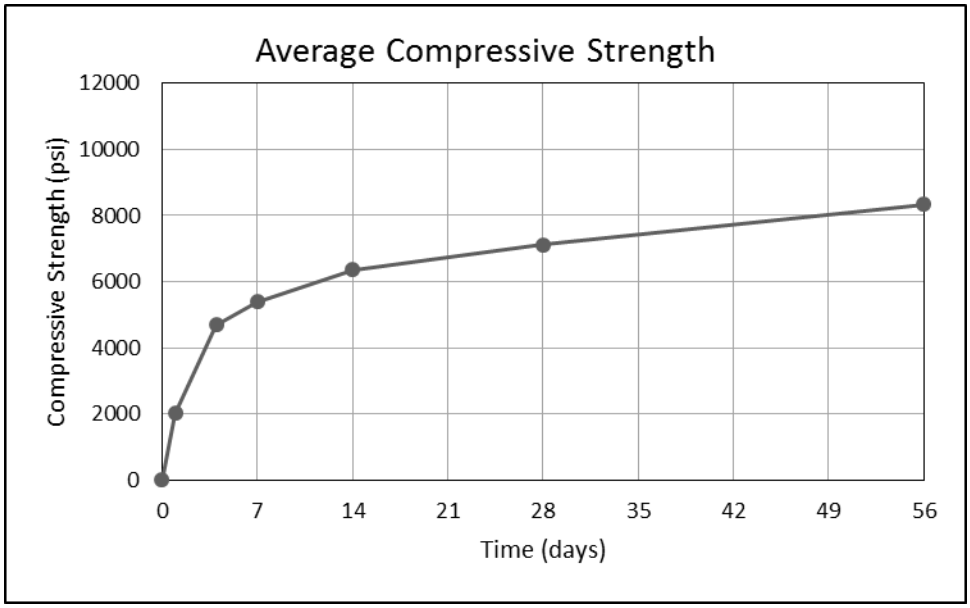

Figure A25. Average Compressive Strength for Mix F5C

Day	Test 1	Test 2	Test 3	Average
Compression, f_c (psi)				
1	1949	1981	2107	2012
4	4776	4659	4647	4694
7	5315	5514	5324	5384
14	6445	6486	6128	6353
28	7243 7054	7041 7036	7433 6919	7121
56	7588	8344	9091	8341
Split Tensile, f_r (psi)				
28	880	777	784	814
Modulus, E (ksi)				
28	4773	5167	5171	5037

Table A13. Properties of Mix F5C

Figure A26. Mix F5C - 28-day Compressive Failure

Mix F5F

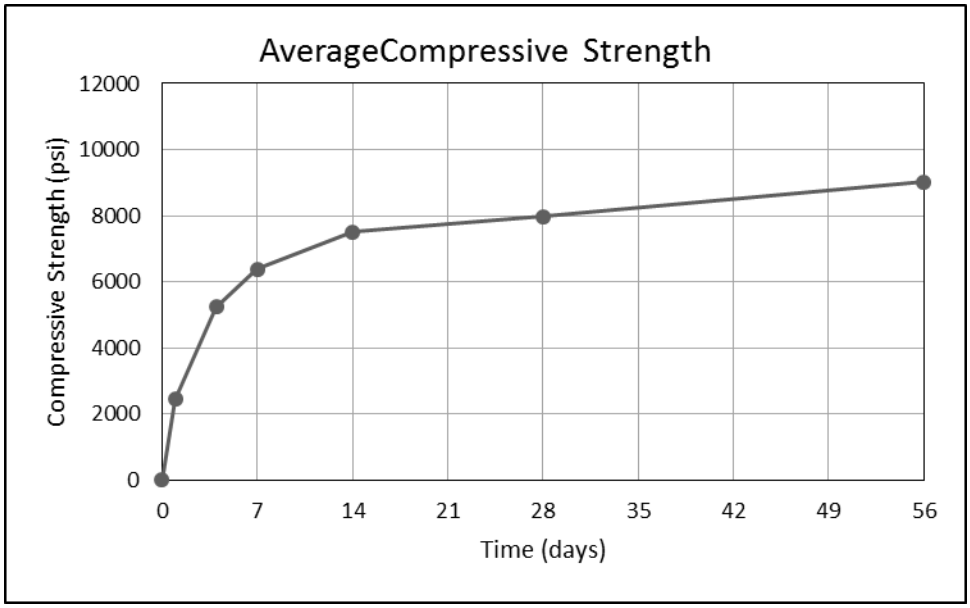

Figure A27. Average Compressive Strength for Mix F5F

Day	Test 1	Test 2	Test 3	Average
Compression, f_c (psi)				
1	2360	2469	2530	2453
4	5019	5353	5377	5250
7	6160	6317	6672	6383
14	7332	7546	7625	7501
28	7925 7903	7890 7903	8119 8099	7973
56	9173	9070	8851	9031
Split Tensile, f_r (psi)				
28	836	800	877	838
Modulus, E (ksi)				
28	5051	4950	4979	4994

Table A14. Properties of Mix F5F

Figure A28. Mix F5F - 28-day Compressive Failure

Mix F5CF

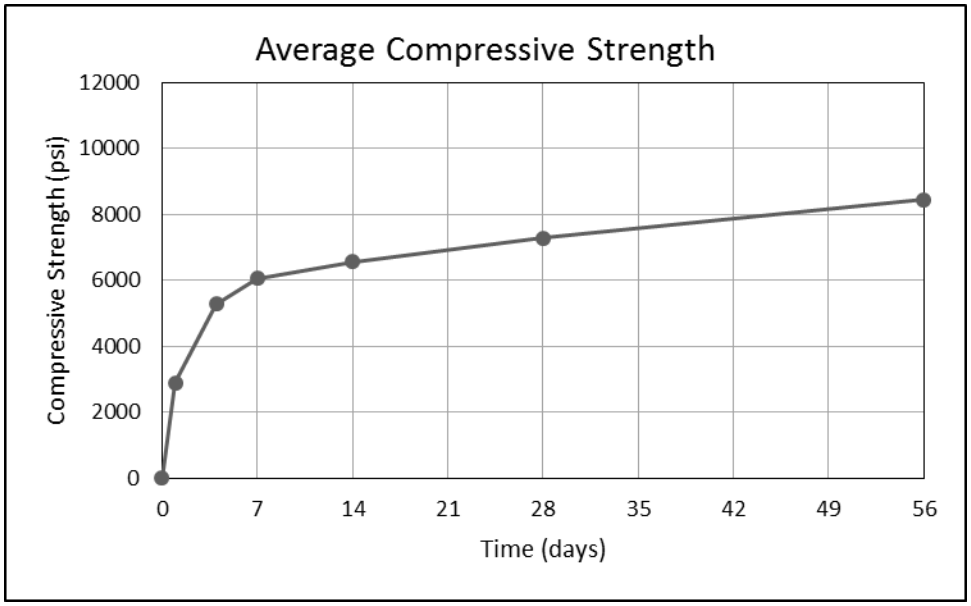

Figure A29. Average Compressive Strength for Mix F5CF

Day	Test 1	Test 2	Test 3	Average
Compression, f_c (psi)				
1	2954	2786	2970	2903
4	5472	5076	5276	5275
7	6148	5958	6064	6057
14	6770	6430	6500	6567
28	7177 7253	7376 7355	7373 7142	7279
56	8212	8209	8930	8450
Split Tensile, f_r (psi)				
28	812	721	763	765
Modulus, E (ksi)				
28	5232	5072	5067	5124

Table A15. Properties of Mix F5CF

Figure A30. Mix F5CF - 28-day Compressive Failure

Mix F10C

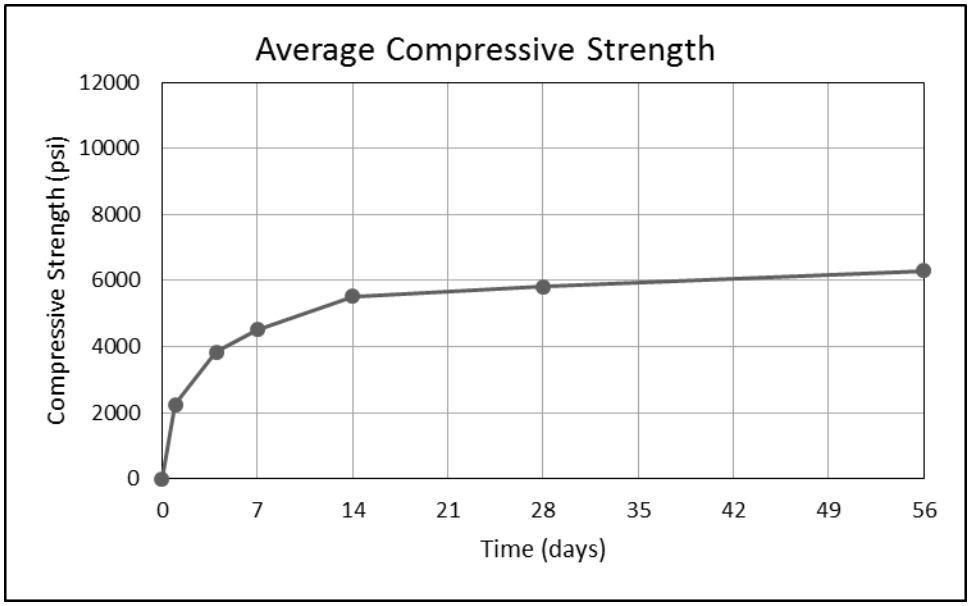

Figure A31. Average Compressive Strength for Mix F10C

Day	Test 1	Test 2	Test 3	Average
Compression, f_c (psi)				
1	2314	2344	2088	2249
4	3712	3988	3801	3834
7	4529	4666	4368	4521
14	5780	5100	5657	5512
28	5952 5783	5768 5949	5703 5730	5814
56	6180	6136	6563	6293
Split Tensile, f_r (psi)				
28	695	658	668	674
Modulus, E (ksi)				
28	5173	5143	4328	4881

Table A16. Properties of Mix F10C

Figure A32. Mix F10C - 28-day Compressive Failure

Mix F10F

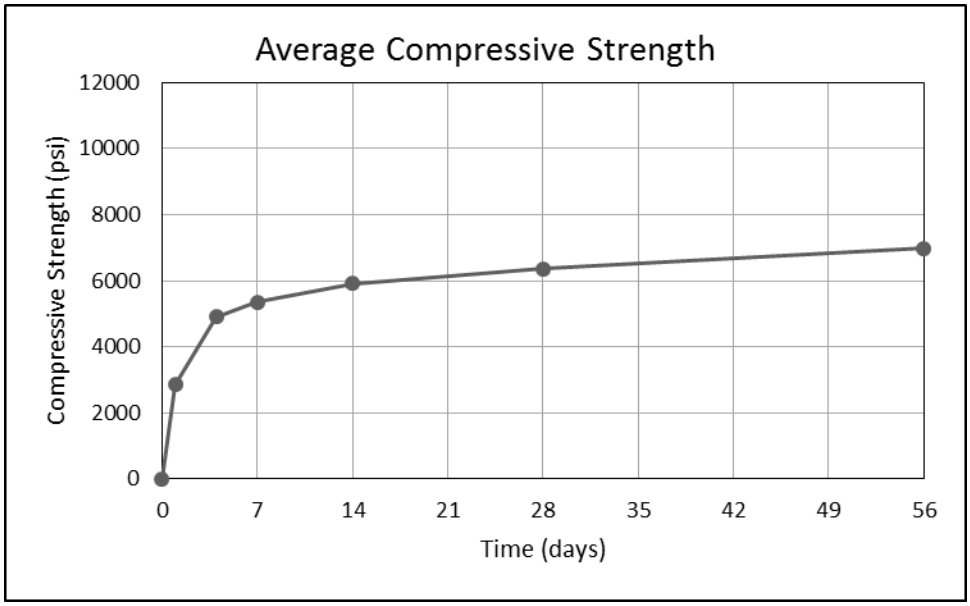

Figure A33. Average Compressive Strength for Mix F10F

Day	Test 1	Test 2	Test 3	Average
Compression, f_c (psi)				
1	2681	2905	2989	2858
4	4845	4974	4892	4904
7	5254	5420	5358	5344
14	6058	6037	5633	5909
28	6134 6905	6403 6368	6067 6242	6353
56	6956	7140	6827	6974
Split Tensile, f_r (psi)				
28	590	652	592	611
Modulus, E (ksi)				
28	4724	4569	4420	4571

Table A17. Properties of Mix F10F

Figure A34. Mix F10F - 28-day Compressive Failure

Mix F10CF

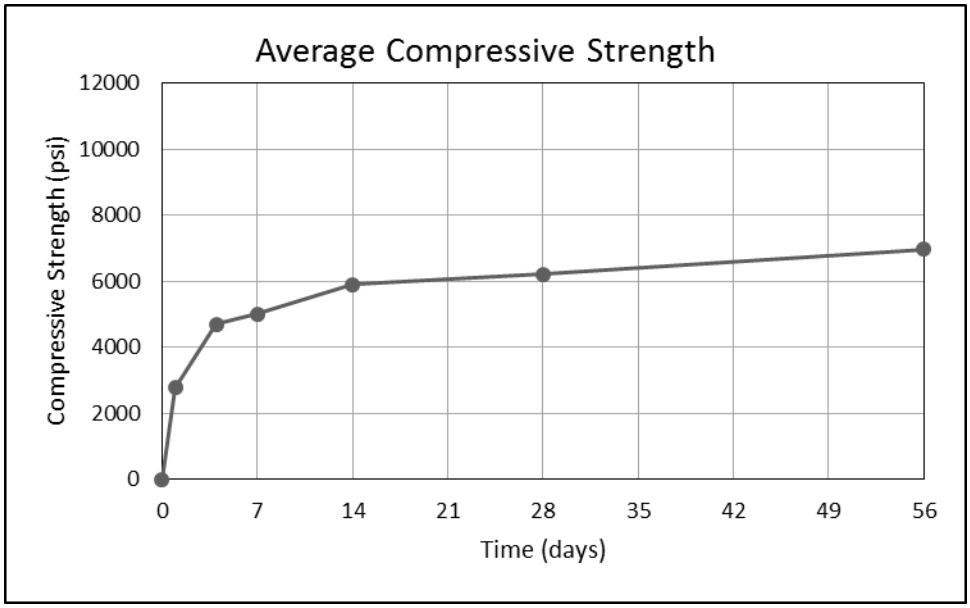

Figure A35. Average Compressive Strength for Mix F10CF

Day	Test 1	Test 2	Test 3	Average
Compression, f_c (psi)				
1	2851	2756	2720	2776
4	4520	4745	4804	4690
7	4856	4956	5202	5005
14	5961	5908	5809	5893
28	6415 6444	5821 6262	6119 6166	6205
56	7170	6859	6888	6972
Split Tensile, f_r (psi)				
28	742	711	766	740
Modulus, E (ksi)				
28	4759	4575	4575	4636

Table A18. Properties of Mix F10CF

Figure A36. Mix F10CF - 28-day Compressive Failure

Mix F15C

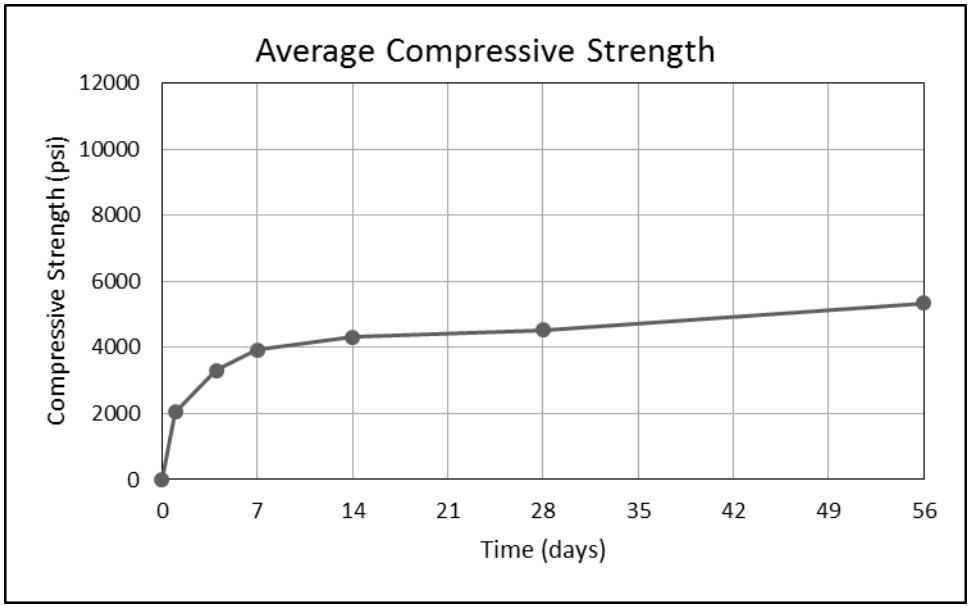

Figure A37. Average Compressive Strength for Mix F15C

Day	Test 1	Test 2	Test 3	Average
Compression, f_c (psi)				
1	1895	2077	2155	2042
4	3226	2941	3733	3300
7	3743	4018	4008	3923
14	4580	4059	4314	4318
28	4470 4206	4701 4777	4118 4865	4523
56	5427	5181	5424	5344
Split Tensile, f_r (psi)				
28	594	670	627	630
Modulus, E (ksi)				
28	3188	4242	4365	3932

Table A19. Properties of Mix F15C

Figure A38. Mix F15C - 28-day Compressive Failure

Mix F15F

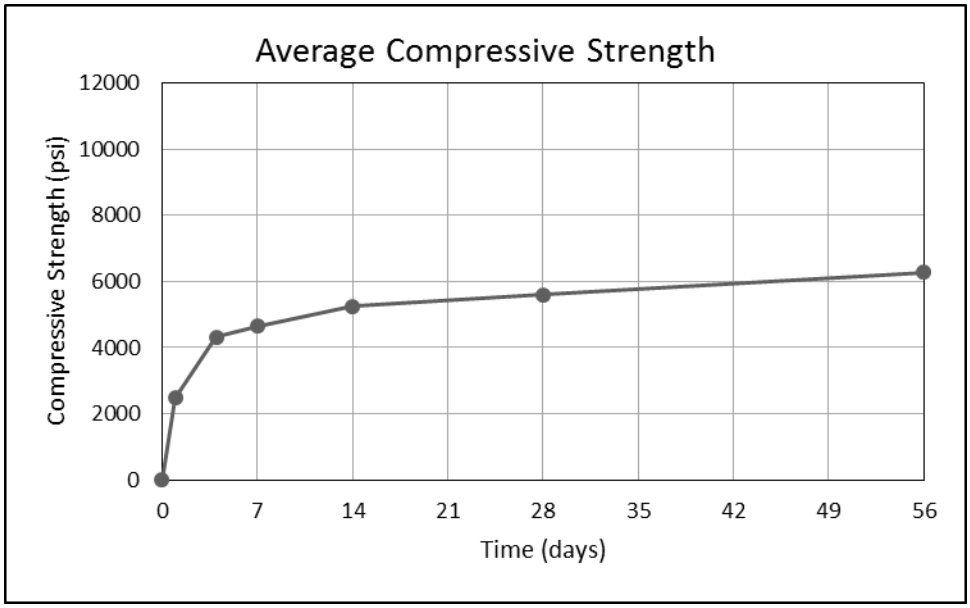

Figure A39. Average Compressive Strength for Mix F15F

Day	Test 1	Test 2	Test 3	Average
Compression, f_c (psi)				
1	2675	2413	2365	2484
4	4292	4143	4532	4322
7	4720	4608	4608	4645
14	5063	5330	5347	5247
28	5653 5764	5545 5515	5627 5533	5606
56	6505	5977	6373	6285
Split Tensile, f_r (psi)				
28	555	599	521	558
Modulus, E (ksi)				
28	3990	4065	4079	4045

Table A20. Properties of Mix F15F

Figure A40. Mix F15F - 28-day Compressive Failure

Mix F15CF

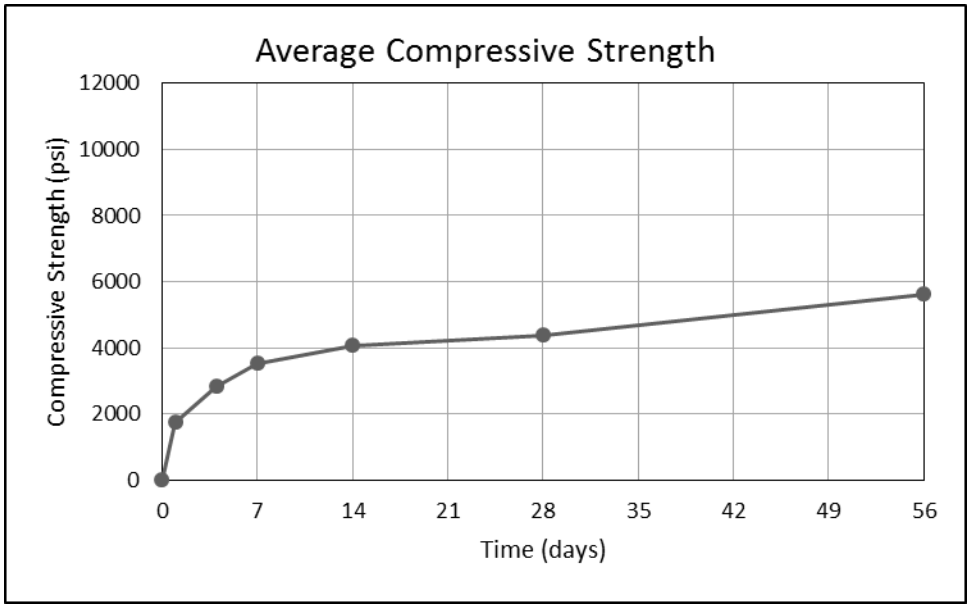

Figure A41. Average Compressive Strength for Mix F15CF

Day	Test 1	Test 2	Test 3	Average
Compression, f_c (psi)				
1	1792	1658	1776	1742
4	2878	2752	2842	2824
7	3602	3510	3460	3524
14	3830	4188	4184	4067
28	3937 4890	4433 4934	3914 4155	4377
56	5425	5448	5975	5616
Split Tensile, f_r (psi)				
28	658	561	570	596
Modulus, E (ksi)				
28	4434	3916	3928	4093

Table A21. Properties of Mix F15CF

Figure A42. Mix F15CF - 28-day Compressive Failure

Mix F2

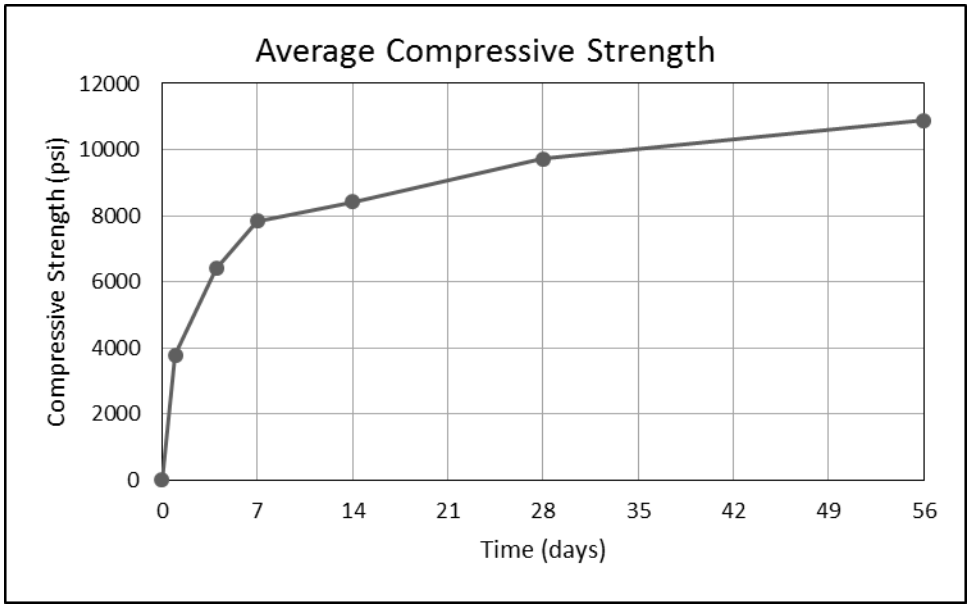

Figure A43. Average Compressive Strength for Mix F2

Day	Test 1	Test 2	Test 3	Average
Compression, f_c (psi)				
1	3831	3845	3710	3795
4	6383	6356	6476	6405
7	7728	8015	7796	7846
14	8259	8368	8646	8424
28	9664 9781	9304 9849	10190 9532	9720
56	10450	11140	11070	10887
Split Tensile, f_r (psi)				
28	915	852	841	869
Modulus, E (ksi)				
28	5537	5458	5508	5501

Table A22. Properties of Mix F2

Figure A44. Mix F2 - 28-day Compressive Failure

APPENDIX B

Rebar

In order to analyze the concrete beams under flexure using strain compatibility, the stress-strain behavior of the half inch diameter steel rebar used as reinforcement in the beams was required. A tension test using an MTS machine was performed on three rebar specimens cut from the same joints of rebar that were used for the beams. All three tests yeilded very similar stress strain plots. The, stress strain plot selected for use in strain compatiblity calculations is shown in Figure B1 below.

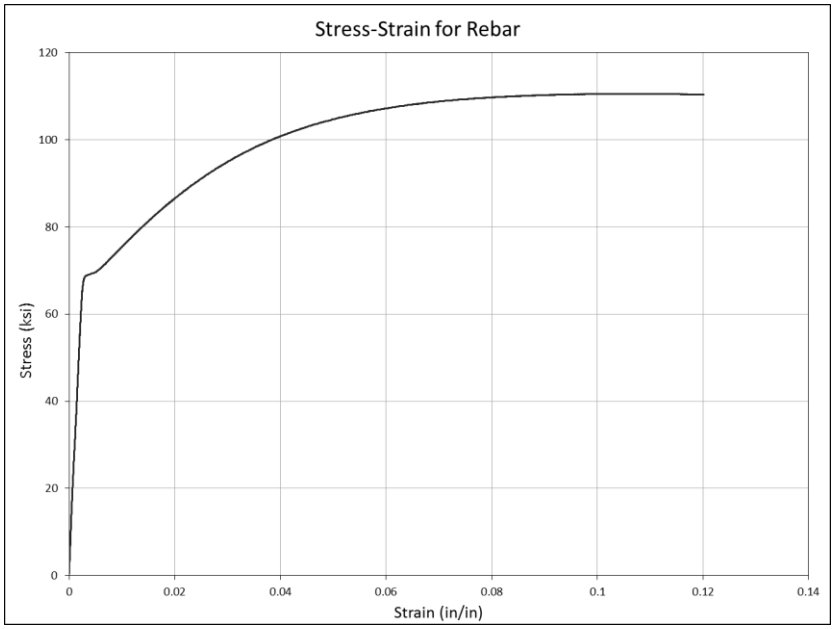

Figure B1. Stress-Strain Curve for Rebar

Using this stress strain curve, the modulus of elasticity, yield stress, proportional limit, and ultimate stress for the steel was determined. The proportional limit was determined to be 61.162 ksi corresponding to a strain of 0.243805%. Adding a linear trendline with the y-intercept set equal to zero to this data set yields an equation in which the slope is defined as the modulus of elasticity. The region labeled y1 shown in Figure B2 represents the initial

straight line portion of the stress strain curve or the point along the curve up to the proportional limit. The modulus of elasticity of the steel was determined to be 27,097 ksi.

Next, the yield stress and strain for the steel were determined. The yield point was determined using the 0.2 percent offset method. This graphical method in displayed in Figure B2. A line was plotted parallel to the straight line portion of the curve offset by 0.2 percent strain that extended beyond the full stress strain curve. The point of intersection of this line and the stress strain curve was taken as the yield point. The yield stress and strain were determined to be 69.394 ksi and 0.4567 percent respectively.

The ultimate stress and strain were determined to be 110.56 ksi and 10.56 percent. In order to simplify the stress strain curve for use in strain compatibility equations, the curve was broken down into different regions as shown in Figure B2. Each region is represented by a linear line. The corresponding linear equations and R^2 values are shown in the figure. The regions were adjusted until the R^2 values were nearly equal to 1 in order to ensure that each region was represented as accurately as possible by the linear equations. The limits to which each of the seven regions apply are shown in Table B1. The limits are represented as corresponding strain values for each region.

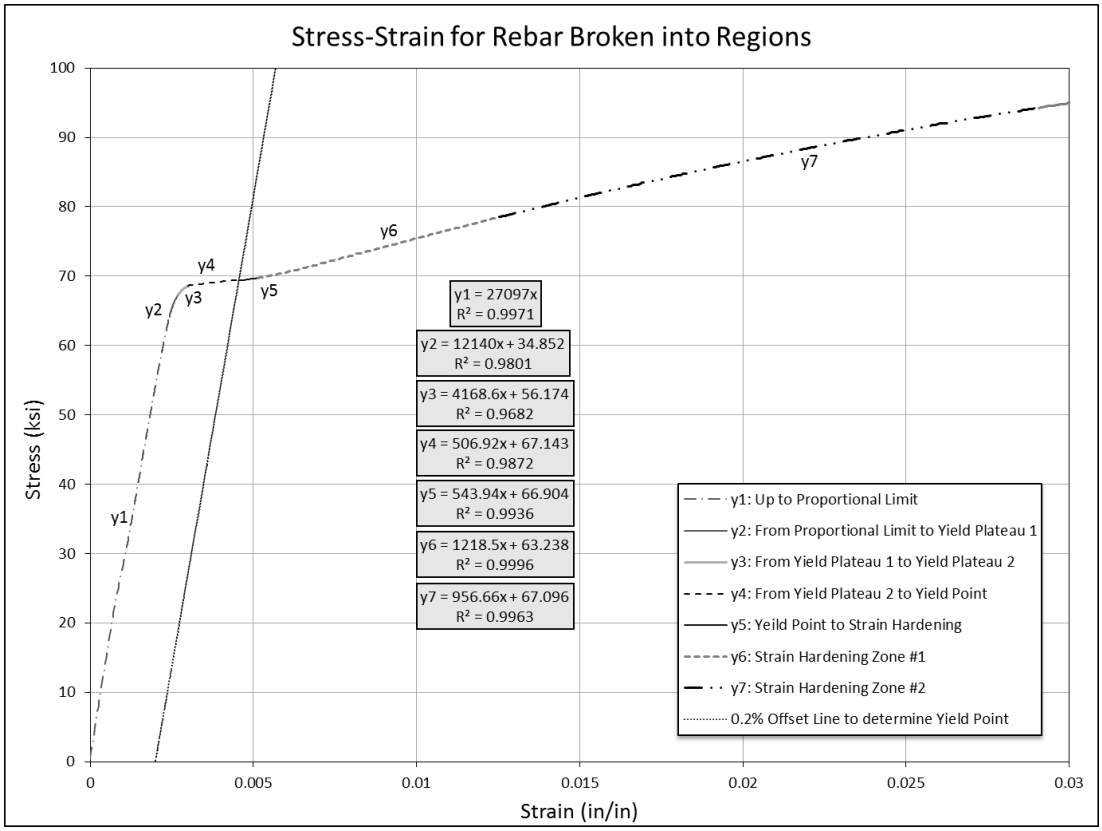

Figure B2. Stress-Strain Curve for Rebar broken into regions

Strain Limits per Region (in/in)		
Region	Lower Limit	Upper Limit
y1	0.0000000	0.0024380
y2	0.0024380	0.0026989
y3	0.0026989	0.0030034
y4	0.0030034	0.0045671
y5	0.0045671	0.0051354
y6	0.0051354	0.0125411
y7	0.0125411	0.0290784

Table B1. Strain Limits per Region for rebar

Concrete

The stress strain relationship of the concrete under compressive load was not determined during the experimental process. For the purposes of strain compatibility, the behavior given by the Modified Hognestad model shown in Figure B3 will be used.

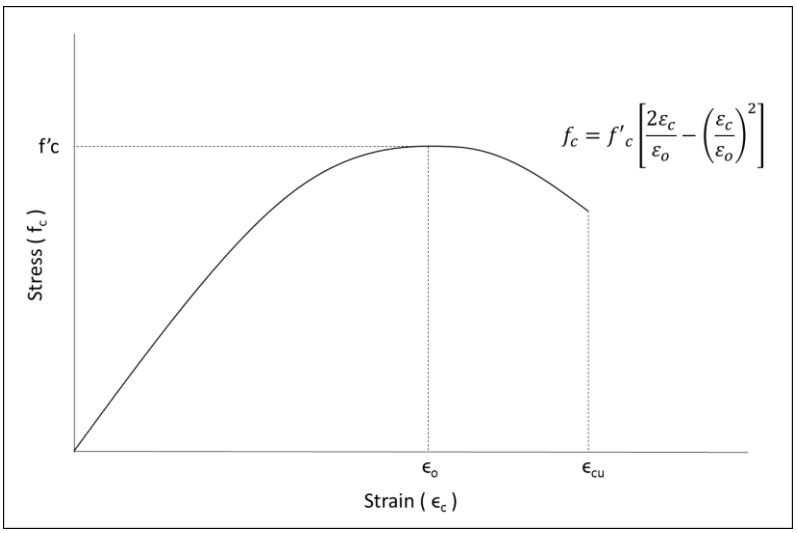

Figure B3. Modified Hognestad model for concrete (Park and Paulay 1975)

The ultimate strain of the concrete in compression (ϵ_{cu}) can vary depending on the type of concrete. Conventional concrete has an ultimate strain of 0.0038 to 0.004. Concrete that has rubber particles incorporated into the mix can have ultimate concrete strains that are 36 to 47 percent higher than plain concrete (Skripkiunas et al. 2007). Fiber-reinforced concrete can have significantly higher ultimate strains depending on the type and amount of fiber used. A lower bound value for the ultimate compressive strength of fiber-reinforced was suggested to be 0.0035 (Swamy and Al-Ta'an 1981; Hassoun and Sahebjam 1985). For the current research, an ultimate strain of 0.004 will be used for plain concrete and an ultimate strain of 0.005 will be used for rubber concrete and fiber-reinforced concrete. As can be seen in the tables of Appendix C, some of the concrete mixes did not reach this ultimate strain before an ultimate stress was reached. For these cases, the concrete strain that corresponded to the ultimate concrete stress was taken as the ultimate concrete strain for that mix.

Fibers

For the mixes that contained fibers, the tensile contribution from the fibers in the cracked section of the beam was taken into consideration. The behavior of steel fiber-

reinforced concrete in tension was idealized using the relationship developed by Chote et al. (2009). This relationship shown in Figure B4 is a strain-softening model. This model was chosen based on the assumption that the fiber-reinforced concrete in this current research would fall into the strain-softening category of fiber-reinforced concrete since rubber particles were added to the mix and little tailoring of the mix was done to create a strain hardening mixture. The factor shown in the diagram labeled "μ" was taken to be equal to 0.5 for use in this investigation. The ultimate tensile strain of the fiber-reinforced concrete (ϵ_{tu}) was taken as 0.025 (Vandewalle 2003). The ultimate tensile strength of the concrete (σ_{cr}) will be taken as the splitting tensile strength (f_r) for each mix as determined by this research.

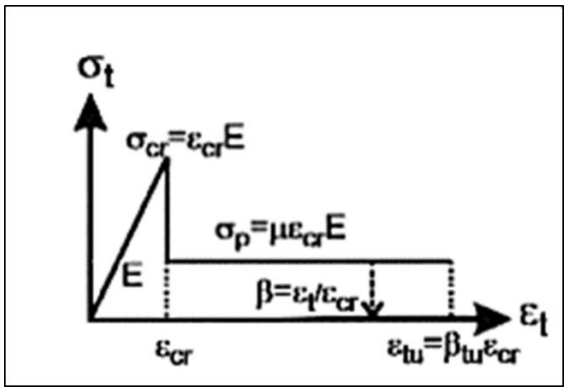

Figure B4. Idealized material model for strain-softening fiber-reinforced concrete (Soranakom and Mobasher 2009)

Strain Compatibility

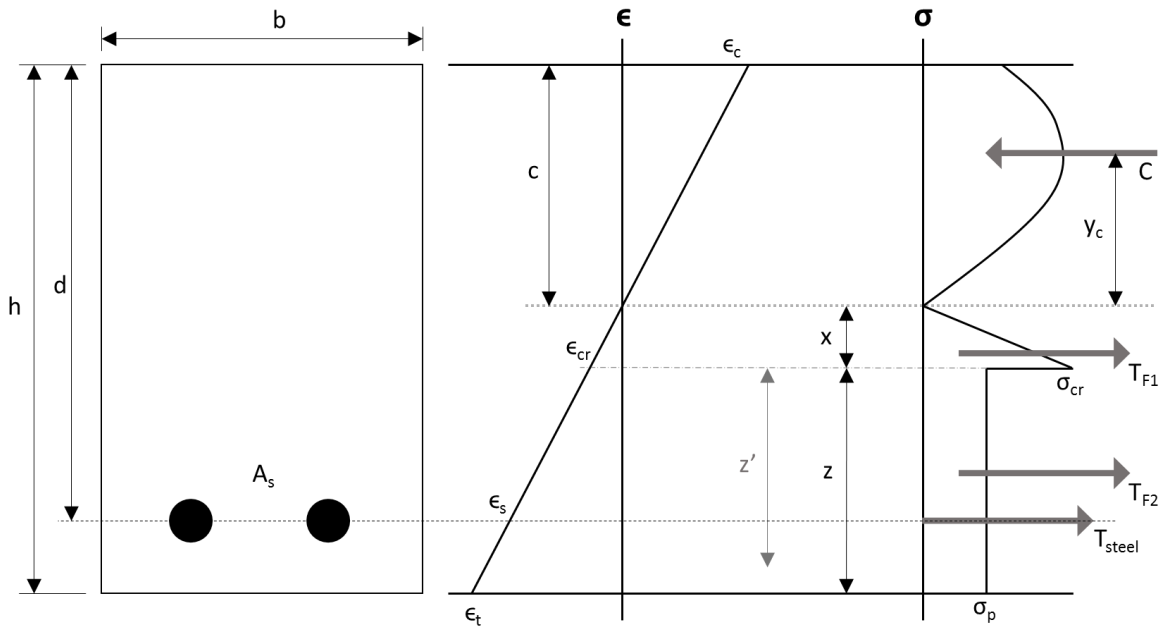

Figure B5. Relationship between stresses and strains on the beam cross-section

Using the relationship between the stress and strains of the concrete, rebar and fibers as shown in Figure B5, the moment capacity and curvature of the beam under flexural loading were calculated for various points in order to develop moment curvature plots. The moment curvature plots were then used to create the load deflection plots for the beams through the use of the conjugate beam method.

The moment curvature relationship was constructed by determining the corresponding moment and curvature value using the relationship shown in Figure B5. To demonstrate the function of the relationship in Figure B5, a sample calculation for Mix F15CF will be performed.

The moment curvature plot was based on the following points during the loading process of the beam: No load, @ Cracking, $f_c = 0.4f_{c\,(56\ days)}$, $\epsilon_s = 0.003$, $\epsilon_s = 0.0045$ (yield), $\epsilon_c = 0.0027$, $\epsilon_c = 0.003$, $\epsilon_c = 0.0038$, $\epsilon_c = 0.00387$. The point $\epsilon_c = 0.00387$ is the ultimate

strain the concrete is able to withstand in the stress strain relationship model. Strains above this value resulted in decreasing values in load carrying capacity.

For the most part, the strategy for computing moment and curvature values at these points is similar. For this sample calculation, the point where the strain in the concrete equals 0.003 ($\epsilon_c = 0.003$) will be explained.

Properties of the Beam and Rebar			
b =	8 in	A_{steel} =	0.3927 in^2
h =	4 in	$A_{concrete}$ =	32 in^2
y_{steel} =	1 in	$y_{concrete}$ =	2 in
d =	3 in	E_{steel} =	27097 ksi
$y_{concrete}$ =	2 in	$E_{Concrete}$ =	4093 ksi
$f_r = \sigma_{cr}$ =	596 psi	$f_{c\ 56\ days}$ =	5616 psi

Table B2. Properties of Beam and Rebar for Mix F15CF

Step 1: Determine ϵ_o

Assume f_c linear up to $0.4*f_{c\ 56\ days}$

$$f_c = 0.4 \times 5616\ psi = 2246.4\ psi = 2.2464\ ksi$$

$$\varepsilon_c = \frac{f_c}{E_{concrete}} = \frac{2.2464\ ksi}{4093\ ksi} = 0.000549$$

Using the Modified Hognestad equation, plug this stress and strain value in for the concrete and solve for the unknown variable ϵ_o.

$$f_c = f'_c \left[\frac{2\varepsilon_c}{\varepsilon_o} - \left(\frac{\varepsilon_c}{\varepsilon_o}\right)^2\right]$$

$$2246.4\ psi = 5616\ psi\ x \left[\frac{2(0.000549)}{\varepsilon_o} - \left(\frac{0.000549}{\varepsilon_o}\right)^2\right]$$

$$\varepsilon_o = 0.002435$$

Step 2: Determine Depth to Neutral Axis (c)

Determining the depth to the neutral axis using strain compatibility is an iterative process. The iterations were carried out using Microsoft Excel. The value of *c* determined in Excel will be given here to avoid showing iterations.

$$c = 0.89345\ inches$$

Step 3: Compute Curvature (φ)

$$\varphi = \frac{\varepsilon_c}{c} = \frac{0.003}{0.89345\ inches} = \frac{0.003358}{inches} = 33.58 \times 10^{-4} in^{-1}$$

Step 4: Compute Compressive Force (C)

$$C = b\int_0^c f_c\, dx \quad where \quad f_c = f'_c\left[\frac{2x\varphi}{\varepsilon_o} - \left(\frac{x\varphi}{\varepsilon_o}\right)^2\right]$$

$$C = bf'_c\left[\frac{c^2\varphi}{\varepsilon_o} - \frac{c^3\varphi^2}{3{\varepsilon_o}^2}\right]$$

$$C = (8\ in)(5.616\ ksi)\left[\frac{(0.89345^2)(0.003358)}{0.002435} - \frac{(0.89345^3)(0.003358^2)}{3(0.002435^2)}\right]$$

$$C = 29.14\ kips$$

Step 5: Compute Tensile Force from Rebar (T_{steel})

$$\varepsilon_s = \varepsilon_c\left(\frac{d-c}{c}\right) = 0.003\left(\frac{3 - 0.89345}{0.89345}\right)$$

$$\varepsilon_s = 0.007073$$

Using Table B1 the strain falls into region *y6.* Thus, the linear equation used to calculate the stress in the steel is as follows:

$$y6 = 1218.5x + 63.238 \qquad where\ x = \varepsilon_s\ and\ y6 = stress\ in\ the\ steel\ f_s$$

$$f_s = 1218.5(0.007073) + 63.238$$

$$f_s = 71.86\ ksi$$

$$T_{steel} = A_{steel} f_s$$

$$T_{steel} = (0.3927)(71.86)$$

$$T_{steel} = 28.22\ kips$$

Step 6: Compute Tensile Force from Fibers (T_{F1} & T_{F2})

$$\varepsilon_{cr} = \frac{\sigma_{cr}}{E_{concrete}} = \frac{0.596\ ksi}{4093\ ksi} = 0.000146$$

$$\sigma_p = \mu \varepsilon_{cr} E_{concrete} = (0.5)(0.000146)(4093ksi) = 0.2982\ ksi$$

Define distance (x):

$$x = \frac{\varepsilon_{cr} c}{\varepsilon_c} = \frac{(0.000146)(0.89345)}{0.003}$$

$$x = 0.0434\ inches$$

Define distance (z) & (z'):

Check to make sure that ε_t is less than $\varepsilon_{tu} = 0.025$. If it is less than, use the distance (z) shown on Figure B5. This means that the full depth of the beam from a distance (x) away from the neutral axis to the bottom of the beam contributes to the fiber tensile force (T_{F2}). If ε_t is greater than $\varepsilon_{tu} = 0.025$ use the distance (z') shown on Figure B5 to a strain corresponding to $\varepsilon_{tu} = 0.025$. This means that the tensile force from the fibers in the post peak region will not extend to the bottom of the beam since the ultimate strain of the fiber-

reinforced concrete was reached. The distance to which the post peak region of the fiber-reinforced concrete stress strain curve extends toward the bottom of the beam from a distance (x) away from the neutral axis is defined as (z').

$$\varepsilon_t = \left(\frac{\varepsilon_c}{c}\right)(h-c) = \left(\frac{0.003}{0.89345}\right)(4-0.89345)$$

$$\varepsilon_t = 0.0104 < 0.025 \qquad OK \qquad Use\ \ distance\ z$$

$$z = h - c - x$$

$$z = 4 - 0.89345 - 0.0434$$

$$z = 3.063\ inches$$

$$T_{F1} = 0.5\sigma_{cr}x = 0.5(0.596)(0.0434)$$

$$T_{F1} = 0.0129\ kips$$

$$T_{F2} = \sigma_p z = (0.2982)(3.063)$$

$$T_{F2} = 0.9135\ kips$$

Step 7: Make Compressive Force equal Tensile Forces

At this point, the sum of the compressive forces must equal the sum of the tensile forces. If the forces do not equal, iterate the depth to the neutral axis *c* until equilibrium is obtained.

$$C = T_{steel} + T_{F1} + T_{F2}$$

$$29.14 = 28.22 + 0.0129 + 0.9135$$

$$29.1445 = 29.1445$$

*Significant digits carried out in Excel. Equilibrium is reached at this point.

Step 8: Compute Moment (M)

The distance (y_c) from the neutral axis to the center of the compressive force of the concrete (C) is given by the following equation:

$$y_c = \frac{\int_0^c x\left[\frac{2x\varphi}{\varepsilon_o} - \left(\frac{x\varphi}{\varepsilon_o}\right)^2\right]dx}{\int_0^c \left[\frac{2x\varphi}{\varepsilon_o} - \left(\frac{x\varphi}{\varepsilon_o}\right)^2\right]dx} = \left[\frac{8\varepsilon_o c - 3c^2\varphi}{12\varepsilon_o - 4c\varphi}\right]$$

$$y_c = \left[\frac{8(0.002435)(0.89345) - 3(0.89345)^2(0.003358)}{12(0.002435) - 4(0.89345)(0.003358)}\right]$$

$$y_c = 0.544\ inches$$

The moment was calculated by taking a moment about the location of the compressive force. The general equation developed is as follows:

$$M = T_{F1}\left(y_c + \frac{2}{3}x\right) + T_{F2}\left(y_c + x + \frac{1}{2}z\right) + T_{steel}(d - c - y_c)$$

$$M = 0.0129\left(0.544 + \frac{2}{3}(0.0434)\right) + 0.9135\left(0.544 + 0.0434 + \frac{1}{2}(3.063)\right)$$

$$+ 28.22(3 - 0.89345 + 0.544)$$

$$M = 76.73\ kip\ inches$$

Step 9: Compute the Load (P) and corresponding Deflection (Δ)

As previously mentioned, the method used to develop the load deflection plot from the moment curvature plot was the conjugate beam method. The process of calculating the deflection corresponding to the moment and curvature point is not shown in this example since it is a fairly common procedure. The deflection value determined for this point is shown below. The relationship between moment (M) and load (P) was determined earlier in this paper to be M = 10P.

$$P = \frac{M}{10\ inches} = \frac{76.73\ kip\ inches}{10\ inches}$$

$$P = 7.673\ kips$$

$$\Delta = 0.531\ inches$$

These values along with all the load and deflection values for each point mentioned above for each mix can be found in the tables of Appendix C. The full load deflection plots developed for each beam for each mix can be found in the figures of Appendix C

APPENDIX C

Mix PL1

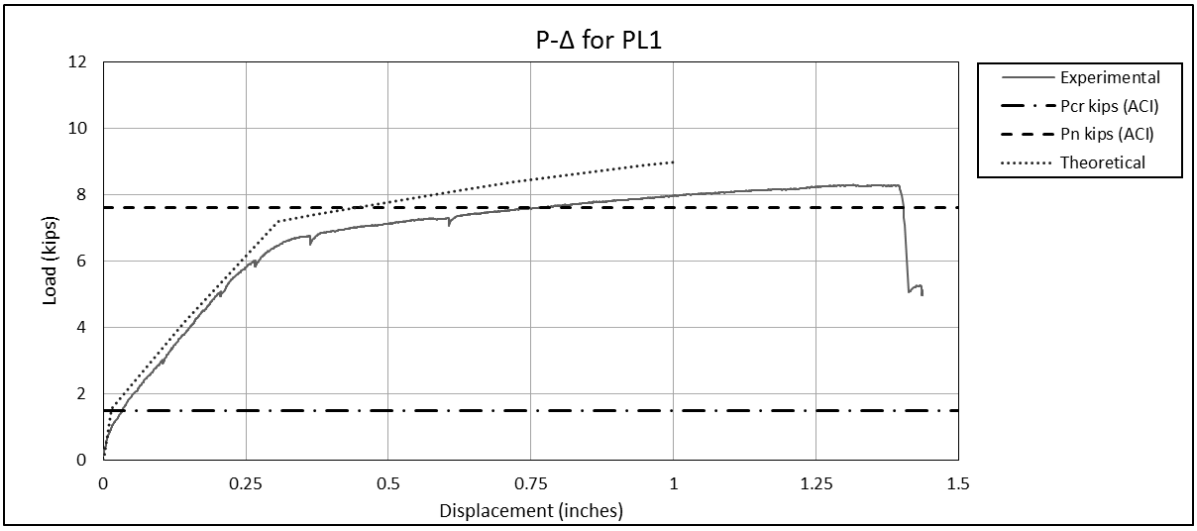

Figure C1. Load vs Deflection Plot for Beam – Mix PL1

PL1 - Theoretical Values		
Point	P (kips)	Δ (in)
No Load	0.000	0.000
Cracking	1.553	0.014
$f_c = 0.4f_{c\,(56\ days)}$	4.161	0.143
$\epsilon_s = 0.003$	7.191	0.307
$\epsilon_s = 0.0045$ (yield)	7.386	0.371
$\epsilon_c = 0.0027$	8.149	0.631
$\epsilon_c = 0.003$	8.375	0.720
$\epsilon_c = 0.0038$	8.890	0.952
$\epsilon_c = 0.004$	8.982	1.003
ACI Cracking Load - Pcr (kips) =		1.491
ACI Nominal Load - Pn (kips) =		7.595

Table C1. Theoretical Load and Deflection Values for Mix PL1

Figure C2. Flexure test on beam – Mix PL1

Mix 5C

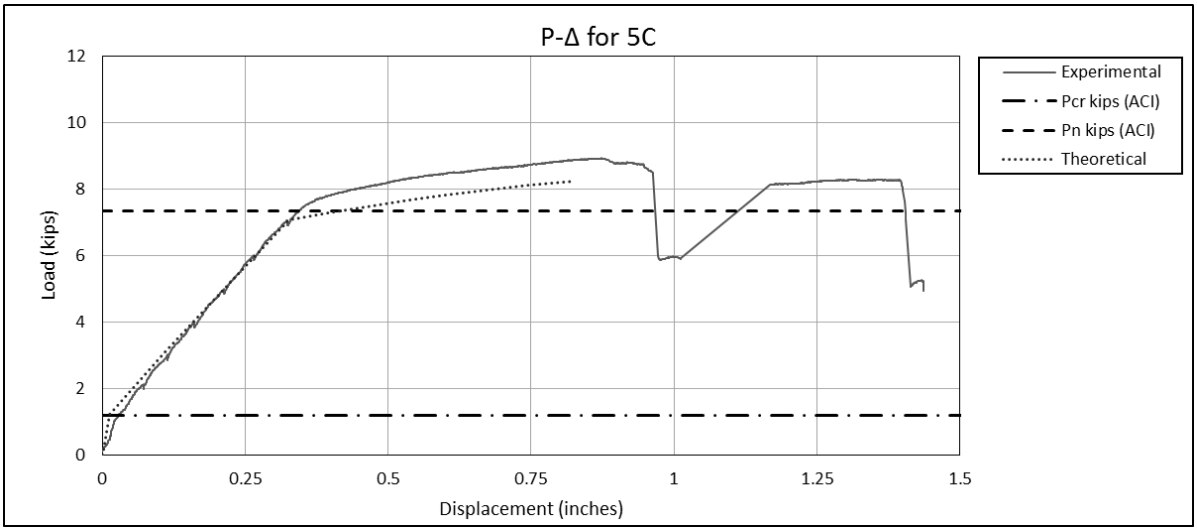

Figure C3. Load vs Deflection Plot for Beam – Mix 5C

5C - Theoretical Values		
Point	P (kips)	Δ (in)
No Load	0.000	0.000
Cracking	1.236	0.013
$f_c = 0.4f_{c\,(56\ days)}$	3.105	0.110
$\epsilon_s = 0.003$	7.090	0.327
$\epsilon_s = 0.0045$ (yield)	7.279	0.394
$\epsilon_c = 0.0027$	7.678	0.537
$\epsilon_c = 0.003$	7.834	0.599
$\epsilon_c = 0.0038$	8.131	0.744
$\epsilon_c = 0.00447$	8.248	0.824
ACI Cracking Load - Pcr (kips) =		1.187
ACI Nominal Load - Pn (kips) =		7.357

Table C2. Theoretical Load and Deflection Values for Mix 5C

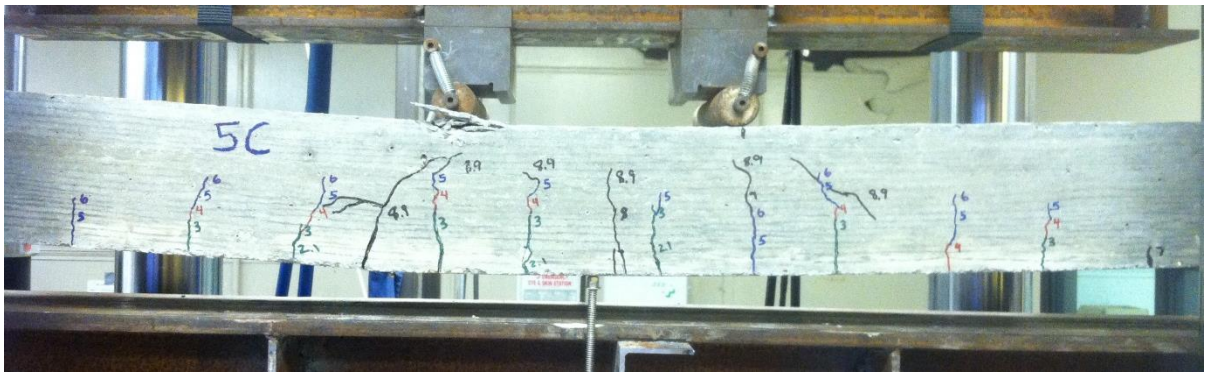

Figure C4. Flexure test on beam – Mix 5C

Mix 5F

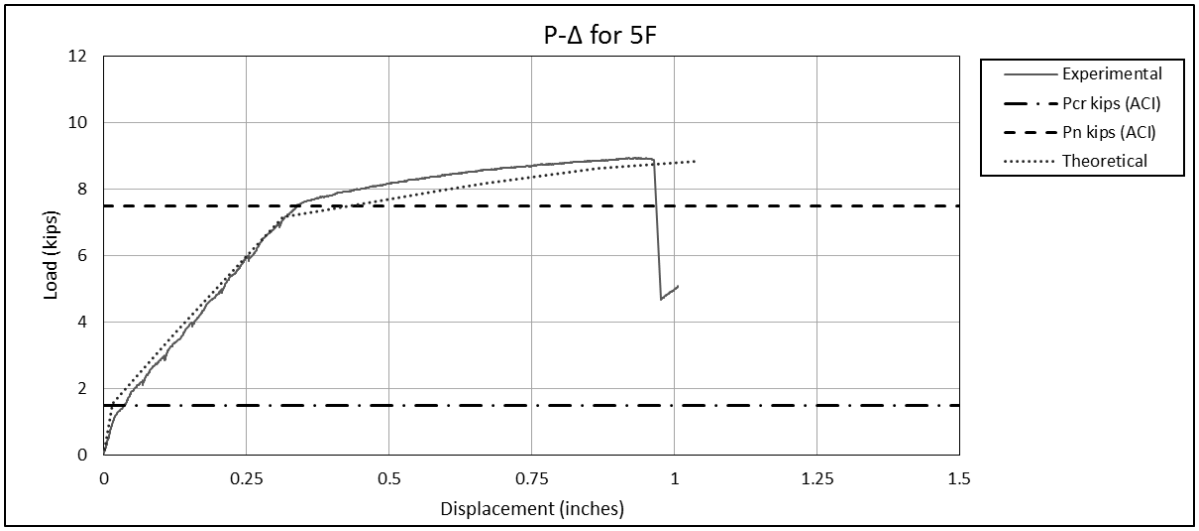

Figure C5. Load vs Deflection Plot for Beam – Mix 5F

5F - Theoretical Values		
Point	P (kips)	Δ (in)
No Load	0.000	0.000
Cracking	1.541	0.015
$f_c = 0.4f_{c\,(56\ days)}$	3.655	0.124
$\epsilon_s = 0.003$	7.158	0.314
$\epsilon_s = 0.0045$ (yield)	7.351	0.379
$\epsilon_c = 0.0027$	7.974	0.593
$\epsilon_c = 0.003$	8.170	0.671
$\epsilon_c = 0.0038$	8.618	0.866
$\epsilon_c = 0.00492$	8.825	1.038
ACI Cracking Load - Pcr (kips) =		1.481
ACI Nominal Load - Pn (kips) =		7.505

Table C3. Theoretical Load and Deflection Values for Mix 5F

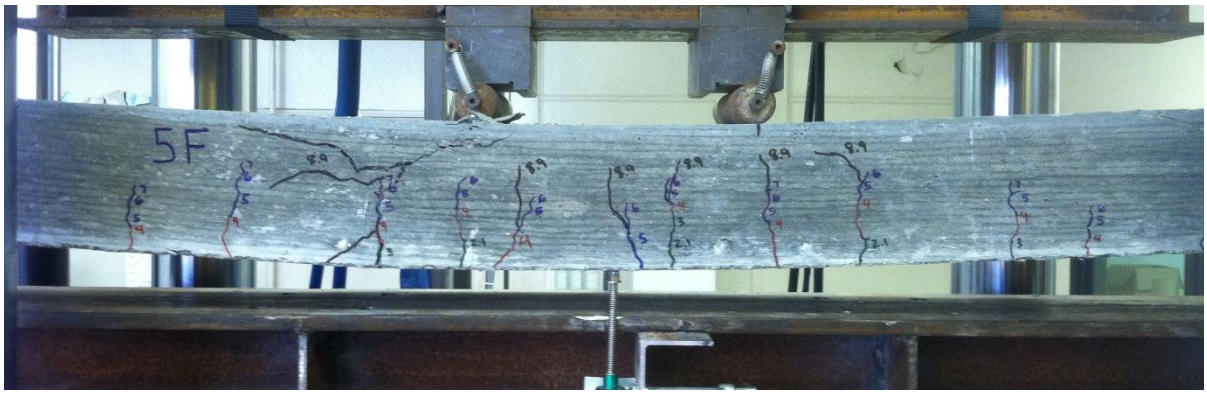

Figure C6. Flexure test on beam – Mix 5F

Mix 5CF

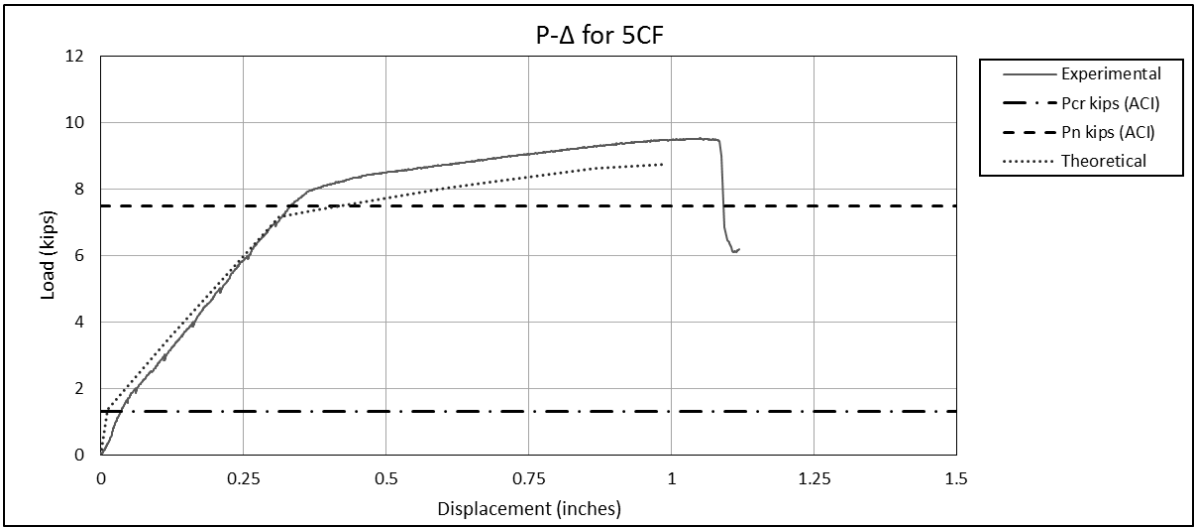

Figure C7. Load vs Deflection Plot for Beam – Mix 5CF

5CF - Theoretical Values		
Point	P (kips)	Δ (in)
No Load	0.000	0.000
Cracking	1.363	0.012
$f_c = 0.4f_{c\,(56\ days)}$	3.579	0.122
$\epsilon_s = 0.003$	7.174	0.312
$\epsilon_s = 0.0045$ (yield)	7.364	0.377
$\epsilon_c = 0.0027$	8.018	0.604
$\epsilon_c = 0.003$	8.208	0.681
$\epsilon_c = 0.0038$	8.622	0.867
$\epsilon_c = 0.00465$	8.755	0.989
ACI Cracking Load - Pcr (kips) =		1.309
ACI Nominal Load - Pn (kips) =		7.503

Table C4. Theoretical Load and Deflection Values for Mix 5CF

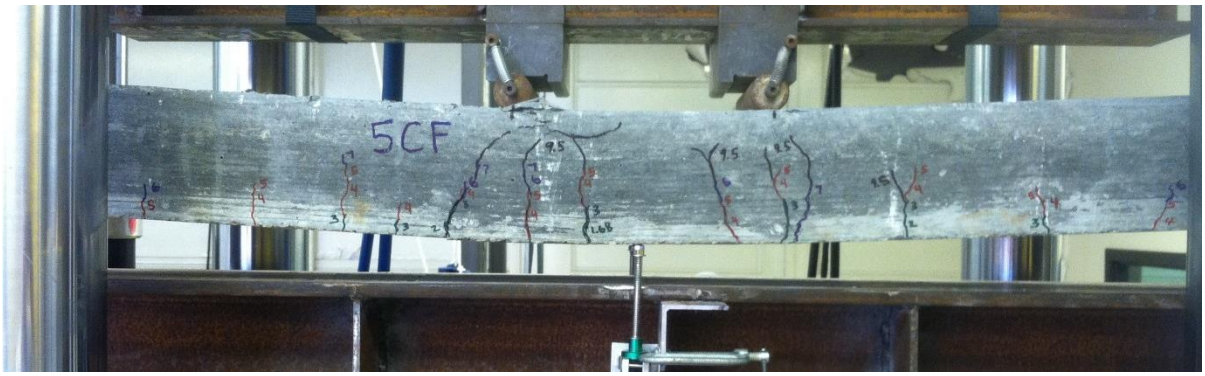

Figure C8. Flexure test on beam – Mix 5CF

Mix 10C

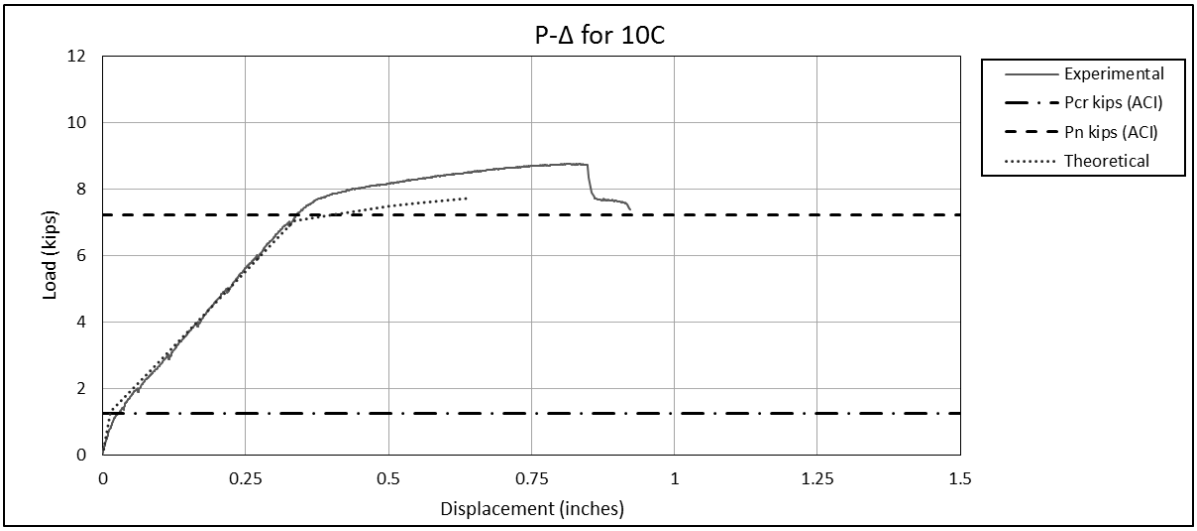

Figure C9. Load vs Deflection Plot for Beam – Mix 10C

10C - Theoretical Values		
Point	P (kips)	Δ (in)
No Load	0.000	0.000
Cracking	1.300	0.014
$f_c = 0.4f_{c\,(56\ days)}$	2.680	0.092
$\epsilon_s = 0.003$	7.047	0.334
$\epsilon_s = 0.0045$ (yield)	7.224	0.401
$\epsilon_c = 0.0027$	7.480	0.503
$\epsilon_c = 0.003$	7.589	0.552
$\epsilon_c = 0.00376$	7.712	0.643
ACI Cracking Load - Pcr (kips) =		1.251
ACI Nominal Load - Pn (kips) =		7.221

Table C5. Theoretical Load and Deflection Values for Mix 10C

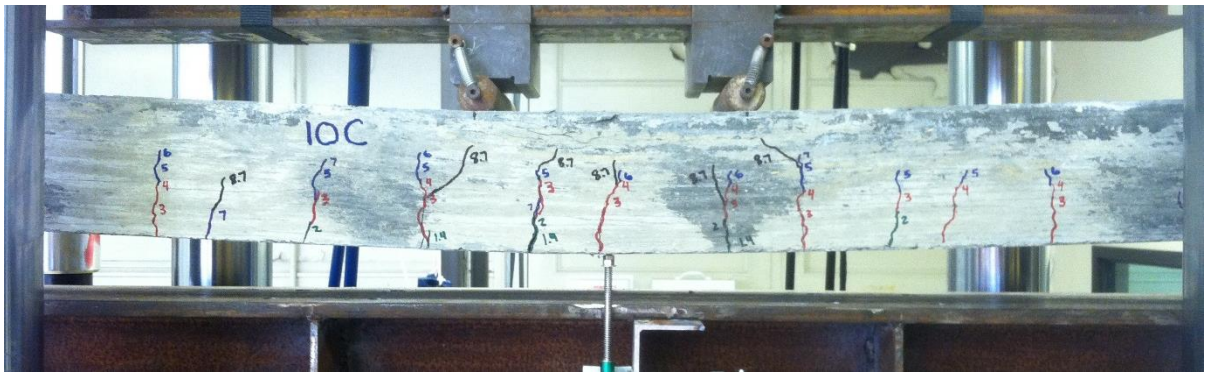

Figure C10. Flexure test on beam – Mix 10C

Mix 10F

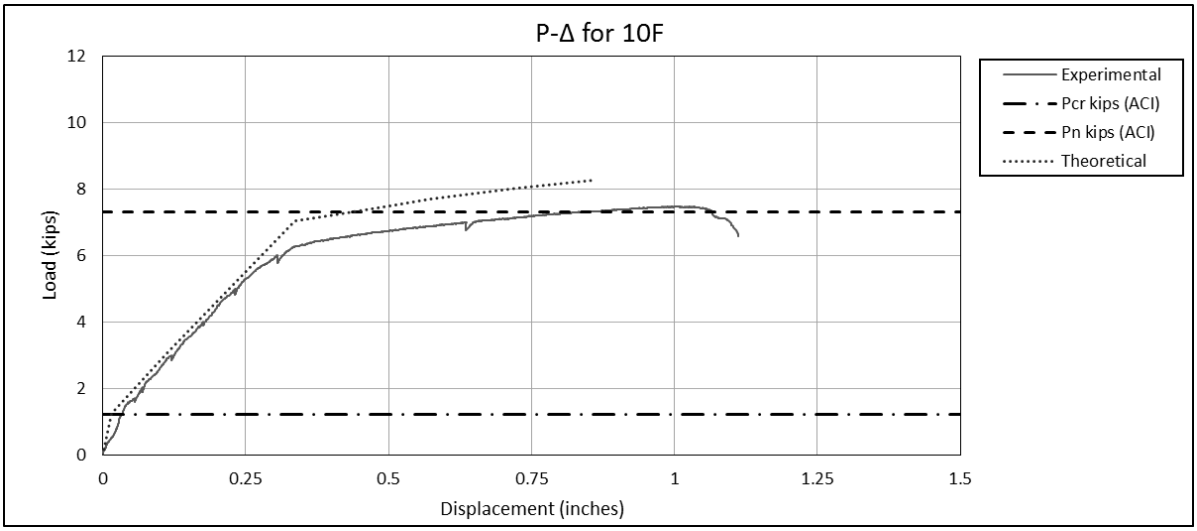

Figure C11. Load vs Deflection Plot for Beam – Mix 10F

10F - Theoretical Values		
Point	P (kips)	Δ (in)
No Load	0.000	0.000
Cracking	1.260	0.015
$f_c = 0.4f_{c\,(56\ days)}$	3.134	0.116
$\epsilon_s = 0.003$	7.040	0.336
$\epsilon_s = 0.0045$ (yield)	7.234	0.404
$\epsilon_c = 0.0027$	7.533	0.511
$\epsilon_c = 0.003$	7.696	0.572
$\epsilon_c = 0.0038$	8.040	0.725
$\epsilon_c = 0.00475$	8.261	0.857
ACI Cracking Load - Pcr (kips) =		1.211
ACI Nominal Load - Pn (kips) =		7.327

Table C6. Theoretical Load and Deflection Values for Mix 10F

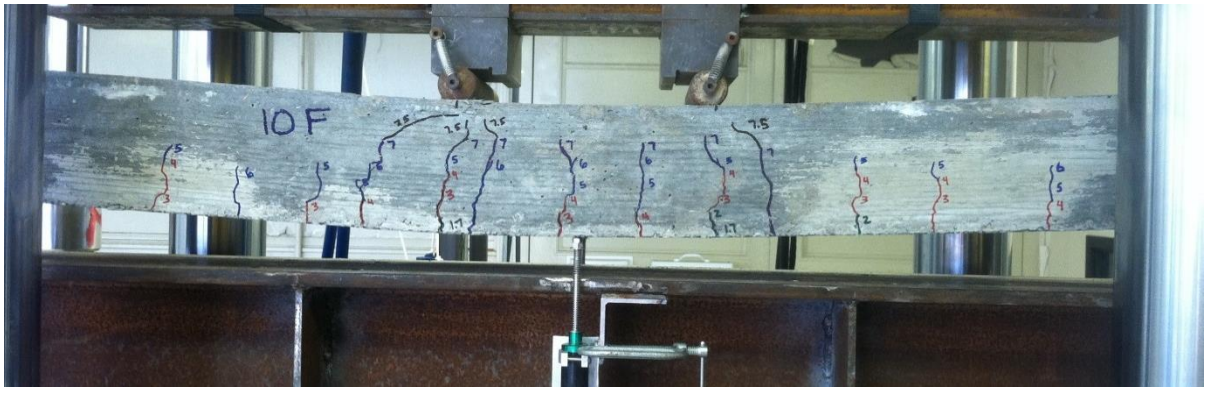

Figure C12. Flexure test on beam – Mix 10F

Mix 10CF

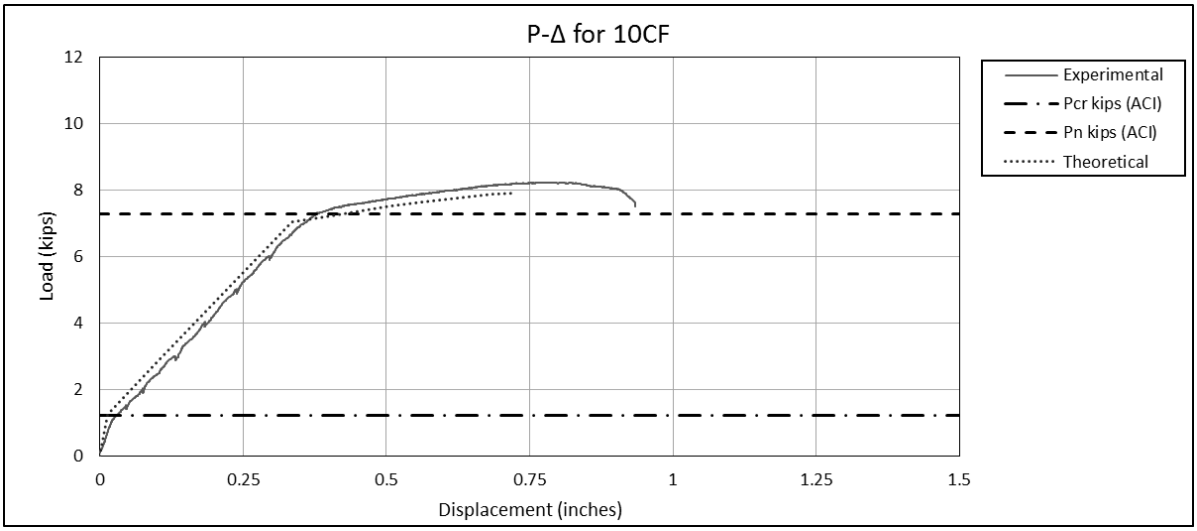

Figure C13. Load vs Deflection Plot for Beam – Mix 10CF

10CF - Theoretical Values		
Point	P (kips)	Δ (in)
No Load	0.000	0.000
Cracking	1.249	0.014
$f_c = 0.4f_{c\,(56\ days)}$	2.850	0.102
$\epsilon_s = 0.003$	7.042	0.335
$\epsilon_s = 0.0045$ (yield)	7.228	0.403
$\epsilon_c = 0.0027$	7.503	0.507
$\epsilon_c = 0.003$	7.639	0.561
$\epsilon_c = 0.0038$	7.871	0.684
$\epsilon_c = 0.0042$	7.899	0.722
ACI Cracking Load - Pcr (kips) =		1.201
ACI Nominal Load - Pn (kips) =		7.261

Table C7. Theoretical Load and Deflection Values for Mix 10CF

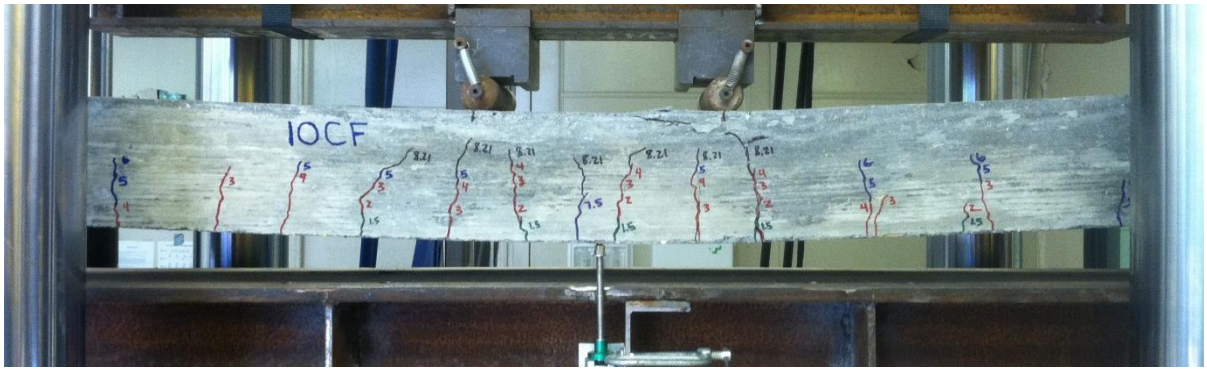

Figure C14. Flexure test on beam – Mix 10CF

Mix 15C

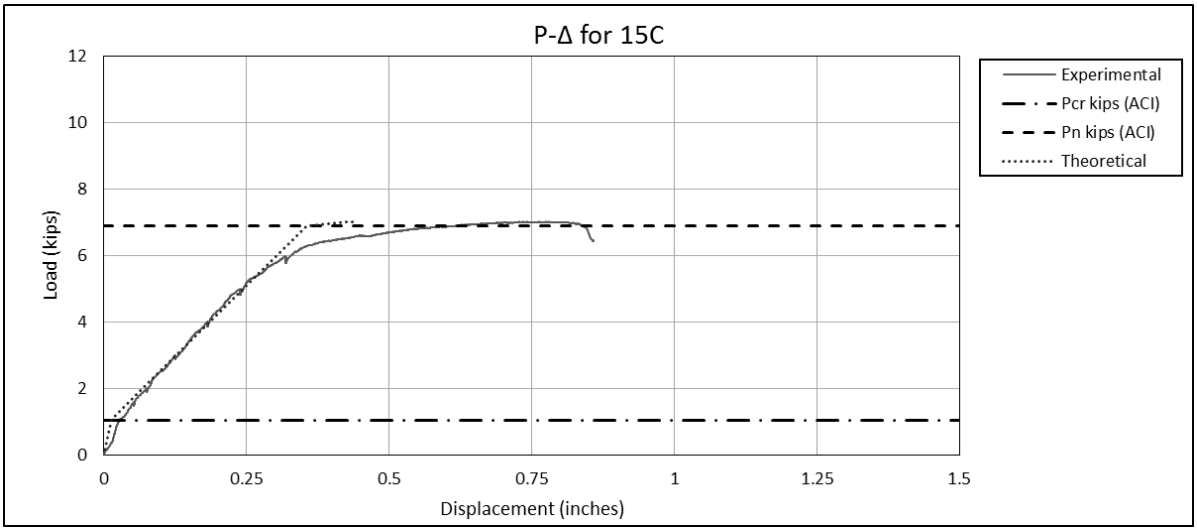

Figure C15. Load vs Deflection Plot for Beam – Mix 15C

15C - Theoretical Values		
Point	P (kips)	Δ (in)
No Load	0.000	0.000
Cracking	1.088	0.013
$f_c = 0.4f_{c\,(56\ days)}$	2.078	0.072
$\epsilon_s = 0.003$	6.895	0.355
$\epsilon_s = 0.0045$ (yield)	7.003	0.425
$\epsilon_c = 0.0027$	7.009	0.438
$\epsilon_c = 0.00275$	7.009	0.441
ACI Cracking Load - Pcr (kips) =		1.047
ACI Nominal Load - Pn (kips) =		6.897

Table C8. Theoretical Load and Deflection Values for Mix 15C

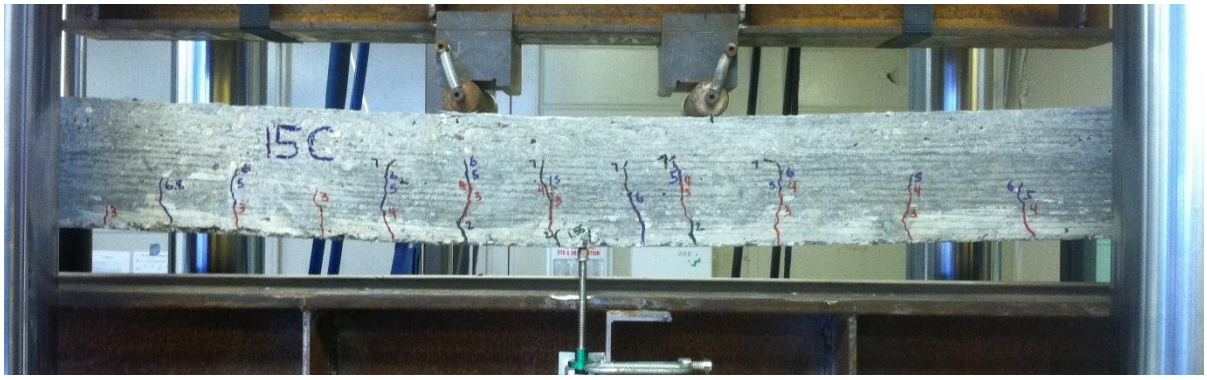

Figure C16. Flexure test on beam – Mix 15C

Mix 15F

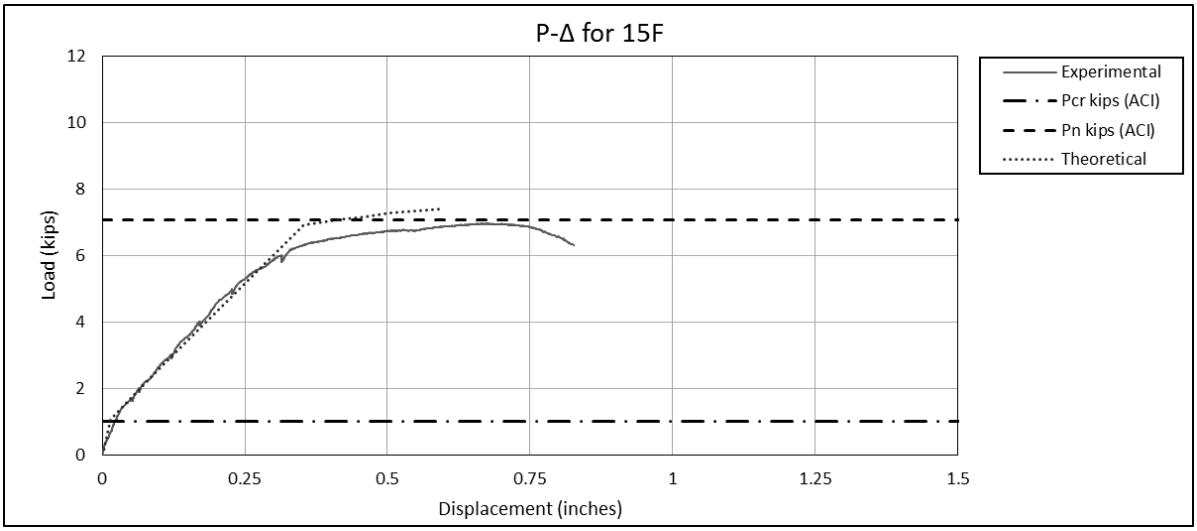

Figure C17. Load vs Deflection Plot for Beam – Mix 15F

15F - Theoretical Values		
Point	P (kips)	Δ (in)
No Load	0.000	0.000
Cracking	1.055	0.014
$f_c = 0.4f_{c\,(56\ days)}$	2.460	0.093
$\epsilon_s = 0.003$	6.933	0.354
$\epsilon_s = 0.0045$ (yield)	7.106	0.424
$\epsilon_c = 0.0027$	7.167	0.459
$\epsilon_c = 0.003$	7.272	0.502
$\epsilon_c = 0.0038$	7.408	0.593
$\epsilon_c = 0.00385$	7.409	0.597
ACI Cracking Load - Pcr (kips) =		1.015
ACI Nominal Load - Pn (kips) =		7.060

Table C9. Theoretical Load and Deflection Values for Mix 15F

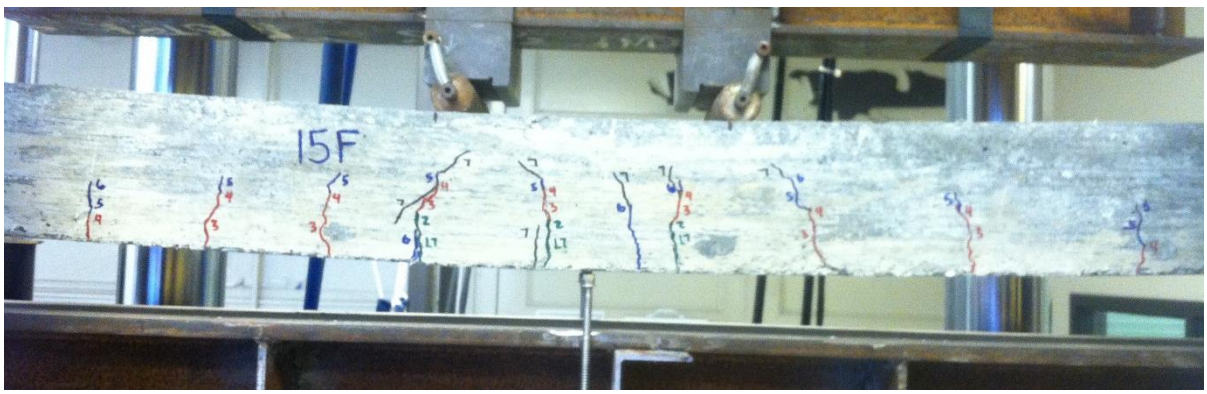

Figure C18. Flexure test on beam – Mix 15F

Mix 15CF

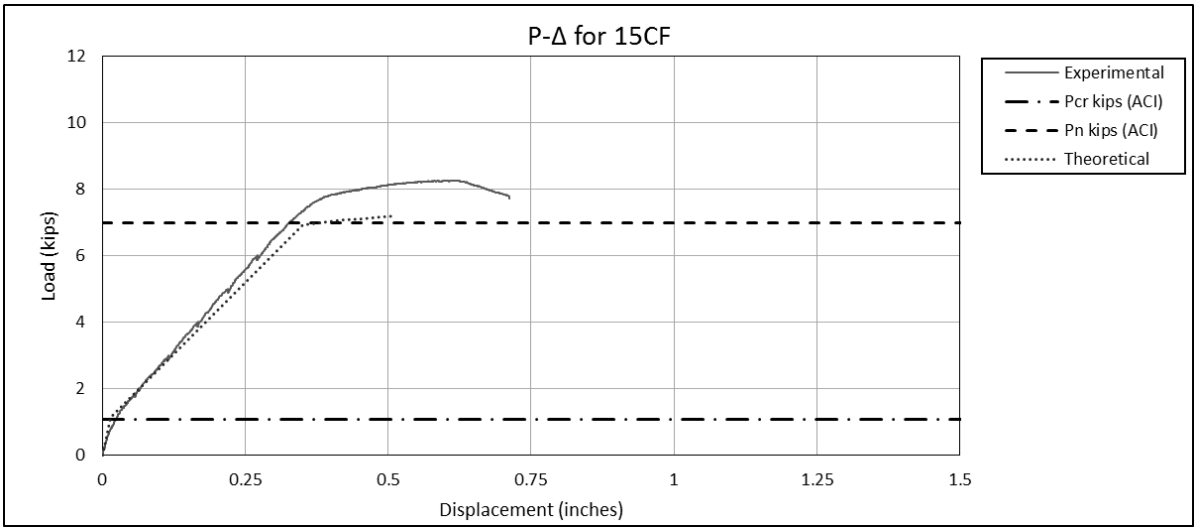

Figure C19. Load vs Deflection Plot for Beam – Mix 15CF

15CF - Theoretical Values		
Point	P (kips)	Δ (in)
No Load	0.000	0.000
Cracking	1.132	0.014
$f_c = 0.4f_{c\,(56\ days)}$	2.262	0.080
$\epsilon_s = 0.003$	6.936	0.351
$\epsilon_s = 0.0045$ (yield)	7.085	0.420
$\epsilon_c = 0.0027$	7.126	0.454
$\epsilon_c = 0.003$	7.184	0.488
$\epsilon_c = 0.00326$	7.202	0.512
ACI Cracking Load - Pcr (kips) =		1.090
ACI Nominal Load - Pn (kips) =		6.998

Table C10. Theoretical Load and Deflection Values for Mix 15CF

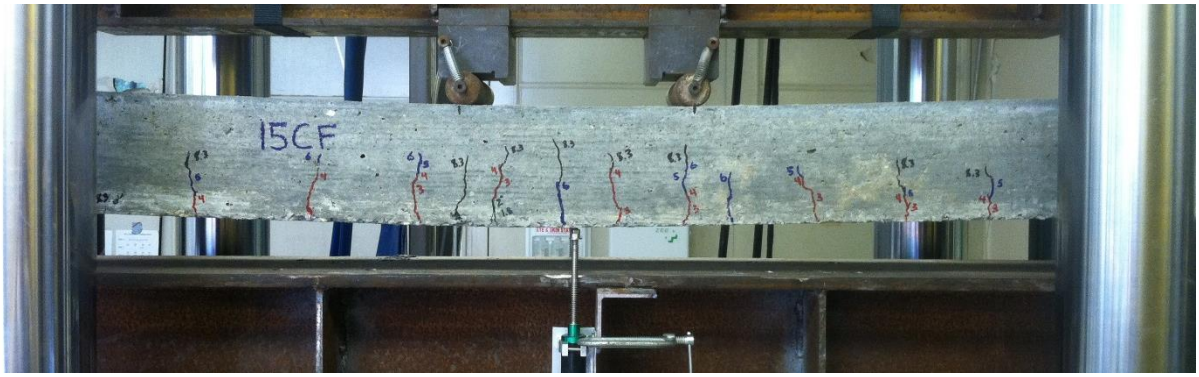

Figure C20. Flexure test on beam – Mix 15CF

Mix PL2

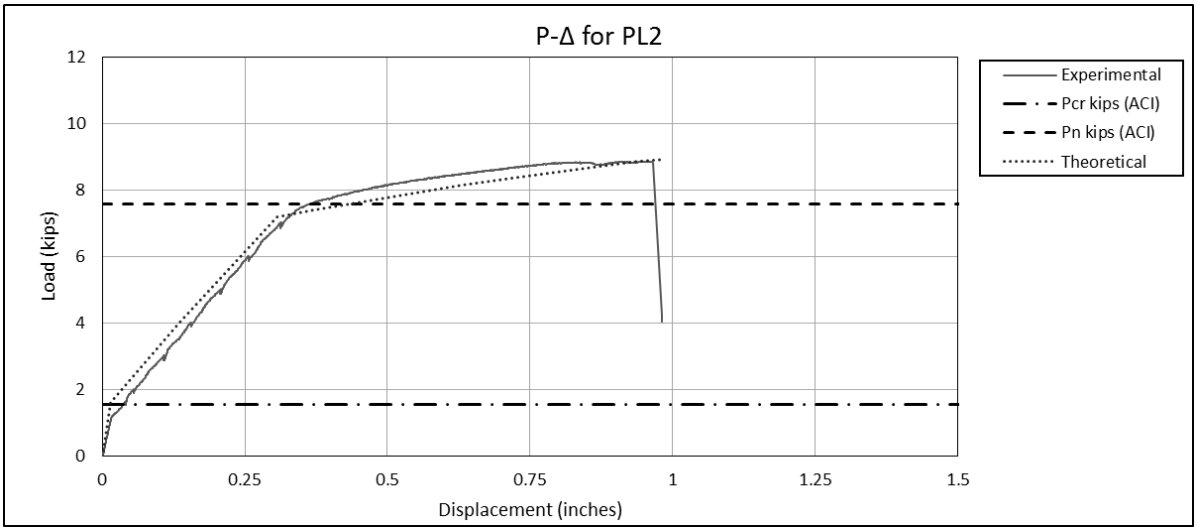

Figure C21. Load vs Deflection Plot for Beam – Mix PL2

PL2 - Theoretical Values		
Point	P (kips)	Δ (in)
No Load	0.000	0.000
Cracking	1.592	0.014
$f_c = 0.4f_{c\,(56\ days)}$	3.992	0.135
$\epsilon_s = 0.003$	7.194	0.307
$\epsilon_s = 0.0045$ (yield)	7.387	0.371
$\epsilon_c = 0.0027$	8.144	0.630
$\epsilon_c = 0.003$	8.362	0.717
$\epsilon_c = 0.0038$	8.846	0.937
$\epsilon_c = 0.004$	8.927	0.985
ACI Cracking Load - Pcr (kips) =		1.529
ACI Nominal Load - Pn (kips) =		7.576

Table C11. Theoretical Load and Deflection Values for Mix PL2

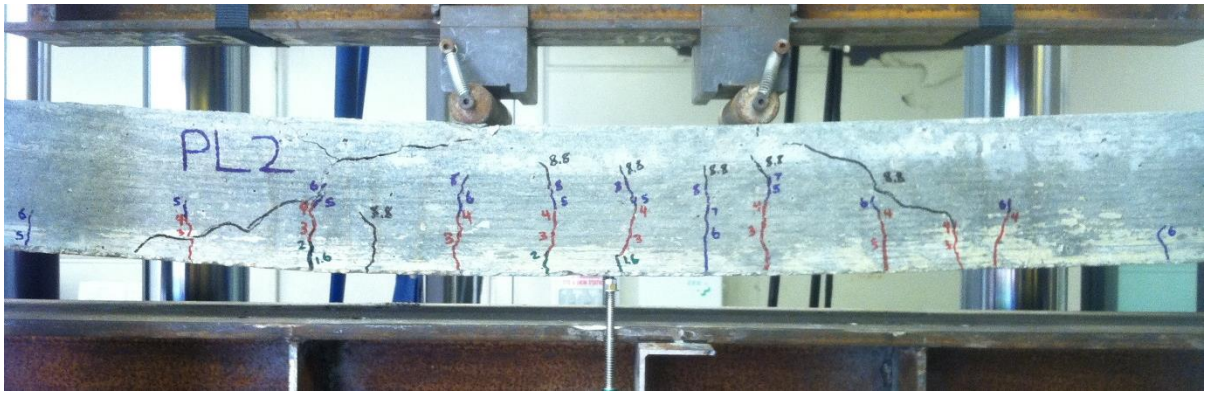

Figure C22. Flexure test on beam – Mix PL2

Mix F1

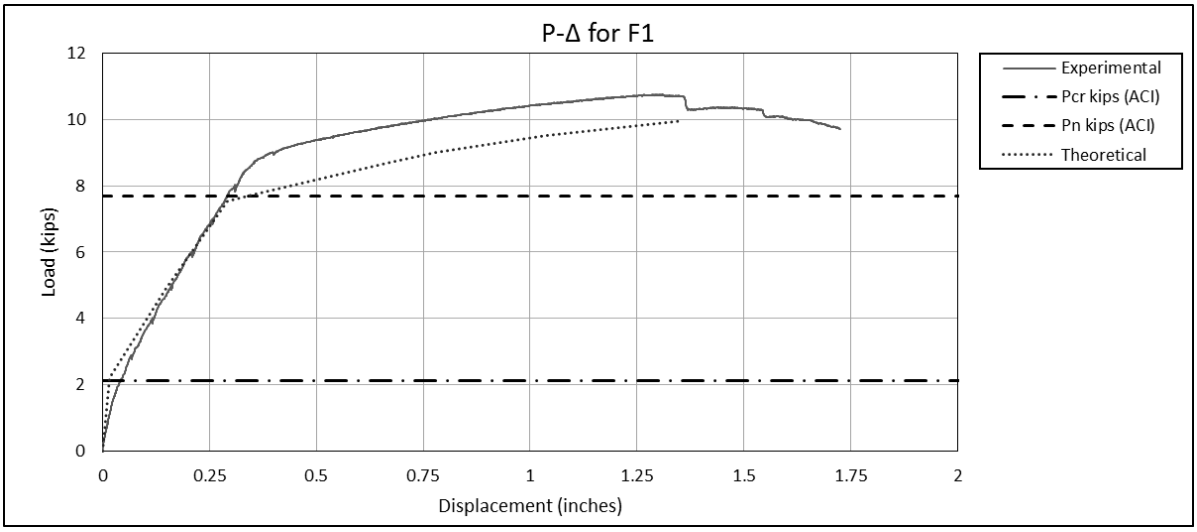

Figure C23. Load vs Deflection Plot for Beam – Mix F1

F1 - Theoretical Values		
Point	P (kips)	Δ (in)
No Load	0.000	0.000
Cracking	2.215	0.018
$f_c = 0.4f_{c\,(56\ days)}$	4.897	0.150
$\epsilon_s = 0.003$	7.542	0.293
$\epsilon_s = 0.0045$ (yield)	7.746	0.357
$\epsilon_c = 0.0027$	8.690	0.673
$\epsilon_c = 0.003$	8.994	0.778
$\epsilon_c = 0.0038$	9.512	1.036
$\epsilon_c = 0.005$	9.971	1.358
ACI Cracking Load - Pcr (kips) =		2.129
ACI Nominal Load - Pn (kips) =		7.698

Table C12. Theoretical Load and Deflection Values for Mix F1

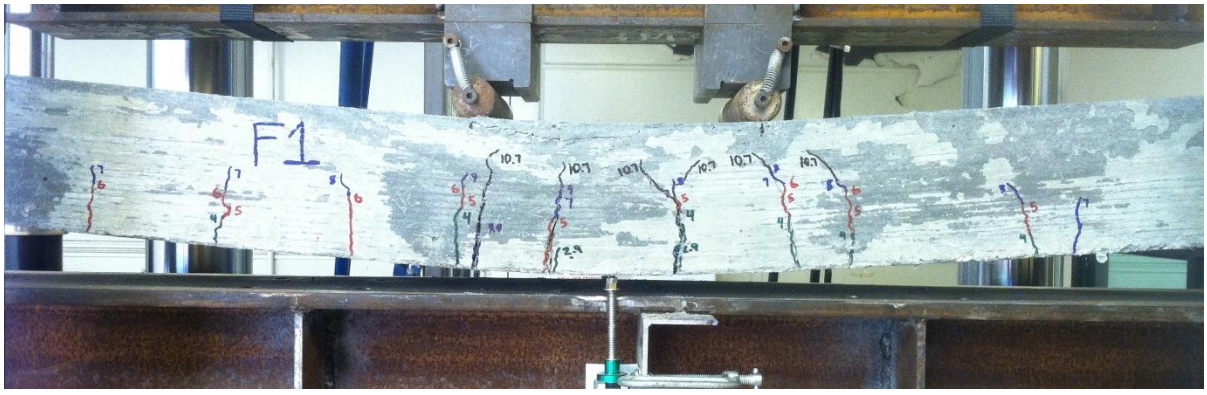

Figure C24. Flexure test on beam – Mix F1

Mix F5C

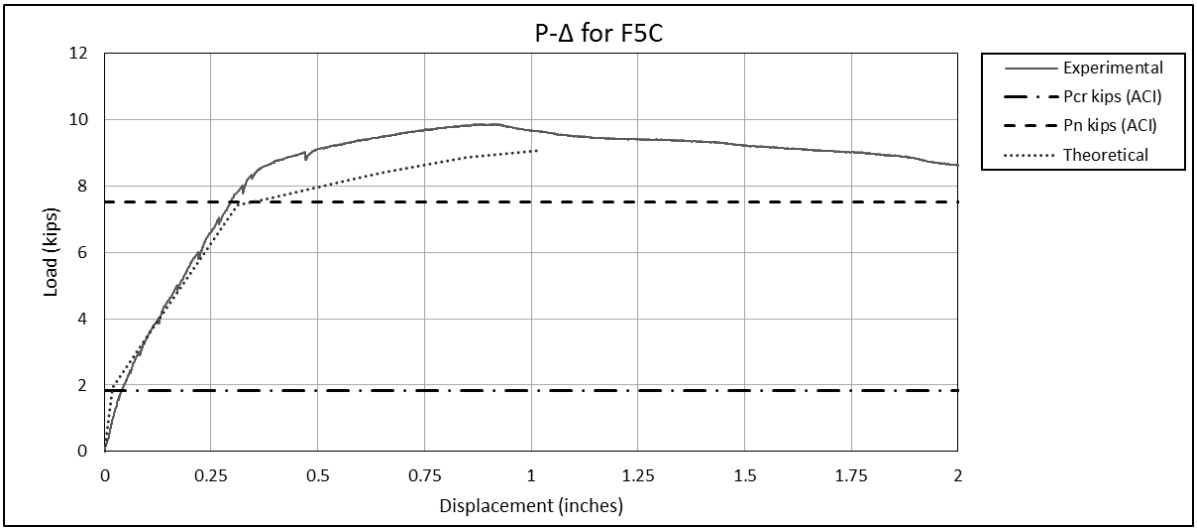

Figure C25. Load vs Deflection Plot for Beam – Mix F5C

F5C - Theoretical Values		
Point	P (kips)	Δ (in)
No Load	0.000	0.000
Cracking	1.922	0.018
$f_c = 0.4f_{c\,(56\ days)}$	3.773	0.116
$\epsilon_s = 0.003$	7.410	0.313
$\epsilon_s = 0.0045$ (yield)	7.611	0.378
$\epsilon_c = 0.0027$	8.209	0.580
$\epsilon_c = 0.003$	8.404	0.656
$\epsilon_c = 0.0038$	8.857	0.848
$\epsilon_c = 0.00492$	9.065	1.019
ACI Cracking Load - Pcr (kips) =		1.849
ACI Nominal Load - Pn (kips) =		7.521

Table C13. Theoretical Load and Deflection Values for Mix F5C

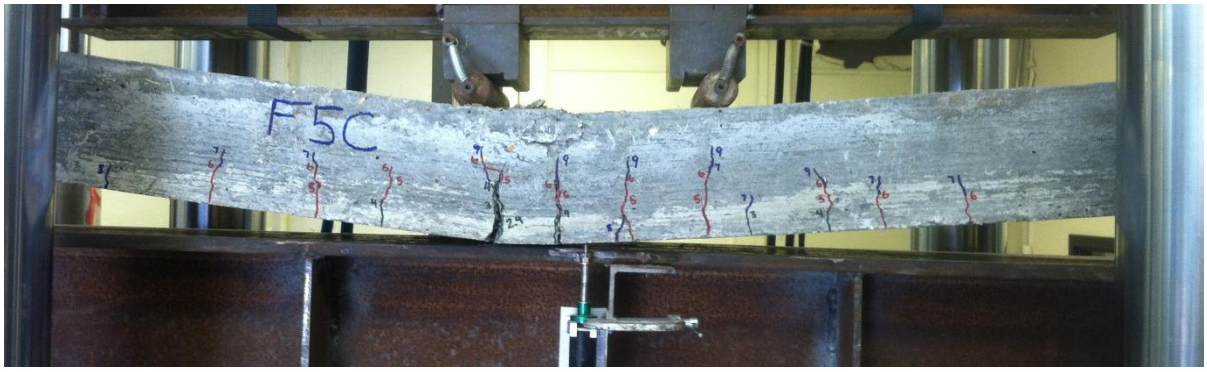

Figure C26. Flexure test on beam – Mix F5C

Mix F5F

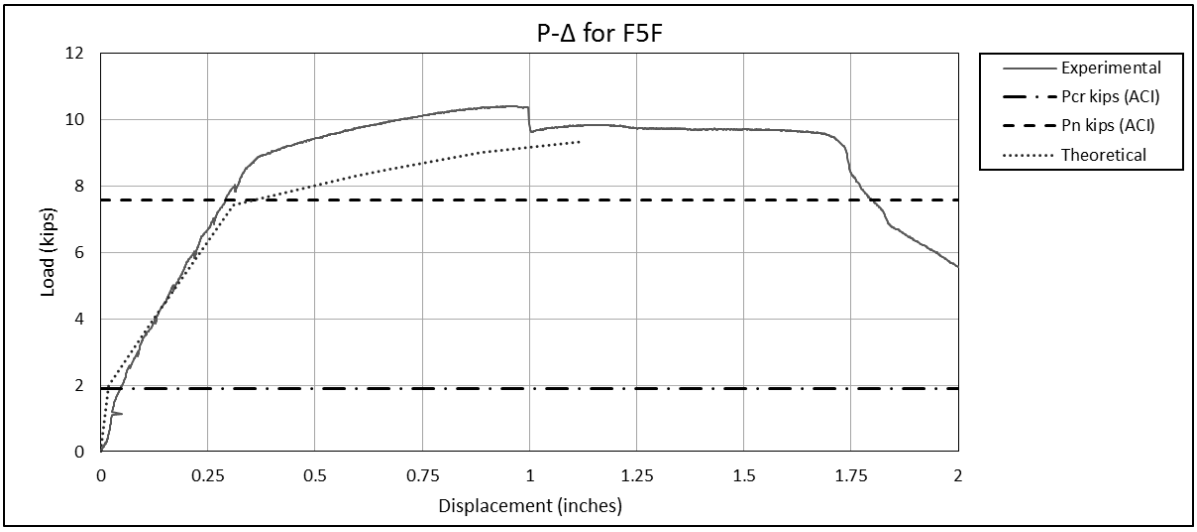

Figure C27. Load vs Deflection Plot for Beam – Mix F5F

F5F - Theoretical Values		
Point	P (kips)	Δ (in)
No Load	0.000	0.000
Cracking	1.981	0.019
$f_c = 0.4f_{c\,(56\ days)}$	4.094	0.129
$\epsilon_s = 0.003$	7.426	0.310
$\epsilon_s = 0.0045$ (yield)	7.630	0.376
$\epsilon_c = 0.0027$	8.278	0.591
$\epsilon_c = 0.003$	8.492	0.673
$\epsilon_c = 0.0038$	8.999	0.887
$\epsilon_c = 0.005$	9.346	1.125
ACI Cracking Load - Pcr (kips) =		1.906
ACI Nominal Load - Pn (kips) =		7.571

Table C14. Theoretical Load and Deflection Values for Mix F5F

Figure C28. Flexure test on beam – Mix F5F

Mix F5CF

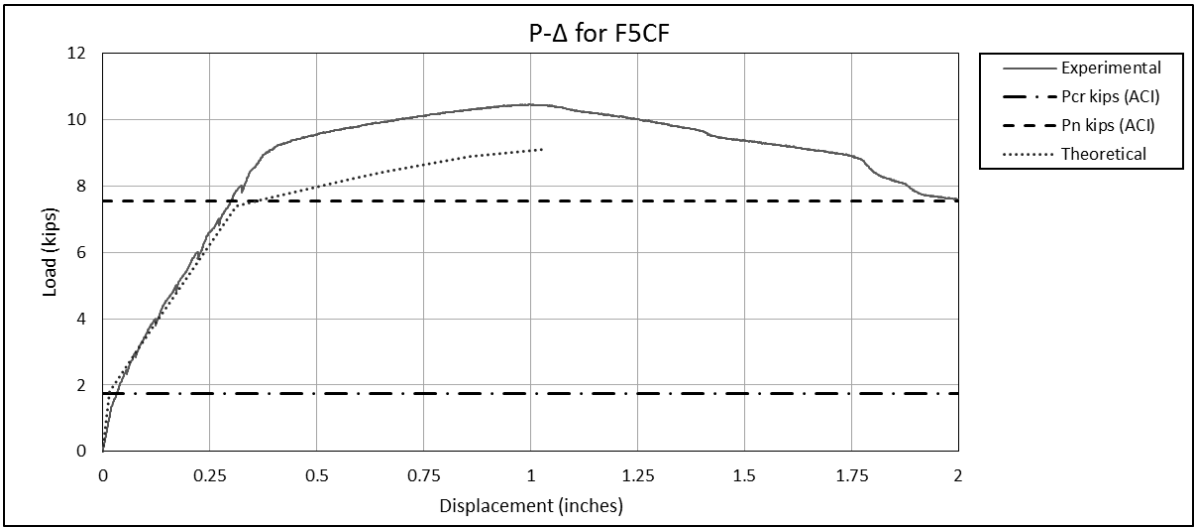

Figure C29. Load vs Deflection Plot for Beam – Mix F5CF

F5CF - Theoretical Values		
Point	P (kips)	Δ (in)
No Load	0.000	0.000
Cracking	1.807	0.017
$f_c = 0.4f_{c\,(56\ days)}$	3.796	0.119
$\epsilon_s = 0.003$	7.403	0.312
$\epsilon_s = 0.0045$ (yield)	7.604	0.377
$\epsilon_c = 0.0027$	8.227	0.588
$\epsilon_c = 0.003$	8.424	0.665
$\epsilon_c = 0.0038$	8.876	0.859
$\epsilon_c = 0.0049$	9.084	1.029
ACI Cracking Load - Pcr (kips) =		1.738
ACI Nominal Load - Pn (kips) =		7.529

Table C15. Theoretical Load and Deflection Values for Mix F5CF

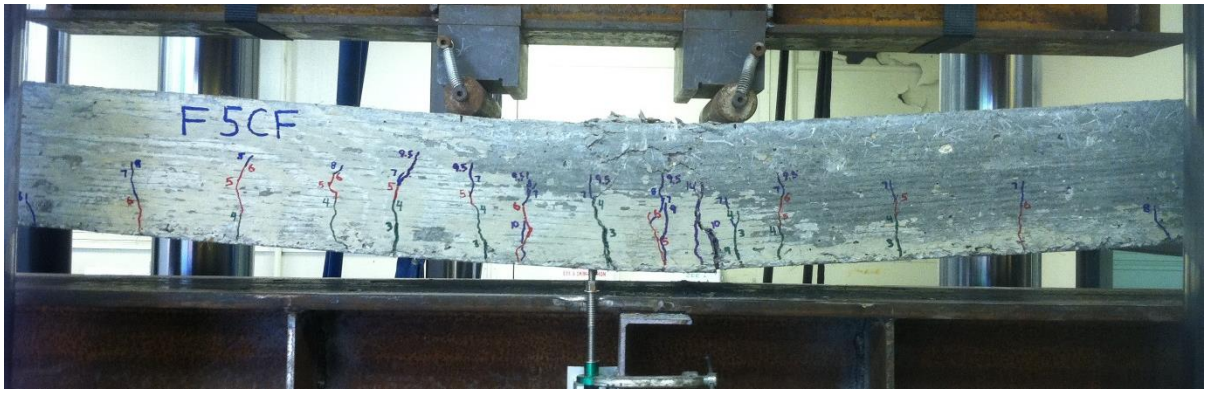

Figure C30. Flexure test on beam – Mix F5CF

Mix F10C

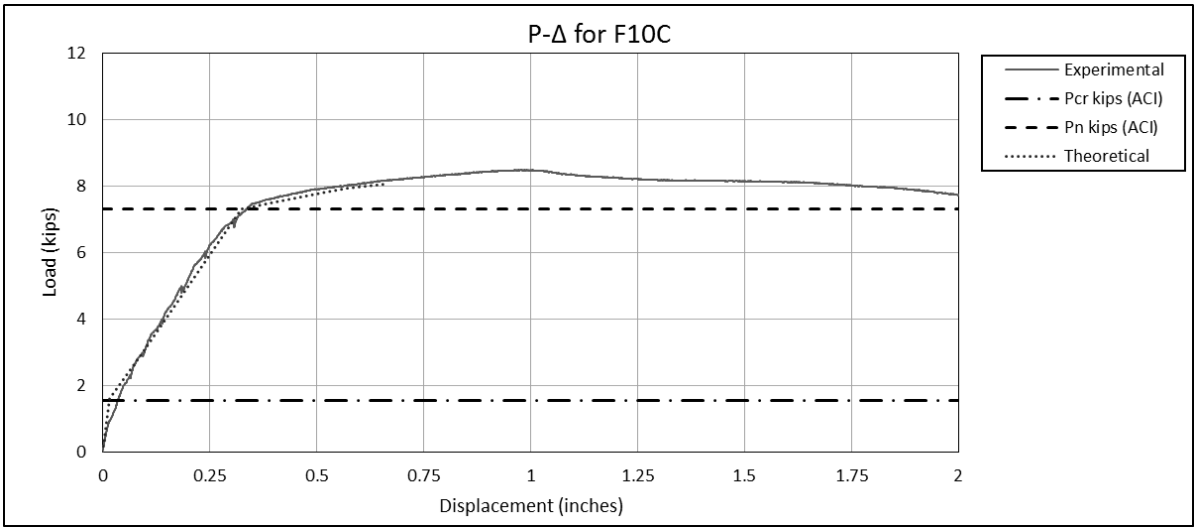

Figure C31. Load vs Deflection Plot for Beam – Mix F10C

F10C - Theoretical Values		
Point	P (kips)	Δ (in)
No Load	0.000	0.000
Cracking	1.594	0.015
$f_c = 0.4f_{c\,(56\ days)}$	2.881	0.087
$\epsilon_s = 0.003$	7.300	0.325
$\epsilon_s = 0.0045$ (yield)	7.484	0.391
$\epsilon_c = 0.0027$	7.820	0.520
$\epsilon_c = 0.003$	7.933	0.571
$\epsilon_c = 0.0037$	8.051	0.658
ACI Cracking Load - Pcr (kips) =		1.535
ACI Nominal Load - Pn (kips) =		7.308

Table C16. Theoretical Load and Deflection Values for Mix F10C

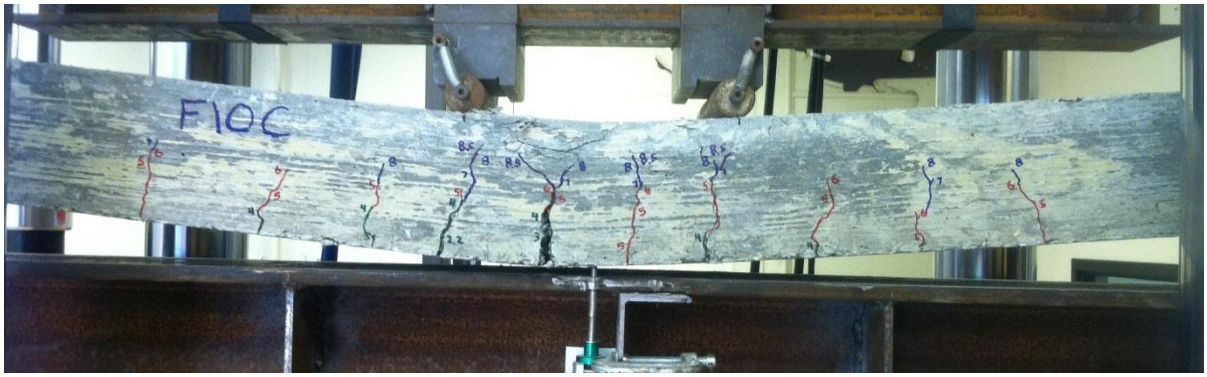

Figure C32. Flexure test on beam – Mix F10C

Mix F10F

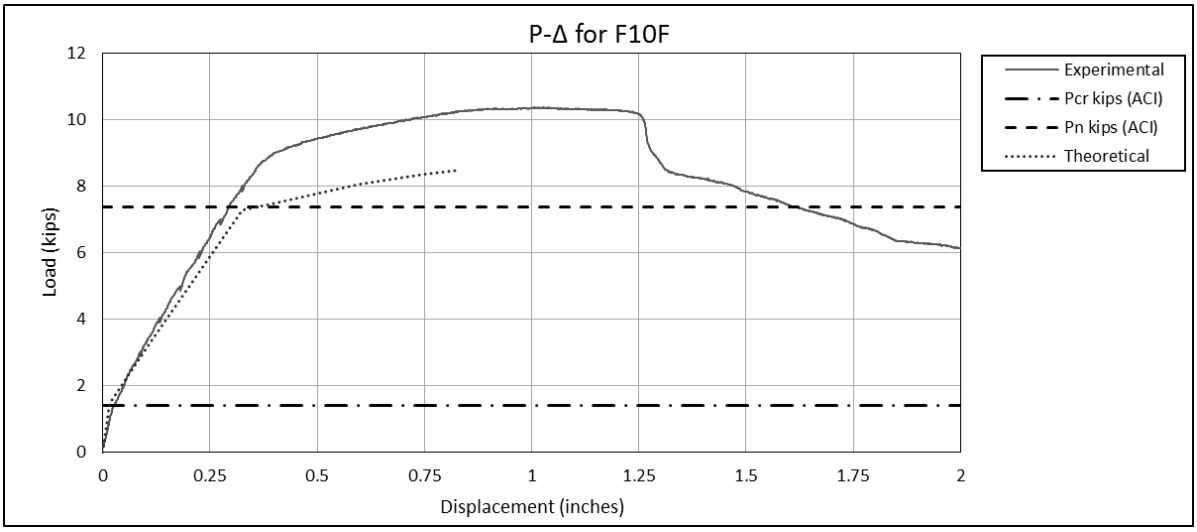

Figure C33. Load vs Deflection Plot for Beam – Mix F10F

F10F - Theoretical Values		
Point	P (kips)	Δ (in)
No Load	0.000	0.000
Cracking	1.456	0.015
$f_c = 0.4f_{c\,(56\ days)}$	3.255	0.108
$\epsilon_s = 0.003$	7.285	0.325
$\epsilon_s = 0.0045$ (yield)	7.481	0.392
$\epsilon_c = 0.0027$	7.892	0.536
$\epsilon_c = 0.003$	8.054	0.599
$\epsilon_c = 0.0038$	8.367	0.748
$\epsilon_c = 0.0044$	8.499	0.828
ACI Cracking Load - Pcr (kips) =		1.400
ACI Nominal Load - Pn (kips) =		7.392

Table C17. Theoretical Load and Deflection Values for Mix F10F

Figure C34. Flexure test on beam – Mix F10F

Mix F10CF

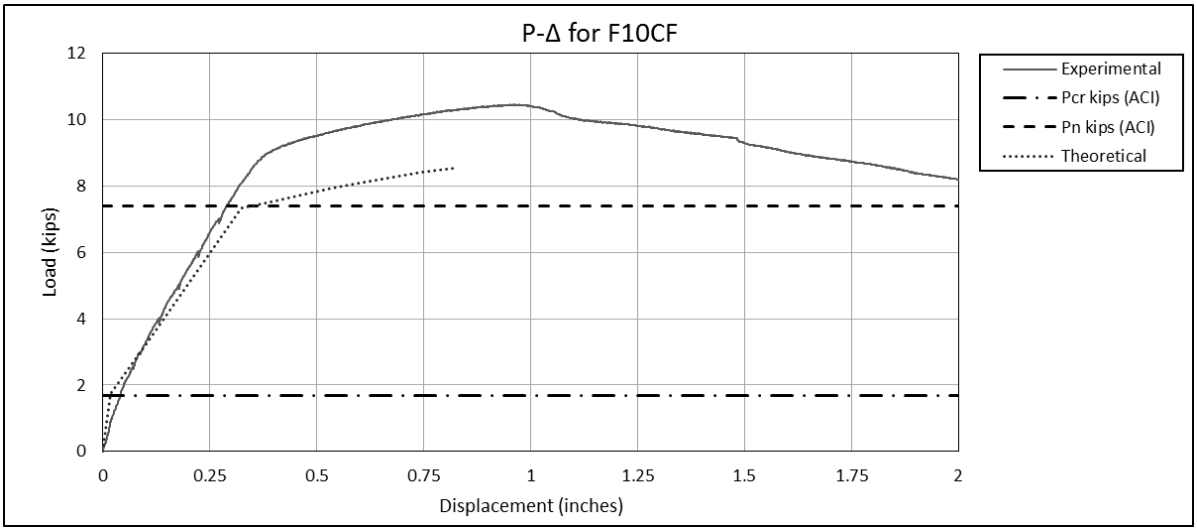

Figure C35. Load vs Deflection Plot for Beam – Mix F10CF

F10CF - Theoretical Values		
Point	P (kips)	Δ (in)
No Load	0.000	0.000
Cracking	1.758	0.018
$f_c = 0.4f_{c\,(56\ days)}$	3.248	0.101
$\epsilon_s = 0.003$	7.327	0.324
$\epsilon_s = 0.0045$ (yield)	7.524	0.390
$\epsilon_c = 0.0027$	7.933	0.534
$\epsilon_c = 0.003$	8.092	0.597
$\epsilon_c = 0.0038$	8.392	0.742
$\epsilon_c = 0.0044$	8.511	0.817
ACI Cracking Load - Pcr (kips) =		1.693
ACI Nominal Load - Pn (kips) =		7.392

Table C18. Theoretical Load and Deflection Values for Mix F10CF

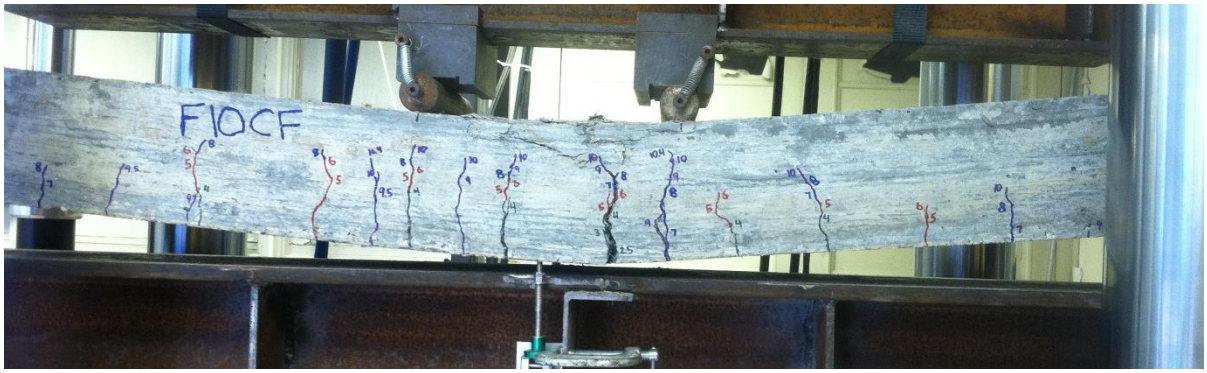

Figure C36. Flexure test on beam – Mix F10CF

Mix F15C

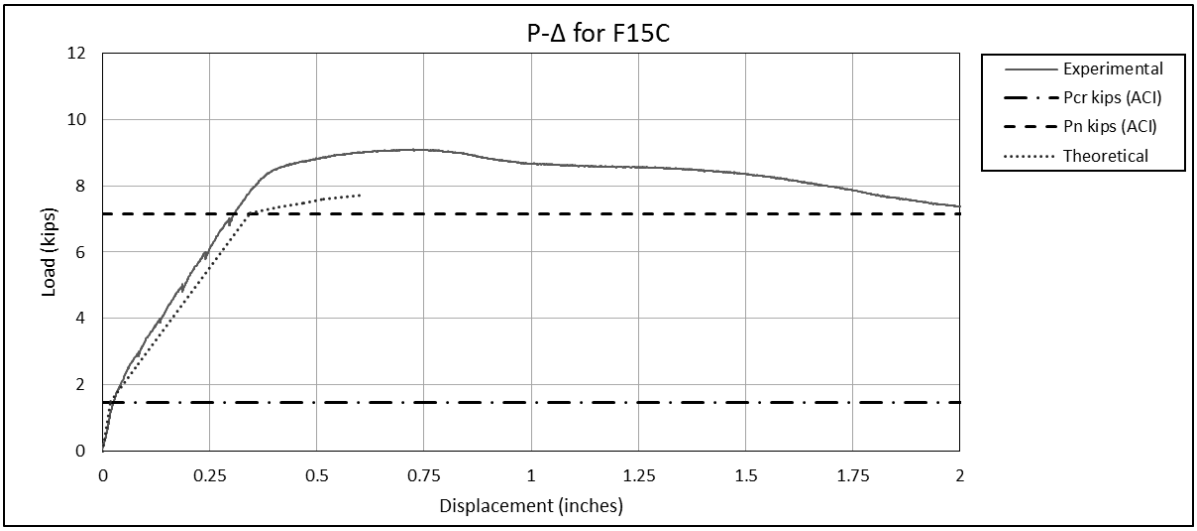

Figure C37. Load vs Deflection Plot for Beam – Mix F15C

F15C - Theoretical Values		
Point	P (kips)	Δ (in)
No Load	0.000	0.000
Cracking	1.518	0.018
$f_c = 0.4f_{c\,(56\ days)}$	2.632	0.085
$\epsilon_s = 0.003$	7.170	0.344
$\epsilon_s = 0.0045$ (yield)	7.350	0.413
$\epsilon_c = 0.0027$	7.479	0.471
$\epsilon_c = 0.003$	7.586	0.516
$\epsilon_c = 0.0038$	7.714	0.607
ACI Cracking Load - Pcr (kips) =		1.462
ACI Nominal Load - Pn (kips) =		7.153

Table C19. Theoretical Load and Deflection Values for Mix F15C

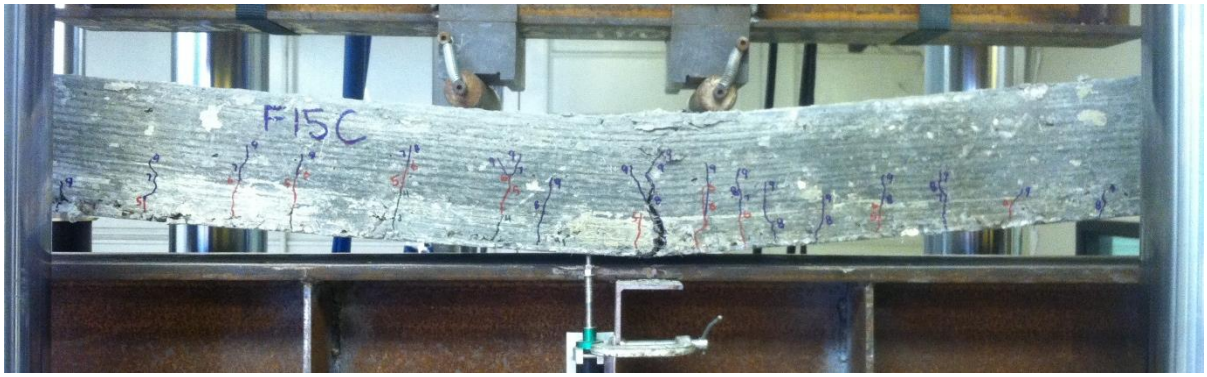

Figure C38. Flexure test on beam – Mix F15C

Mix F15F

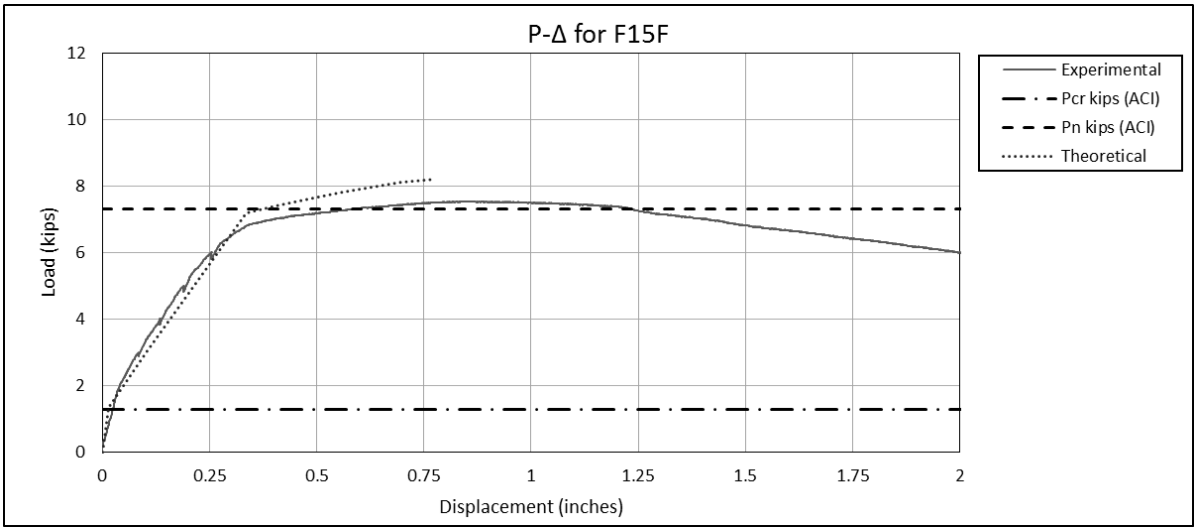

Figure C39. Load vs Deflection Plot for Beam – Mix F15F

F15F - Theoretical Values		
Point	P (kips)	Δ (in)
No Load	0.000	0.000
Cracking	1.343	0.015
$f_c = 0.4f_{c\,(56\ days)}$	3.055	0.106
$\epsilon_s = 0.003$	7.206	0.336
$\epsilon_s = 0.0045$ (yield)	7.402	0.404
$\epsilon_c = 0.0027$	7.672	0.502
$\epsilon_c = 0.003$	7.822	0.559
$\epsilon_c = 0.0038$	8.114	0.696
$\epsilon_c = 0.00448$	8.203	0.774
ACI Cracking Load - Pcr (kips) =		1.292
ACI Nominal Load - Pn (kips) =		7.306

Table C20. Theoretical Load and Deflection Values for Mix F15F

Figure C40. Flexure test on beam – Mix F15F

Mix F15CF

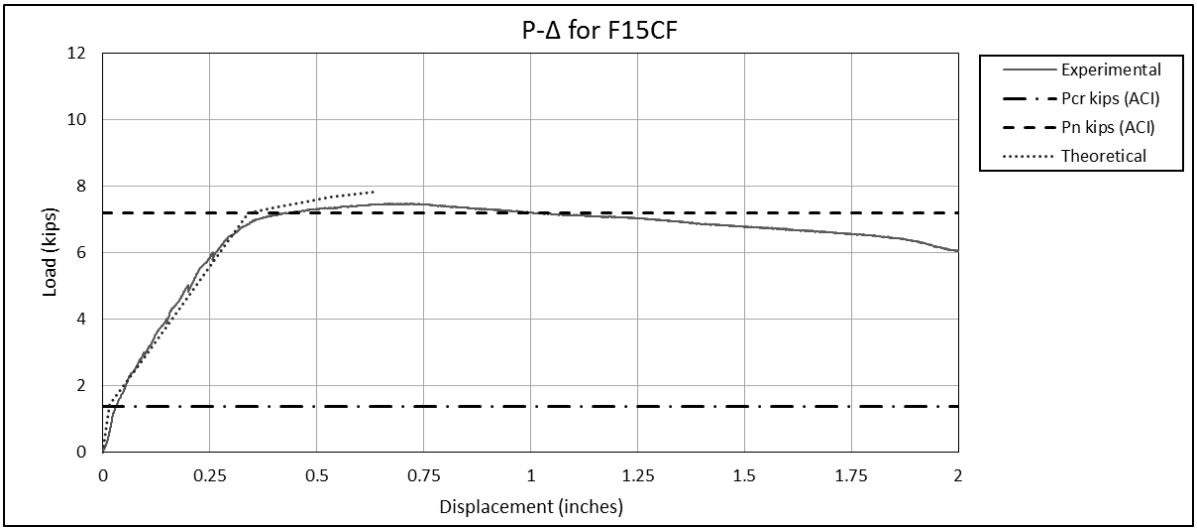

Figure C41. Load vs Deflection Plot for Beam – Mix F15CF

F15CF - Theoretical Values		
Point	P (kips)	Δ (in)
No Load	0.000	0.000
Cracking	1.432	0.016
$f_c = 0.4f_{c\,(56\ days)}$	2.726	0.089
$\epsilon_s = 0.003$	7.189	0.339
$\epsilon_s = 0.0045$ (yield)	7.373	0.408
$\epsilon_c = 0.0027$	7.558	0.483
$\epsilon_c = 0.003$	7.673	0.531
$\epsilon_c = 0.0038$	7.826	0.630
$\epsilon_c = 0.00387$	7.827	0.636
ACI Cracking Load - Pcr (kips) =		1.379
ACI Nominal Load - Pn (kips) =		7.203

Table C21. Theoretical Load and Deflection Values for Mix F15CF

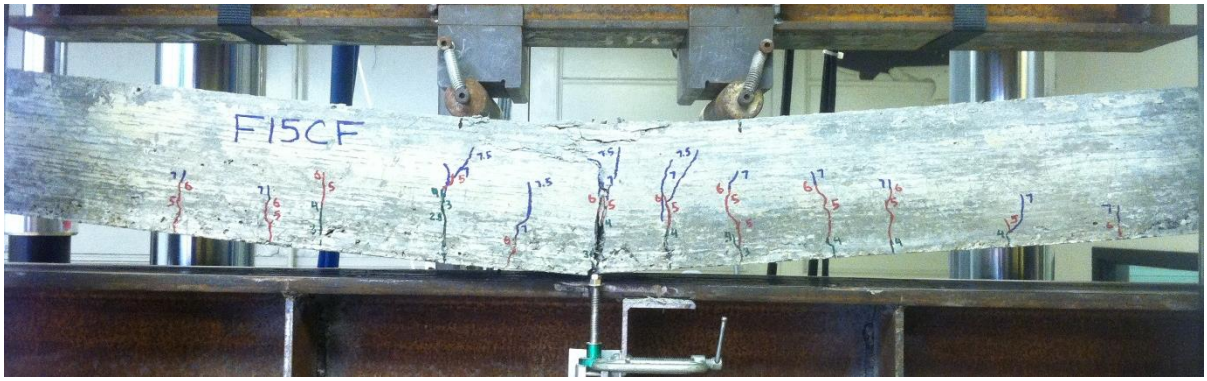

Figure C42. Flexure test on beam – Mix F15CF

Mix F2

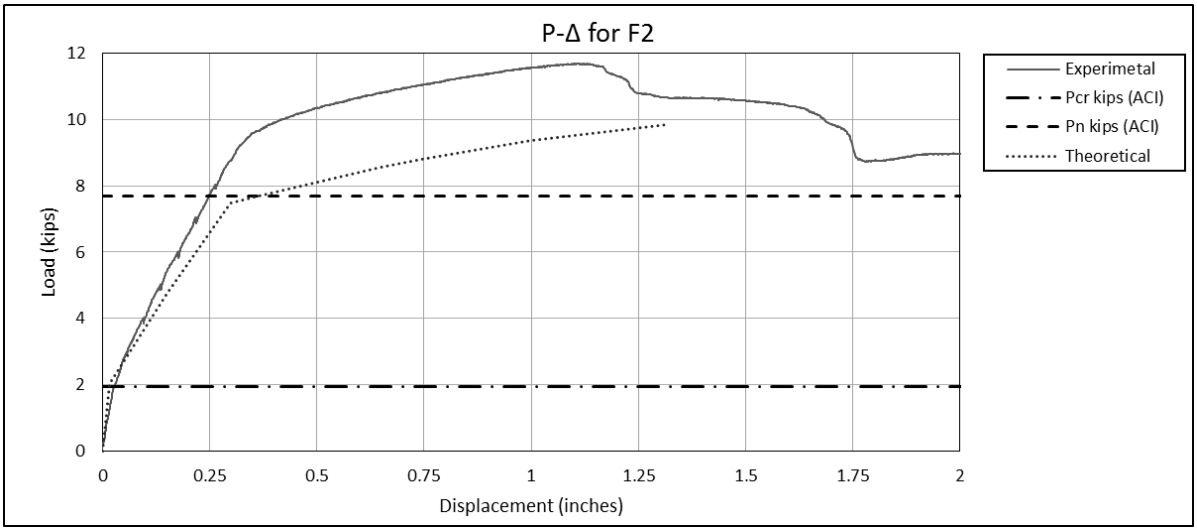

Figure C43. Load vs Deflection Plot for Beam – Mix F2

F2 - Theoretical Values		
Point	P (kips)	Δ (in)
No Load	0.000	0.000
Cracking	2.044	0.018
$f_c = 0.4f_{c\,(56\ days)}$	4.764	0.150
$\epsilon_s = 0.003$	7.491	0.299
$\epsilon_s = 0.0045$ (yield)	7.696	0.363
$\epsilon_c = 0.0027$	8.550	0.647
$\epsilon_c = 0.003$	8.799	0.743
$\epsilon_c = 0.0038$	9.364	0.999
$\epsilon_c = 0.005$	9.832	1.314
ACI Cracking Load - Pcr (kips) =		1.964
ACI Nominal Load - Pn (kips) =		7.674

Table C22. Theoretical Load and Deflection Values for Mix F2

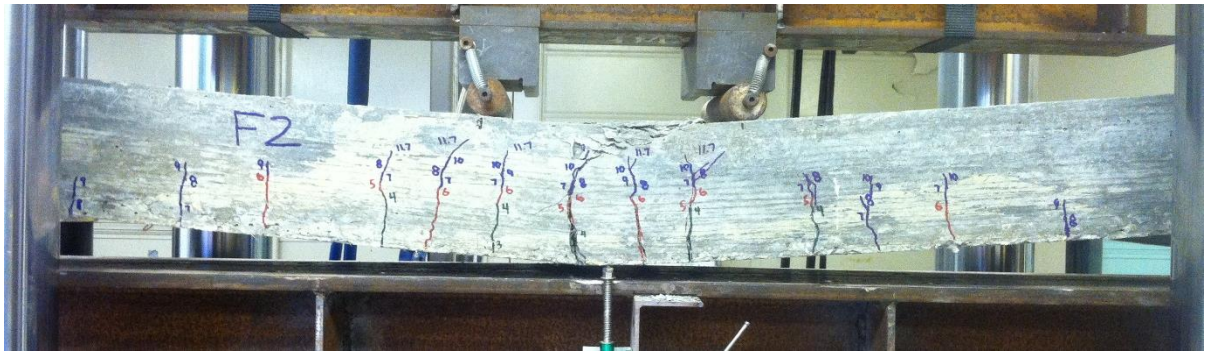

Figure C44. Flexure test on beam – Mix F2

Helminger, Nicholas P. Bachelor of Science, University of Louisiana at Lafayette, Spring 2013; Master of Science, University of Louisiana at Lafayette, Fall 2014
Major: Engineering, Civil Engineering option
Title of Thesis: Material and Flexural Properties of Fiber Reinforced Rubber Concrete
Thesis Director: Dr. Chris Carroll
Pages in Thesis: 193; Words in Abstract: 238

ABSTRACT

The purpose of this research is to determine the material properties of rubber concrete with the addition of fibers, and to determine optimal mixture dosages of rubber and fiber in concrete for structural applications. Fiber-reinforced concrete and rubberized concrete have been researched separately extensively, but this research intends to combine both rubber and fiber in a concrete matrix in order to create a composite material, fiber-reinforced rubber concrete (FRRC). Sustainability has long been important in engineering design, but much of the previous research performed on sustainable concrete does not result in a material that can be used for practical purposes. While still achieving a material that can be used for structural applications, economical considerations were given when choosing the proportions and types of constituents in the concrete mix. Concrete mixtures were designed, placed, and tested in accordance with common procedures and standards, with an emphasis on practicality. Properties that were investigated include compressive strength, tensile strength, modulus of elasticity, toughness, and ductility. The basis for determining the optimal concrete mixture is one that is economical, practical, and exhibits ductile properties with a significant strength. Results show that increasing percentages of rubber tend to decrease workability, unit weight, compressive strength, split tensile strength, and modulus of elasticity while the toughness is increased. The addition of steel needle fibers to rubber concrete increases unit weight, compressive strength, split tensile strength, modulus of elasticity, toughness, and ductility of the composite material.

BIOGRAPHICAL SKETCH

Nicholas Helminger was born on October 14, 1990 and grew up in Mansura, Louisiana. His parents are Chad and Laura Helminger and he has a younger brother, Alex. Nicholas graduated from the University of Louisiana at Lafayette in May 2013 with a Bachelor of Science in Civil Engineering. He graduated Magna Cum Laude and was named outstanding graduate of his class by the Department of Civil Engineering. Nicholas is a member of ASCE, ACI, and Chi Epsilon, and plans to continue his involvement in these societies in his professional career.